

# Efekti konačne veličine u XY lancu

---

**Marić, Vanja**

**Master's thesis / Diplomski rad**

**2017**

*Degree Grantor / Ustanova koja je dodijelila akademski / stručni stupanj:* **University of Zagreb, Faculty of Science / Sveučilište u Zagrebu, Prirodoslovno-matematički fakultet**

*Permanent link / Trajna poveznica:* <https://um.nsk.hr/um:nbn:hr:217:052835>

*Rights / Prava:* [In copyright](#)/[Zaštićeno autorskim pravom.](#)

*Download date / Datum preuzimanja:* **2024-11-18**



*Repository / Repozitorij:*

[Repository of the Faculty of Science - University of Zagreb](#)



UNIVERSITY OF ZAGREB  
FACULTY OF SCIENCE  
DEPARTMENT OF PHYSICS

Vanja Marić

FINITE-SIZE EFFECTS IN THE XY CHAIN

Master Thesis

Zagreb, 2017

SVEUČILIŠTE U ZAGREBU  
PRIRODOSLOVNO-MATEMATIČKI FAKULTET  
FIZIČKI ODSJEK

Vanja Marić

EFEKTI KONAČNE VELIČINE U XY LANCU

Diplomski rad

Zagreb, 2017.

UNIVERSITY OF ZAGREB  
FACULTY OF SCIENCE  
DEPARTMENT OF PHYSICS

INTEGRATED UNDERGRADUATE AND GRADUATE UNIVERSITY  
PROGRAMME IN PHYSICS

**Vanja Marić**

Master Thesis

# **Finite-Size Effects in the XY Chain**

Advisor: Professor Fabio Franchini, dr. sc.

Co-Advisor: Professor Denis Sunko, prof. dr. sc.

Master Thesis grade: \_\_\_\_\_

Committee: 1. \_\_\_\_\_

2. \_\_\_\_\_

3. \_\_\_\_\_

Master Thesis defence date: \_\_\_\_\_

Zagreb, 2017

First, I would like to thank my advisor Dr. Sc. Fabio Franchini for turning his ideas into a topic of this thesis and for his guidance and assistance throughout the process.

I would also like to thank Professor Denis Sunko for co-advising the thesis.

I thank Ira Schneider for help with the English language.

Finally, I wish to thank my parents for their continuous support throughout my study.

# Efekti konačne veličine u XY lancu

## Sažetak

XY lanac u poprečnom magnetskom polju je prototipni egzaktno rješiv model sa zanimljivim i poželjnim svojstvima: njegov dvodimenzionalni fazni dijagram, karakteriziran parametrom anizotropije i snagom vanjskog magnetskog polja, sadrži dva različita kvantna prijelaza na temperaturi apsolutne nule, a model se uvijek može preslikati u sistem slobodnih (bez spina) fermiona. Jedan od faznih prijelaza je klasa univerzalnosti slobodnih fermiona ( $c = 1$  CFT), a drugi je klasa univerzalnosti 1D kvantnog Isingovog modela ( $c = 1/2$  CFT). XY lanac je zapravo generalizacija Isingovog lanca. Dok se obje linije faznih prijelaza mogu opisati konformalnom teorijom polja (CFT), bikritična točka u kojoj se te linije susreću je nekonformalna, jer ima kvadratičan spektar.

Cilj diplomskog rada je uočiti nekonformalnu prirodu bikritične točke u XY lancu u numeričkom eksperimentu kroz veličine dostupne također u modelima koji nisu egzaktno rješivi, kao što su entropija zapetljanosti i svojstvene vrijednosti reducirane matrice gustoće. Na taj način želimo u budućnosti predložiti numeričke provjere je li multikritična točka u proizvoljnom modelu konformalna ili nije.

Najprije uvodimo XY lanac i koristeći standarde analitičke tehnike pronalazimo njegovo mikroskopsko rješenje. Kao i Isingov model XY lanac pokazuje fazu slomljene  $Z_2$  simetrije, u kojoj postoje dva degenerirana osnovna stanja u termodinamičkom limesu velikog sistema. Primijetivši manjak rezultata o egzaktnoj degeneraciji osnovnog stanja, istražujemo problem koristeći numeričke i analitičke metode. Analitička metoda, koja uključuje kompleksnu analizu i Fourierov red, dala je odgovor za Isingov model. Koristeći tu metodu za općenitiji XY lanac pronalazimo ovisnost degeneracije o broju spinova u slučaju iščezavajućeg magnetskog polja i pokazujemo odsutnost degeneracije kada je parametar anizotropije veći od 1 i broj spinova paran.

Vraćajući se glavnom cilju rada, izvodimo svojstvene vrijednosti reducirane matrice gustoće i entropiju zapetljanosti u XY lancu te konstruiramo numerički algoritam za njihovo računanje. Uspijevamo primijetiti nekonformalnu prirodu bikritične točke uspoređivanjem entropije zapetljanosti i najveće svojstvene vrijednosti reducirane matrice gustoće s predviđanjima konformalne teorije polja u blizini i daleko od

bikritične točke.

Ključne riječi: XY lanac u poprečnom magnetskom polju, zapetljanost, kvantni fazni prijelazi, degenerirana osnovna stanja, nekonformalna točka

# Finite-Size Effects in the XY chain

## Abstract

The XY chain in a transverse field is a prototypical exactly solvable model with interesting and desirable properties: its two dimensional phase diagram, characterized by an anisotropy parameter and the strength of an external magnetic field, hosts two different quantum phase transitions at zero temperature, while the model can always be mapped into a system of free (spin-less) fermions. One of the phase transitions is the universality of free fermions ( $c = 1$  CFT), while the other is that of the 1D quantum Ising model ( $c = 1/2$  CFT). As a matter of fact, the XY chain is a generalization of the Ising chain. While both lines of phase transitions can be described by Conformal Field Theory, the bi-critical point at which these lines meet is non-conformal, since it has a quadratic spectrum.

The aim of this thesis is to observe the non-conformal nature of the bi-critical point in the XY chain in a numerical experiment through quantities accessible also in non-exactly solvable models, such as the entanglement entropy and the eigenvalues of the reduced density matrix. In this way, we want to propose in the future numerical tests whether a multi-critical point in an arbitrary model is conformal or not.

First we introduce the XY chain and using standard analytical methods find its microscopic solution. Like the Ising model, the XY chain has a phase of broken  $Z_2$  symmetry, where the model shows two degenerate ground states in the thermodynamic limit of infinite system length. Having noticed a scarcity of results on the exact energy degeneracy between two putative ground states, we examine the problem using numerical and analytical methods. The analytical method, employing complex analysis and Fourier series, has given a definite answer for the Ising model. Using this method for the more general XY chain we find the dependence of the exact degeneracy on the number of spins in the special case of zero magnetic field and show the absence of an exact degeneracy when the anisotropy is greater than 1 and the number of spins is even.

Coming back to the main aim of the thesis, we derive the reduced density matrix eigenvalues and the entanglement entropy in the XY chain and construct a numerical algorithm for calculating them. We accomplish to discriminate the non-conformal



nature of the bi-critical point by comparing the entanglement entropy and the largest reduced density matrix eigenvalue with the conformal field theory predictions near and far from the bi-critical point.

Keywords: XY chain in a transverse magnetic field, entanglement, quantum phase transitions, ground state degeneracy, non-conformal point

# Contents

<b>1</b>	<b>Introduction</b>	<b>1</b>
<b>2</b>	<b>Solving the XY chain</b>	<b>6</b>
2.1	Introduction . . . . .	6
2.2	Diagonalization of a quadratic form in Fermi operators . . . . .	7
2.3	Jordan-Wigner transformation . . . . .	8
2.4	Diagonalization of the XY chain . . . . .	10
2.5	Ground state . . . . .	22
2.6	Critical properties . . . . .	25
2.7	Correlation functions . . . . .	27
<b>3</b>	<b>Ground state degeneracy in the XY chain</b>	<b>33</b>
3.1	Introduction . . . . .	33
3.2	Known results . . . . .	34
3.3	Numerical results . . . . .	36
3.4	Analytical results . . . . .	38
<b>4</b>	<b>Entanglement in the XY chain</b>	<b>47</b>
4.1	Introduction . . . . .	47
4.2	Reduced density matrix and the entanglement entropy . . . . .	47
4.3	Reduced density matrix of the XY chain . . . . .	50
4.4	Double scaling limit . . . . .	55
4.5	Methodology . . . . .	58
4.6	Results . . . . .	62
<b>5</b>	<b>Conclusion</b>	<b>70</b>
<b>6</b>	<b>Prošireni sažetak</b>	<b>72</b>
6.1	Uvod . . . . .	72
6.2	Rješavanje XY lanca . . . . .	74
6.3	Degeneracija osnovnog stanja u XY lancu . . . . .	77
6.4	Zapetljanost u XY lancu . . . . .	80
6.5	Zaključak . . . . .	82
6.6	HR nazivi slika i tablica . . . . .	84



# 1 Introduction

The one-dimensional XY chain in a transverse magnetic field is a prototypical quantum-mechanical model for magnetic-orderings in spin systems. It is a generalization of the one-dimensional quantum Ising model with whom it shares a property of describing a chain of spins which interact with their nearest neighbors and with an external magnetic field. It is more general than the Ising model because in addition to the interaction of the  $x$  components of the spins we also have the interaction of the  $y$  components which is in general different, therefore the model is called the XY chain. The difference between the interaction of  $x$  and  $y$  components is described by the so-called *anisotropy parameter*  $\gamma$ . Explicitly, the XY chain in a transverse magnetic field is given by the Hamiltonian [2]

$$H = J \sum_{j=1}^N [(1 + \gamma)S_j^x S_{j+1}^x + (1 - \gamma)S_j^y S_{j+1}^y + hS_j^z]. \quad (1.1)$$

The introduced Hamiltonian describes  $N$  three-dimensional 1/2-spin variables on a one dimensional lattice. Spin operators are represented by matrices  $S_j^\alpha = 1/2\sigma_j^\alpha$ , where  $\sigma_j^\alpha$  are Pauli matrices for  $\alpha = x, y, z$ . The magnetic field points in the  $z$ -direction and it's magnitude is described by a parameter  $h$ . The interaction between the spins is such that it can be neglected in the direction of the magnetic field. The parameter  $J$  defines the energy scale. The 1D Quantum Ising model is obtained for  $\gamma = 1$ . Another special case,  $\gamma = 0$ , is known in the literature as the XX model. A graphical representation of the XY chain is given in Figure 1.1.

We'll assume periodic boundary conditions  $S_{N+1}^\alpha = S_1^\alpha$  in (1.1). Open boundary conditions are for most of the systems more realistic but, as usual, we expect that the boundary conditions shouldn't be important for large systems. It can be shown explicitly that in the XY chain the same phases exist regardless of the boundary conditions but the mathematical way to describe them using open boundary conditions is somewhat different [2]. Periodic boundary conditions can also be a more realistic option, if the system is closed in a ring.

Because of the symmetries of the model we can always assume  $\gamma \geq 0$ ,  $h \geq 0$ . Namely, a rotation around  $z$ -axis by  $\pi/2$  interchanges  $x$  and  $y$  spin interactions and corresponds to  $\gamma \rightarrow -\gamma$ . The case  $h < 0$  can be described as the case  $h > 0$  with the

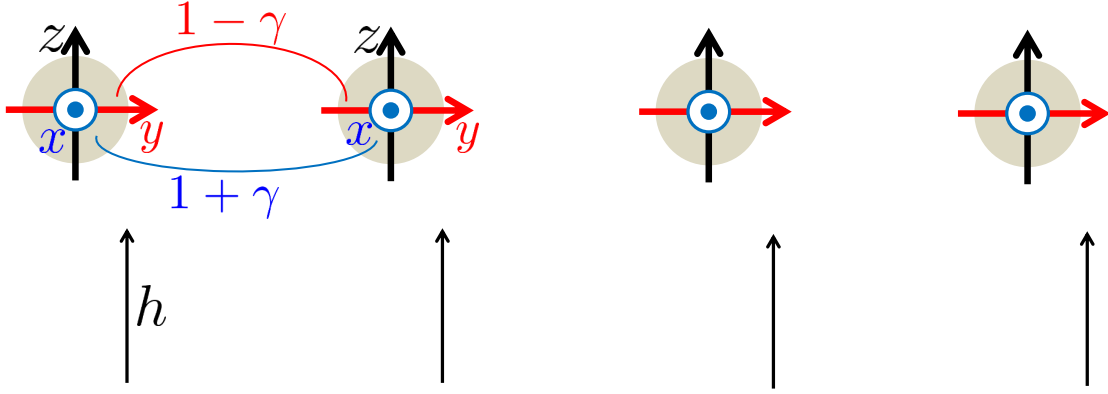


Figure 1.1: A graphical representation of the XY chain, where the chain propagates in the  $y$  direction and is orthogonal to the external magnetic field. The external magnetic field  $h$  points in the  $z$ -direction and interacts with  $z$  components of spins. Spins interact with their nearest neighbours through their  $x$  and  $y$  components. The difference between the interaction of  $x$  and  $y$  components is described by *anisotropy parameter*  $\gamma$ .

change of the direction of the  $z$ -axis followed by a rotation by  $\pi/2$  around it.

The case  $J < 0$  is usually called the ferromagnetic case and the case  $J > 0$  anti-ferromagnetic. It is easy to justify this terminology when we look at the simple case  $\gamma = 1$  and  $h = 0$ , which describes the Ising model without magnetic field. The ground state for  $J < 0$  has all the spins aligned in the parallel way along the  $x$ -direction, while for  $J > 0$  the nearest spins are antiparallel (staggered).

The XY chain in a transverse field is an exactly solvable and free model. The ground state, all the excitations, the free energy, the entanglement entropy and virtually every other quantity can be found exactly. This fact makes the XY chain a very good model to test general theoretical hypotheses, in addition to being an interesting generalization of historically very important Ising model. The one-dimensional systems are important in general because of existence of exact methods for solving them and powerful approximate approaches. On the other hand they are possible to realize experimentally using, for example, trapped cold atoms in optical lattices. Specifically, spin-spin interactions between neighboring atoms can be implemented by bringing the atoms together to a single site and carrying out controlled collisions [30]. Analytical tractability on one side and possibility of experimental realization on the other makes one-dimensional spin systems important also for quantum information and quantum computation. The XY chain in particular has been examined theoretically also for this purpose [31] [6].

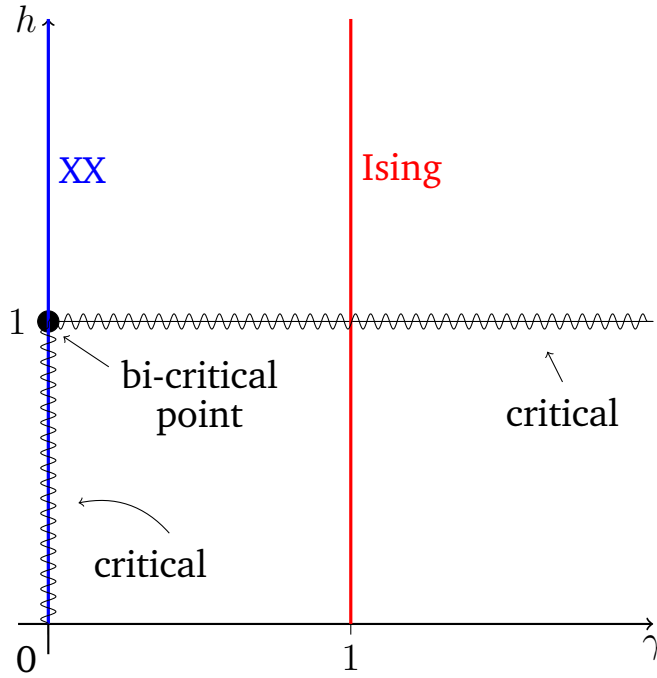


Figure 1.2: Critical regions in the  $(\gamma, h)$  parameter space for the XY model. The XX model,  $\gamma = 0$ , is critical in the interval  $h \in [0, 1]$ . The whole  $h = 1$  line is also critical and includes the familiar Ising phase transition at  $\gamma = 1$ . Two critical lines meet at the bi-critical point  $(0, 1)$ .

The XY chain in a transverse field has a rich and non-trivial  $(\gamma, h)$  phase diagram. It shows two quantum phase transitions (QPT) at zero temperature, i.e. with the system in its ground state. The critical lines are  $h = 1$  and  $\gamma = 0, h \leq 1$ , and they intersect at the bi-critical point  $(\gamma, h) = (0, 1)$ . The phase diagram is shown in Figure 1.2.

One of the most fundamental and fascinating features of quantum mechanics is entanglement. This phenomenon has been the basis for the development of new branches such as quantum information and computation . A recent and rich field of research concerns the understanding of the role of entanglement in many-body systems [9]. A quantity which has been successful as an entanglement measure is the entanglement entropy. A principal reason for this is simple laws governing its behavior at and close to the critical points, given by conformal field theory [9]. Conformal field theory (CFT) is a powerful analytical method to describe the low-energy behavior of systems at and near criticality. Together with the density matrix renormalization group procedure to obtain the reduced density matrix eigenvalues one has both analytical and numerical methods to study the systems which are not exactly solvable and to calculate quantities which would otherwise be hard or even

impossible. Within the CFT description the system's universality is characterized by a pure number called *central charge*. Each phase transition has its central charge  $c$  which is a single number. For example, in the XY chain the QPT at  $h = 1$  has central charge  $c = 1/2$ , while the QPT at  $\gamma = 0$ ,  $h \leq 1$ , has central charge  $c = 1$  [2]. Universality classes for one-dimensional systems are qualitatively different from higher dimensional analogues. For example, lattice fermions in three and higher dimensions typically behave like a Fermi liquid, while in one dimension we have a Luttinger liquid [32]. The problem with the CFT description is that CFT itself doesn't know when it fails. The CFT is valid as long as we are not too far from the criticality, in the Hamiltonian parameters. How far we can be is set by the correlation length  $\xi$ , a characteristic length-scale in the system. There are general principles that help us in determining the regime of validity of the CFT description, and they might also depend on the quantities we want to address. However, it is important to also have the microscopic solution of the model in order to check these general principles or to address more peculiar properties.

The multi-critical points, i.e. points where more quantum phase transitions meet, are special for CFT. In their vicinity the CFT might be and might not be valid. In the former case we say that the multi-critical point is *conformal*, while in the latter case we say that it is *non-conformal*. For exactly solvable models we can determine whether the multi-critical point is conformal or not by examination of the properties of the Hamiltonian spectrum, but in general this is a difficult task. For example, the XY chain is exactly solvable and we know that its bi-critical point  $(\gamma, h) = (0, 1)$  is non-conformal.

The aim of this thesis is to observe the non-conformal nature of the bi-critical point in the XY chain in a numerical experiment through quantities accessible also in non-exactly solvable models. In this way want to propose in the future numerical tests whether a multi-critical point in an arbitrary model is conformal or not. Quantities accessible in an arbitrary model are the reduced density matrix eigenvalues and the entanglement entropy. The idea is to examine the behavior of these quantities in an exactly solvable XY chain and see how the CFT prediction breaks close to the non-conformal bi-critical point. The XY chain is exactly solvable so we know its microscopic details and we can calculate the characteristic length-scale to make some predictions where the CFT should be valid. We calculate the reduced density matrix

eigenvalues and the entanglement entropy for the XY chain and examine how these quantities behave in the phase diagram where the CFT prediction should be valid. We establish the agreement with the CFT prediction for some characteristic length-scale in the system. Then we specifically examine how the RDM eigenvalues and the entanglement entropy behave close to the non-conformal bi-critical point for a similar characteristic length-scale. We want to find out in which way, if it is noticeable, the CFT prediction breaks.

In Section 2 the XY chain is solved. The ground state energy and all the excitations are found. The critical properties and the correlation functions are also discussed. The ground state of the XY chain can be degenerate in general, which is also connected to the breaking of the discrete  $Z_2$  symmetry. The degeneracy depends on the size of the system  $N$ . Because of the lack of results on the degeneracy in the XY chain we devote the entire Section 3 to the study of it. In this way we get a more complete understanding of the model. In Section 4 first the reduced density matrix eigenvalues and the entanglement entropy are found exactly for a finite block of spins in a large chain, and numerical algorithm for their calculation is discussed. Then some CFT and other predictions on the behavior of these quantities are discussed in the double-scaling limit, i.e. the limit of a large subsystem in a very large system. The numerically calculated behavior of these quantities in a finite system is compared to the double-scaling limit. Finally, the breaking of the CFT prediction close to the bi-critical point is examined.



## 2 Solving the XY chain

### 2.1 Introduction

The XY chain was introduced and solved in the case of zero magnetic field by Lieb, Schultz and Mattis in 1961 [3]. They introduced it as an exactly solvable model that bears a strong resemblance to the Heisenberg model, to gain further insight into the effects of anisotropy in one dimension. The Heisenberg model is described by the Hamiltonian

$$H = J \sum_{j=1}^N [S_j^x S_{j+1}^x + S_j^y S_{j+1}^y + S_j^z S_{j+1}^z] \quad (2.1)$$

and it is historically the first exactly solved model [2]. The XY model in a transverse external magnetic field was also introduced and solved in 1960s [4] [5].

The XY chain is solved by mapping it first into a system of fermions via the so-called Jordan-Wigner transformation and then bringing it to a form of free fermions. To motivate such mapping in subsection 2.2 we explain how a general quadratic form in fermions can be brought to a form of free fermions. The described procedure was found by Lieb, Shultz and Mattis and was used to solve the original model. However, the XY chain can be solved by more direct standard procedure. In subsection 2.3 we explain a mapping of a system of spins into a system of fermions in general. Then in subsection 2.4 the Jordan-Wigner transformation for the XY chain is introduced and the Hamiltonian is brought to a form of free fermions, we say the Hamiltonian is diagonalized. Once the Hamiltonian is diagonalized we can find the ground state, ground state energy and all the excitations, as is discussed in subsection 2.5. In subsection 2.6 on the basis of the found energies the critical properties are examined. Namely, Figure 1.2 is justified and it is shown that the bi-critical point is non-conformal. In subsection (2.7) it is discussed how can critical properties be approached by examining the correlation functions. Some expressions which will be used in Section 4 are derived and some results important for this thesis are quoted, most importantly the expression for the correlation length.

## 2.2 Diagonalization of a quadratic form in Fermi operators

A Hamiltonian quadratic in fermionic operators  $c_i$  can most generally be written in a form

$$H = \sum_{i,j} [A_{ij}c_i^\dagger c_j + \frac{1}{2}(B_{ij}c_i c_j - B_{ij}^*c_i^\dagger c_j^\dagger)] + const_0, \quad (2.2)$$

where  $const_0$  is a real constant, matrix  $\mathbf{A}$  made out of coefficients  $A_{ij}$  is hermitian and matrix  $\mathbf{B}$  made out of coefficients  $B_{ij}$  is antisymmetric. Form (2.2) can be inferred from the hermicity requirement of the Hamiltonian, i.e. the requirement  $H = H^\dagger$ . Fermi operators  $c_i$  satisfy (anti)commutation relations:

$$\{c_i, c_j\} = 0, \quad (2.3a)$$

$$\{c_i, c_j^\dagger\} = \delta_{ij}. \quad (2.3b)$$

Lieb, Schultz and Mattis have, in the same paper where they introduced the XY model [3], described the procedure how any Hamiltonian quadratic in Fermi operators with real coefficients  $A_{ij}$  and  $B_{ij}$  can be diagonalized. We'll review their method, without deriving it, to motivate the Jordan-Wigner transformation in the next subsections. They have shown that we can always find a canonical linear transformation

$$\chi_i = \sum_k (g_{ik}c_k + h_{ik}c_k^\dagger), \quad (2.4a)$$

$$\chi_i^\dagger = \sum_k (g_{ik}c_k^\dagger + h_{ik}c_k), \quad (2.4b)$$

with the  $g_{ki}$  and  $h_{ki}$  real which gives for Hamiltonian  $H$  the form

$$H = \sum_i \Lambda_i \chi_i^\dagger \chi_i + const. \quad (2.5)$$

The transformation is canonical in the sense that  $\chi_i$  are also Fermi operators:

$$\{\chi_i, \chi_j\} = 0, \quad (2.6a)$$

$$\{\chi_i, \chi_j^\dagger\} = \delta_{ij}. \quad (2.6b)$$

The first step in finding the right transformation is solving the eigenvalue problem for the matrix

$$(\mathbf{A} - \mathbf{B})^T(\mathbf{A} - \mathbf{B})\mathbf{u}_i = \Lambda_i^2\mathbf{u}_i \quad (2.7)$$

We can infer from the form of the matrix  $(\mathbf{A} - \mathbf{B})^T(\mathbf{A} - \mathbf{B})$  that it is symmetric and has non-negative eigenvalues. The energies  $\Lambda_i$  are given by the square root of the eigenvalues. The sign of the energies is arbitrary. Changing the sign corresponds to the redefinition  $\chi_i \leftrightarrow \chi_i^\dagger$ . Next step in finding the transformation is calculating the new vectors  $\mathbf{v}_i$  from the eigenvectors  $\mathbf{u}_i$  using the expression

$$\mathbf{v}_i = \frac{1}{\Lambda_i}(\mathbf{A} - \mathbf{B})\mathbf{u}_i. \quad (2.8a)$$

If some of the energies  $\Lambda_i$  are equal to zero then we calculate the new vector  $\mathbf{v}_i$  by solving the equation

$$(\mathbf{A} - \mathbf{B})^T\mathbf{v}_i = \mathbf{0}. \quad (2.8b)$$

Finally, the linear coefficients  $g_{ik}$  and  $h_{ik}$  in (2.4) are obtained from the components of the vectors  $\mathbf{u}_i$  and  $\mathbf{v}_i$  using expressions

$$g_{ik} = \frac{1}{2}[(\mathbf{u}_i)_k + (\mathbf{v}_i)_k], \quad (2.9a)$$

$$h_{ik} = \frac{1}{2}[(\mathbf{u}_i)_k - (\mathbf{v}_i)_k]. \quad (2.9b)$$

Choosing the normalized vectors  $\mathbf{u}_i$  and  $\mathbf{v}_i$  guarantees us that operators  $\chi_i$  are fermionic. The constant in the diagonalized Hamiltonian (2.5) is given by

$$const = \frac{1}{2} \sum_i (\mathbf{A}_{ii} - \Lambda_i) + const_0. \quad (2.10)$$

### 2.3 Jordan-Wigner transformation

This subsection is based on [8]. Jordan-Wigner transformation is a mapping of a system of interacting spins into a system of Fermions. This means that with a suitable definition of a fermionic operators  $c_i$  we express our spin Hamiltonian in the form which contains only fermionic operators. Furthermore, if the Hamiltonian can be expressed as a quadratic form in fermionic operators (2.2) it can always be brought

to a simple form of free Fermions (2.5). Let's suppose that we have mapped a system of  $N$  interacting spins to a system of  $N$  interacting fermions (2.2) and see what it means.

Let's take a look at the number operators  $c_i^\dagger c_i$ . Each of them is a Hermitian operator. From this fact follows [1] that each has a complete orthonormal system of eigenstates with real eigenvalues. A system of  $N$  spins is described by a Hilbert space of dimension  $2^N$  so each of the operators  $c_i^\dagger c_i$  has  $2^N$  eigenstates. However, the operators  $c_i$  are fermionic and from commutation relations (2.3) follows that their eigenvalues can assume only values 0 and 1. Explicitly, let us assume that the state  $|\psi\rangle$  is an eigenstate of  $c_i^\dagger c_i$  with the eigenvalue  $\lambda$ :

$$c_i^\dagger c_i |\psi\rangle = \lambda |\psi\rangle.$$

But from the commutation relations (2.3) we have

$$(c_i^\dagger c_i)^2 = c_i^\dagger c_i,$$

from which follows that  $\lambda$  has to be 0 or 1.

There are precisely  $2^{N-1}$  eigenvalues of the operator  $c_i^\dagger c_i |\psi\rangle$  with the eigenvalue 1 and with the eigenvalue 0. This again follows from commutation relations. Explicitly, if we suppose that there exists an eigenstate  $|1\rangle$  with eigenvalue 1 then the state  $c_i |1\rangle$  is normalized and has an eigenvalue 0:

$$(c_i^\dagger c_i) c_i |1\rangle = 0.$$

Similarly, if there is an eigenstate  $|0\rangle$  with the eigenvalue 0 there is a corresponding orthogonal state with the eigenvalue 1:

$$(c_i^\dagger c_i) c_i^\dagger |0\rangle = c_i^\dagger |0\rangle.$$

Furthermore, again from the commutation relations, the operators  $c_i^\dagger c_i$  for  $i = 1, \dots, N$  are mutually commuting:

$$[c_i^\dagger c_i, c_j^\dagger c_j] = 0. \tag{2.11}$$

From this fact follows [1] that operators  $c_i^\dagger c_i$  have a complete orthonormal set of common eigenstates. From previous considerations it is clear that half of those eigenstates will be the eigenstate of the particular  $c_i^\dagger c_i$  with the eigenvalue zero, and another half of them with the eigenvalue 1. We can write the generic basis state as  $|n_1 n_2 \dots n_N\rangle$ , where  $n_i$  can assume values 0 or 1 and we consider it the number of particles. We have:

$$c_i^\dagger c_i |n_1 \dots n_i \dots n_N\rangle = n_i |n_1 \dots n_i \dots n_N\rangle . \quad (2.12)$$

If we define the vacuum state  $|0\rangle$  as the state with no particles

$$c_i^\dagger c_i |0\rangle = 0 \quad \text{for any } i, \quad (2.13)$$

we can also write

$$|n_1 n_2 \dots n_N\rangle = (c_1^\dagger)^{n_1} (c_2^\dagger)^{n_2} \dots (c_N^\dagger)^{n_N} |0\rangle . \quad (2.14)$$

State (2.14) is antisymmetric to the interchange of two particles. If the Hamiltonian is quadratic as (2.2) then it will also commute with operators  $c_i^\dagger c_i$  and the states (2.14) will also be the eigenstates of the Hamiltonian, that is they will satisfy the Schrödinger equation.

Finally, if we bring the Hamiltonian to the diagonal form (2.5) since the previous analysis is also valid for fermions  $\chi_q$  we can easily find the energies

$$E_{n_1 n_2 \dots n_N} = \sum_{i=1}^N \Lambda_i n_i + \text{const} . \quad (2.15)$$

## 2.4 Diagonalization of the XY chain

Diagonalization of the XY Hamiltonian in this subsection is based on [2]. The XY Hamiltonian (1.1) in terms of Pauli spin operators reads

$$H = \frac{J}{2} \sum_{j=1}^N \left( \frac{1+\gamma}{2} \sigma_j^x \sigma_{j+1}^x + \frac{1-\gamma}{2} \sigma_j^y \sigma_{j+1}^y + h \sigma_j^z \right) . \quad (2.16)$$

The Hamiltonian also takes a simple form when written in terms of Pauli raising

and lowering operators defined with

$$\sigma^\pm = \frac{1}{2}(\sigma^x \pm i\sigma^y). \quad (2.17)$$

The Hamiltonian reads

$$H = \frac{J}{2} \sum_{j=1}^N \left[ (\sigma_j^+ \sigma_{j+1}^- + \gamma \sigma_j^+ \sigma_{j+1}^+ + \text{h.c.}) + h\sigma_j^z \right], \quad (2.18)$$

where h.c. stands for the hermitian conjugate of the expression in the brackets.

We'll review the properties of Pauli spin operators [7]. Pauli spin operators on a particular site  $j$  satisfy relations

$$[\sigma_j^\alpha, \sigma_j^\beta] = 2i\varepsilon_{\alpha\beta\gamma}\sigma_j^\gamma, \quad (2.19a)$$

$$\{\sigma_j^\alpha, \sigma_j^\beta\} = 2\delta_{\alpha\beta}, \quad (2.19b)$$

where Greek letters  $\alpha, \beta, \gamma$  stand for  $x, y$  or  $z$ ,  $\varepsilon_{\alpha\beta\gamma}$  is the antisymmetric Levi-Civita symbol and  $\delta_{\alpha\beta}$  is the Kronecker delta. Between different sites we have

$$[\sigma_i^\alpha, \sigma_j^\beta] = 0 \quad \text{for } i \neq j. \quad (2.19c)$$

We see that Pauli spin operators  $\sigma_j^\alpha$  are not Fermi operators. Between different sites they satisfy bosonic commutation relations and on a particular site they behave fermionically. Similarly the set of operators  $\sigma_j^-, \sigma_j^+ = (\sigma_j^-)^\dagger$  and  $\sigma_j^z$  is also not a set of Fermi operators. On a particular site  $j$  they satisfy the relations

$$[\sigma_j^+, \sigma_j^-] = \sigma_j^z, \quad (2.20a)$$

$$[\sigma_j^z, \sigma_j^+] = \sigma_j^+, \quad (2.20b)$$

$$\{\sigma_j^+, \sigma_j^-\} = 1, \quad (2.20c)$$

$$\{\sigma_j^z, \sigma_j^+\} = 0, \quad (2.20d)$$

which are again fermionic, but again between sites they satisfy bosonic commutation relations

$$[\sigma_i^z, \sigma_j^+] = [\sigma_i^-, \sigma_j^+] = 0 \quad \text{for } i \neq j. \quad (2.20e)$$

Now we introduce the Jordan-Wigner transformation for the XY chain and reformulate the Hamiltonian in terms of Fermi operators. The suitable Fermi operators for the Jordan-Wigner transformation are

$$\psi_j = \left( \prod_{l=1}^{j-1} \sigma_l^z \right) \sigma_j^+ \quad (2.21a)$$

and their hermitian conjugates

$$\psi_j^\dagger = \left( \prod_{l=1}^{j-1} \sigma_l^z \right) \sigma_j^- , \quad (2.21b)$$

for  $j = 1, 2, \dots, N$ . We will examine the properties of operators (2.21) and reformulate the Hamiltonian in terms of them using properties (2.19) and (2.20) of Pauli spin operators. As we have already noted, the operators  $\psi_j$  and  $\psi_j^\dagger$  are Fermi operators:

$$\{\psi_i, \psi_j\} = 0 , \quad (2.22a)$$

$$\{\psi_i, \psi_j^\dagger\} = \delta_{ij} , \quad (2.22b)$$

which can be shown using the properties of Pauli spin operators. If we define  $\psi_{N+1}$  in the same way, as

$$\psi_{N+1} = \left( \prod_{l=1}^N \sigma_l^z \right) \sigma_{N+1}^+ = \left( \prod_{l=1}^N \sigma_l^z \right) \sigma_1^+$$

it doesn't satisfy the Fermi commutation relations with other operators (2.21). That's why we'll abort this definition.

Our Hilbert space is a tensor product of  $N$  spin 1/2 Hilbert spaces. We represent the  $\sigma^z$  eigenstates in the following way:

$$\sigma^z |\uparrow\rangle = |\uparrow\rangle , \quad \sigma^z |\downarrow\rangle = -|\downarrow\rangle .$$

The basis of our Hilbert space are product spin states  $|n_1\rangle \otimes |n_2\rangle \otimes \dots \otimes |n_N\rangle$  or shortly  $|n_1 n_2 \dots n_N\rangle$ , where  $n_i$  stands for  $\uparrow$  or  $\downarrow$ . This states will also be the basis (2.14) because if we identify  $\uparrow$  with 0 and  $\downarrow$  with 1 we see that Fermi operators (2.21) act on the

basis states as

$$\psi_j |n_1 n_2 \dots n_j = 0 \dots n_N\rangle = 0 , \quad (2.24a)$$

$$\psi_j |n_1 n_2 \dots n_j = 1 \dots n_N\rangle = (-1)^{n_1} (-1)^{n_2} \dots (-1)^{n_{j-1}} |n_1 n_2 \dots n_j = 0 \dots n_N\rangle , \quad (2.24b)$$

$$\psi_j^\dagger |n_1 n_2 \dots n_j = 0 \dots n_N\rangle = (-1)^{n_1} (-1)^{n_2} \dots (-1)^{n_{j-1}} |n_1 n_2 \dots n_j = 1 \dots n_N\rangle , \quad (2.24c)$$

$$\psi_j^\dagger |n_1 n_2 \dots n_j = 1 \dots n_N\rangle = 0 , \quad (2.24d)$$

from which follows

$$\psi_j^\dagger \psi_j = n_j |n_1 n_2 \dots n_j \dots n_N\rangle . \quad (2.24e)$$

$$(2.24f)$$

The vacuum state is

$$|0\rangle \equiv |\uparrow_1 \uparrow_2 \dots \uparrow_N\rangle . \quad (2.25)$$

Spin downs  $\downarrow$  are particles and spin ups  $\uparrow$  are holes.

We can express Pauli operator  $\sigma_j^z$  in terms of Fermi operators:

$$\sigma_j^z = 1 - 2\psi_j^\dagger \psi_j , \quad (2.26a)$$

and also  $\sigma_j^+$  and  $\sigma_j^-$ :

$$\sigma_j^+ = \left( \prod_{l=1}^{j-1} 1 - 2\psi_l^\dagger \psi_l \right) \psi_j , \quad (2.26b)$$

$$\sigma_j^- = \left( \prod_{l=1}^{j-1} 1 - 2\psi_l^\dagger \psi_l \right) \psi_j^\dagger , \quad (2.26c)$$

$$(2.26d)$$

for  $j = 1, \dots, N$ . Using (2.26) and Fermi operators properties (2.22) after some algebra we can express the Hamiltonian (2.18) in terms of Fermi operators. We



obtain

$$\begin{aligned}
H = & -\frac{J}{2} \sum_{j=1}^{N-1} (\psi_j \psi_{j+1}^\dagger + \gamma \psi_j \psi_{j+1} + \text{h.c.}) + \frac{J}{2} P (\psi_N \psi_1^\dagger + \gamma \psi_N \psi_1 + \text{h.c.}) \\
& - Jh \sum_{j=1}^N \psi_j^\dagger \psi_j + \frac{1}{2} JNh ,
\end{aligned} \tag{2.27}$$

where we have defined the Hermitian parity operator

$$P = \prod_{l=1}^N \sigma_l^z = \prod_{l=1}^N (1 - 2\psi_l^\dagger \psi_l) . \tag{2.28}$$

The parity operator simply gives a plus sign on a basis state with an even number of particles and a minus sign on a state with an odd number of particles. Schematically,

$$P |\text{even number of particles}\rangle = |\text{even number of particles}\rangle , \tag{2.29a}$$

$$P |\text{odd number of particles}\rangle = - |\text{odd number of particles}\rangle . \tag{2.29b}$$

The Hamiltonian (2.27) consists of terms such as  $\psi_i \psi_j$  and  $\psi_i^\dagger \psi_j$ . It creates and annihilates particles in pairs and that's why it will commute with the parity operator.

Explicitly,

$$[\psi_i \psi_j, P] = 0 , \quad [\psi_i^\dagger \psi_j, P] = 0 . \tag{2.30}$$

and

$$[H, P] = 0 . \tag{2.31}$$

The Hamiltonian is now reformulated in terms of Fermi operators  $\psi_j$  and the parity operator  $P$ . Because of the parity operator  $P$  the Hamiltonian (2.27) is not a quadratic form in Fermi operators (2.2). However, we can separate our theory in two sectors, one with an even number of particles and one with an odd number of particles, so that in each sector the Hamiltonian is quadratic form. We do it by writing the Hamiltonian (2.27) in the form

$$H = \frac{1+P}{2} H^+ + \frac{1-P}{2} H^- , \tag{2.32}$$

where  $H^\pm$  is formally (2.27) with  $P = \pm 1$ :

$$\begin{aligned}
H^\pm = & -\frac{J}{2} \sum_{j=1}^{N-1} (\psi_j \psi_{j+1}^\dagger + \gamma \psi_j \psi_{j+1} + \text{h.c.}) \pm \frac{J}{2} (\psi_N \psi_1^\dagger + \gamma \psi_N \psi_1 + \text{h.c.}) \\
& - Jh \sum_{j=1}^N \psi_j^\dagger \psi_j + \frac{1}{2} JNh,
\end{aligned} \tag{2.33}$$

We'll call the operators  $H^+$  and  $H^-$  also Hamiltonians. Each of them is a quadratic form in Fermi operators (2.2). That's why in principle we could write down the  $N \times N$  matrices **A** and **B**, defined in subsection 2.2, for each of them, diagonalize the matrix  $(\mathbf{A} - \mathbf{B})^T(\mathbf{A} - \mathbf{B})$  and bring them to a diagonal form (2.5). However, this might not be an easy task and there is a method to circumvent it. First, notice that if we define the operator  $\psi_{N+1}$  separately in each sector in the following way:

$$\psi_{N+1} |\text{even number of particles}\rangle = -\psi_1 |\text{even number of particles}\rangle, \tag{2.34a}$$

$$\psi_{N+1} |\text{odd number of particles}\rangle = \psi_1 |\text{odd number of particles}\rangle \tag{2.34b}$$

then we could write the Hamiltonians (2.33) as

$$H^\pm = -\frac{J}{2} \sum_{j=1}^N (\psi_j \psi_{j+1}^\dagger + \gamma \psi_j \psi_{j+1} + \text{h.c.}) - Jh \sum_{j=1}^N \psi_j^\dagger \psi_j + \frac{1}{2} JNh. \tag{2.35}$$

Hamiltonians  $H^\pm$  can from (2.35) be brought to a more useful form, but first we have to introduce a lemma that we will use many times throughout the thesis.

**Lemma.** *Let  $n$  be an arbitrary integer and  $N$  be a natural number. Let us define the set  $X_N$  with  $X_N = \{x_0, x_0 + 1, x_0 + 2, \dots, x_0 + N - 1\}$ . Then*

- if  $x_0$  is an integer:

$$\frac{1}{N} \sum_{x \in X_N} e^{i \frac{2\pi}{N} xn} = \begin{cases} 1 & \text{if } n \text{ is equal to } kN \text{ for some integer } k \\ 0 & \text{otherwise} \end{cases}$$

- if  $x_0 = 1/2$ :

$$\frac{1}{N} \sum_{x \in X_N} e^{i \frac{2\pi}{N} x n} = \begin{cases} (-1)^k & \text{if } n \text{ is equal to } kN \text{ for some integer } k \\ 0 & \text{otherwise} \end{cases}$$

*Proof.* In both cases we can write

$$\frac{1}{N} \sum_{x \in X_N} e^{i \frac{2\pi}{N} x n} = e^{i \frac{2\pi}{N} x_0 n} \frac{1}{N} \sum_{m=0}^{N-1} \left( e^{\frac{2\pi}{N} n} \right)^m .$$

The sum in the right expression is just the sum of the geometric sequence. It is equal to  $N$  if  $n$  is equal to  $kN$  for some integer  $k$ . Otherwise it is zero. In the former case the term in front of the sum is

$$e^{i \frac{2\pi}{N} x_0 n} = e^{i 2\pi x_0 k} ,$$

which is equal to 1 if  $x_0$  is an integer and equal to  $(-1)^k$  if  $x_0 = 1/2$ . Lemma follows from stated.  $\square$

Lemma allows us to write operators (2.21) for all  $j = 1, \dots, N$  as

$$\psi_j = \sum_{l=1}^N \left[ \psi_l \frac{1}{N} \sum_{x \in X_N} e^{i \frac{2\pi}{N} x (j-l)} \right], \quad (2.36)$$

where we can take for  $x_0$  an integer or  $1/2$ , it's not important. But if we take  $x_0 = 1/2$  in the even sector and  $x_0 = 0$  in the odd sector we can also write the operator  $\psi_{N+1}$ , defined in (2.34), in the form (2.36). That's why we will define the operators

$$\psi_q \equiv \frac{1}{\sqrt{N}} \sum_{l=1}^N \psi_l e^{-i \frac{2\pi}{N} q l} \quad (2.37a)$$

for any  $q \in X_N$  with  $x_0 = 1/2$  in the even sector and  $x_0 = 0$  in the odd sector. From (2.36) we see that

$$\psi_j = \frac{1}{\sqrt{N}} \sum_q \psi_q e^{i \frac{2\pi}{N} q j}. \quad (2.37b)$$

for all  $j = 1, \dots, N$ . Relations (2.37) are some kind of Fourier transform. Notice that

the operators  $\psi_q$  defined in (2.37) are periodic with period  $N$ :

$$\psi_q = \psi_{q+N}. \quad (2.38)$$

That's why we could also treat it as a definition for all  $q \in X_N + \mathbb{Z}$ . In each sector operators  $\psi_q$  are Fermi operators:

$$\{\psi_q, \psi_{q'}\} = 0, \quad (2.39a)$$

$$\{\psi_q, \psi_{q'}^\dagger\} = \delta_{qq'}, \quad (2.39b)$$

for any  $q, q' \in X_N$ . This can be shown using the definition (2.37), linearity of the commutators, Fermi relations (2.22) and Lemma. We can reformulate the Hamiltonians (2.35) in terms of Fermi operators  $\psi_q$ . Using (2.37), Fermi relations (2.39) and Lemma after some algebra we obtain for the particular terms of the Hamiltonians (2.35):

$$\sum_{j=1}^N \psi_j^\dagger \psi_{j+1} = \sum_q \psi_q^\dagger \psi_q e^{i\frac{2\pi}{N}q}, \quad (2.40a)$$

$$\sum_{j=1}^N \psi_j^\dagger \psi_{j+1}^\dagger = \sum_q \psi_q^\dagger \psi_{-q}^\dagger e^{i\frac{2\pi}{N}q} = i \sum_q \sin\left(\frac{2\pi}{N}q\right) \psi_q^\dagger \psi_{-q}^\dagger, \quad (2.40b)$$

$$\sum_{j=1}^N \psi_j^\dagger \psi_j = \sum_q \psi_q^\dagger \psi_q. \quad (2.40c)$$

Now using (2.40) we can reformulate the Hamiltonians:

$$H^\pm = J \sum_q \left[ \cos\left(\frac{2\pi}{N}q\right) - h \right] \left( \psi_q^\dagger \psi_q - \frac{1}{2} \right) + \frac{1}{2} i J \gamma \sum_q \sin\left(\frac{2\pi}{N}q\right) \left( \psi_q^\dagger \psi_{-q}^\dagger - \psi_{-q} \psi_q \right). \quad (2.41)$$

We can get rid of the imaginary coefficients in (2.41) with the redefinition  $\psi_q \rightarrow e^{i\pi/4} \psi_q$ . Relations (2.37) become:

$$\psi_q \equiv \frac{e^{i\pi/4}}{\sqrt{N}} \sum_{l=1}^N \psi_l e^{-i\frac{2\pi}{N}ql}, \quad (2.42a)$$

$$\psi_j = \frac{e^{-i\pi/4}}{\sqrt{N}} \sum_q \psi_q e^{i\frac{2\pi}{N}qj}, \quad (2.42b)$$

with the commutation relations (2.39) unchanged. The Hamiltonians  $H^\pm$  in terms of operators (2.42) are given by

$$H^\pm = J \sum_q \left[ \cos\left(\frac{2\pi}{N}q\right) - h \right] \left( \psi_q^\dagger \psi_q - \frac{1}{2} \right) + \frac{1}{2} J \gamma \sum_q \sin\left(\frac{2\pi}{N}q\right) (\psi_q^\dagger \psi_{-q}^\dagger - \psi_{-q} \psi_q) \quad (2.43)$$

This form is more convenient for diagonalization.

In the case  $\gamma = 0$ , which is the XX model, the second term in (2.43) dies and the Hamiltonians  $H^\pm$  are already in the diagonal form (2.5):

$$H^\pm = J \sum_q \left[ \cos\left(\frac{2\pi}{N}q\right) - h \right] \left( \psi_q^\dagger \psi_q - \frac{1}{2} \right), \quad (2.44a)$$

with the energies

$$\Lambda_q = \cos\left(\frac{2\pi}{N}q\right) - h. \quad (2.44b)$$

Notice that substitution  $J \rightarrow -J$  simply corresponds to the redefinition  $\psi_q \leftrightarrow \psi_q^\dagger$ .

In other cases, when  $\gamma \neq 0$ , we can write the Hamiltonians (2.43) in the simple form using the matrix notation:

$$H^\pm = -\frac{1}{2} J \sum_q \begin{pmatrix} \psi_q^\dagger & \psi_{-q} \end{pmatrix} M_q \begin{pmatrix} \psi_q \\ \psi_{-q}^\dagger \end{pmatrix}, \quad (2.45)$$

where  $M_q$  are  $2 \times 2$  symmetric matrices

$$M_q = \begin{pmatrix} h - \cos\left(\frac{2\pi}{N}q\right) & -\gamma \sin\left(\frac{2\pi}{N}q\right) \\ -\gamma \sin\left(\frac{2\pi}{N}q\right) & -\left[ h - \cos\left(\frac{2\pi}{N}q\right) \right] \end{pmatrix} = \begin{pmatrix} a_q & b_q \\ b_q & -a_q \end{pmatrix}. \quad (2.46)$$

Here we have defined the coefficients

$$\begin{aligned} a_q &\equiv h - \cos\left(\frac{2\pi}{N}q\right), \\ b_q &\equiv -\gamma \sin\left(\frac{2\pi}{N}q\right). \end{aligned}$$

Matrix  $M_q$ , defined in (2.46), is diagonal in the odd sector for  $q = 0$  and for  $q = N/2$  in the even or odd sector depending on the parity of  $N$ . Let's first examine the other cases, when  $q \neq 0$  and  $q \neq N/2$ . These are also the cases when  $\psi_q \neq \psi_{-q}$ . The

matrix  $M_q$  is not diagonal in these cases, but since it is symmetric we can diagonalize it with an orthogonal matrix  $O_q$ :

$$M_q = O_q^T D_q O_q, \quad (2.47)$$

where  $D_q$  is a diagonal matrix. The matrix  $O_q^T$  has the matrix  $M_q$  eigenvectors as its columns. It is convenient to define

$$O_q = \begin{pmatrix} \cos \theta_q & -\sin \theta_q \\ \sin \theta_q & \cos \theta_q \end{pmatrix}. \quad (2.48)$$

Then we can write

$$O_q \begin{pmatrix} \psi_q \\ \psi_{-q}^\dagger \end{pmatrix} = \begin{pmatrix} \cos \theta_q \psi_q - \sin \theta_q \psi_{-q}^\dagger \\ \sin \theta_q \psi_q + \cos \theta_q \psi_{-q}^\dagger \end{pmatrix}. \quad (2.49)$$

We get the explicit form of  $\cos \theta_q$ ,  $\sin \theta_q$  and diagonal matrix  $D_q$  by solving the eigenvalue problem for the  $2 \times 2$  matrix (2.46). The solution is:

$$\cos \theta_q = \frac{b_q}{\sqrt{2} \sqrt{a_q^2 + b_q^2 - a_q \sqrt{a_q^2 + b_q^2}}}, \quad (2.50a)$$

$$\sin \theta_q = \frac{a_q - \sqrt{a_q^2 + b_q^2}}{\sqrt{2} \sqrt{a_q^2 + b_q^2 - a_q \sqrt{a_q^2 + b_q^2}}}, \quad (2.50b)$$

and

$$D_q = \begin{pmatrix} \Lambda_q & 0 \\ 0 & -\Lambda_q \end{pmatrix}, \quad (2.51)$$

where we have defined

$$\Lambda_q \equiv \Lambda\left(\frac{2\pi}{N}q\right) \equiv \sqrt{\left[h - \cos\left(\frac{2\pi}{N}q\right)\right]^2 + \gamma^2 \sin^2\left(\frac{2\pi}{N}q\right)}. \quad (2.52)$$

Using (2.50) we can state the following property of  $\cos \theta_q$  and  $\sin \theta_q$  with respect to the change of sign of  $q$ :

$$\cos \theta_{-q} = -\cos \theta_q, \quad \sin \theta_{-q} = \sin \theta_q. \quad (2.53)$$

Now let's look again at (2.49). We see that if we define the operators

$$\chi_q \equiv \cos \theta_q \psi_q - \sin \theta_q \psi_{-q}^\dagger \quad (2.54)$$

because of property (2.53) we can simply write

$$O_q \begin{pmatrix} \psi_q \\ \psi_{-q}^\dagger \end{pmatrix} = \begin{pmatrix} \chi_q \\ -\chi_{-q}^\dagger \end{pmatrix}. \quad (2.55)$$

It turns out that operators (2.54) are also fermionic, as we will show. Operators (2.54) are periodic with period  $N$  as operators  $\psi_q$  in (2.38) because  $\cos \theta_q$  and  $\sin \theta_q$  defined in (2.50) are periodic:

$$\chi_q = \chi_{q+N}. \quad (2.56)$$

We are examining the case when  $q \neq 0$  and  $q \neq N/2$ . From the fact that in this case we have always  $\psi_q \neq \psi_{-q}$  and from (2.22) follows

$$\{\chi_q, \chi_q\} = 0, \quad \{\chi_q, \chi_q^\dagger\} = 1, \quad \{\chi_q, \chi_{-q}^\dagger\} = 0, \quad (2.57a)$$

and using (2.53)

$$\{\chi_q, \chi_{-q}\} = 0. \quad (2.57b)$$

It is also clear that

$$\{\chi_q, \chi_{q'}\} = \{\chi_q, \chi_{q'}^\dagger\} = 0 \quad \text{for } q' \neq q \text{ and } q' \neq N - q. \quad (2.57c)$$

So we have shown that the set of operators (2.54) for  $q \neq 0$ ,  $q \neq N/2$ , is a set of Fermi operators.

Expressions (2.50) are quite complicated. Trigonometric functions of the angle  $2\theta_q$  have simpler expressions and in many cases this will be the only thing we have to know. From (2.50) follows

$$\tan 2\theta_q = \frac{\gamma \sin\left(\frac{2\pi}{N}q\right)}{h - \cos\left(\frac{2\pi}{N}q\right)} \quad (2.58)$$

and

$$e^{i2\theta_q} = \frac{h - \cos\left(\frac{2\pi}{N}q\right) + i\gamma \sin\left(\frac{2\pi}{N}q\right)}{\sqrt{\left[h - \cos\left(\frac{2\pi}{N}q\right)\right]^2 + \gamma^2 \sin^2\left(\frac{2\pi}{N}q\right)}}. \quad (2.59)$$

We will show that operators (2.54) also satisfy Fermi commutation relations.

For  $q = 0$  and  $q = N/2$  the matrix  $M_q$  is already diagonal. Explicitly

$$M_{q=0} = \begin{pmatrix} h-1 & 0 \\ 0 & -(h-1) \end{pmatrix}, \quad (2.60)$$

and

$$M_{q=N/2} = \begin{pmatrix} h+1 & 0 \\ 0 & -(h+1) \end{pmatrix}. \quad (2.61)$$

Expressions (2.50) are not well defined here but we can define the operators  $\chi_q$  here in such way that (2.59) is satisfied and we take any  $\cos\theta_q$  and  $\sin\theta_q$  in agreement with this. The appropriate definition is

$$\chi_{q=0} \equiv \begin{cases} \psi_{q=0}^\dagger & \text{for } h < 1 \\ \psi_{q=0} & \text{for } h > 1 \end{cases}, \quad (2.62a)$$

$$\chi_{q=N/2} \equiv \psi_{q=N/2}. \quad (2.62b)$$

The case  $q = 0$  for  $h = 1$  has (2.59) not well defined, but here the matrix  $M_{q=0}$  is equal to zero so it doesn't appear in the sum and it's not important.

Now we can state that the set of operators  $\chi_q$  defined in (2.54) and (2.62) is a set of Fermi operators:

$$\{\chi_q, \chi_{q'}\} = 0, \quad (2.63a)$$

$$\{\chi_q, \chi_{q'}^\dagger\} = \delta_{qq'}, \quad (2.63b)$$

and we can reformulate the Hamiltonians (2.45) in terms of them. We find

$$H^\pm = -J \sum_q \Lambda_q \left( \chi_q^\dagger \chi_q - \frac{1}{2} \right), \quad (2.64)$$

where  $\Lambda_q$  is given by (2.52). Expression (2.64) is also valid for  $\gamma = 0$  with the



definition in accordance with (2.59) and (2.54):

$$\chi_q \equiv \begin{cases} \psi_q^\dagger & \text{for } h < \cos\left(\frac{2\pi}{N}q\right), \gamma = 0 \\ \psi_q & \text{for } h > \cos\left(\frac{2\pi}{N}q\right), \gamma = 0 \end{cases} . \quad (2.65)$$

The Hamiltonians (2.33) are brought to a diagonal form, from which in the next subsection we will find the spectrum and the eigenstates of the full Hamiltonian (2.32).

## 2.5 Ground state

Now we will examine the ground state of the XY chain, the ground state energy and all the excitations. This subsection is also based on [2]. We will examine the ferromagnetic case  $J < 0$ . Both  $H^+$  and  $H^-$  in (2.64) have  $2^N$  eigenstates. However because of parity requirements only half of the  $H^+$  and half of the  $H^-$  eigenstates will be also the eigenstates of the full Hamiltonian (2.32).

First we will examine the even sector. For the sake of clarity let us suppose that  $\gamma \neq 0$ . The ground state  $|GS^+\rangle$  of the even sector Hamiltonian,  $H^+$  in (2.64), is it's vacuum state:

$$\chi_q |GS^+\rangle = 0 \quad \text{for any } q \in \left\{ \frac{1}{2}, \frac{1}{2} + 1, \dots, \frac{1}{2} + N - 1 \right\} , \quad (2.66)$$

and the ground state energy is

$$E_0^+ = -\frac{1}{2} \sum_{q=0}^{N-1} \Lambda_{q+1/2} . \quad (2.67)$$

However, if this is going to be an eigenstate of the full Hamiltonian (2.32) it must have an even parity. Now we will find the explicit expression for the ground state and see that it has the right parity. Let us recall the vacuum state (2.25) and notice using the definition of operators (2.42) that

$$\psi_q |0\rangle = 0 \quad \text{for any } q . \quad (2.68)$$

To find the ground state we have to notice that the definition (2.54) of operators

$\psi_q$  and commutation relations (2.39) give us

$$\chi_q (\cos \theta_q + \sin \theta_q \psi_q^\dagger \psi_{-q}^\dagger) |0\rangle = 0, \quad (2.69a)$$

from which, using (2.53), also follows

$$\chi_{-q} (\cos \theta_q + \sin \theta_q \psi_q^\dagger \psi_{-q}^\dagger) |0\rangle = 0. \quad (2.69b)$$

Now using (2.69) one can check that correct, normalized, ground state of the even sector Hamiltonian  $H^+$  is:

$$|GS^+\rangle = \prod_{q=0}^{\lfloor \frac{N}{2} \rfloor - 1} (\cos \theta_{q+1/2} + \sin \theta_{q+1/2} \psi_{q+1/2}^\dagger \psi_{-(q+1/2)}^\dagger) |0\rangle. \quad (2.70)$$

In (2.70) the operators  $\psi_q$  are applied in pairs and from (2.42) we can see that this means that operators  $\psi_j$  are also applied in pairs. That's why the state (2.70) has even parity (2.70) and is also an eigenstate of the full Hamiltonian (2.32).

Now we will examine the odd sector. Analogous to the even sector the ground state of the odd sector Hamiltonian  $H^-$  is its vacuum state  $|GS^*\rangle$  :

$$\chi_q |GS^*\rangle = 0 \quad \text{for any } q \in \{0, 1, \dots, N-1\}. \quad (2.71)$$

Because of the definition (2.62) we have to treat separately case  $h < 1$  and case  $h > 1$ . Case  $h > 1$  is analogous to the even sector with the (2.69) unchanged. That's why the ground state of the odd sector Hamiltonian  $H^-$  for  $h > 1$  is

$$|GS^*, h > 1\rangle = \prod_{q=1}^{\lfloor \frac{N-1}{2} \rfloor} (\cos \theta_q + \sin \theta_q \psi_q^\dagger \psi_{-q}^\dagger) |0\rangle. \quad (2.72)$$

However, this state has even parity so the operator  $1 - P$  in (2.32) would rule it out and therefore it is not an eigenstate of the full Hamiltonian (2.32). The eigenstate of the full Hamiltonian should have an excitation. For  $h > 1$  the excitation with the lowest energy is  $q = 0$  because it minimizes the expression (2.52). That's why the odd sector and the full Hamiltonian common eigenstate with the lowest energy is

$$|GS^-, h > 1\rangle = \chi_{q=0}^\dagger |GS^*, h > 1\rangle, \quad (2.73)$$

or written differently

$$|GS^-, h > 1\rangle = \psi_{q=0}^\dagger \prod_{q=1}^{\lfloor \frac{N-1}{2} \rfloor} (\cos \theta_q + \sin \theta_q \psi_q^\dagger \psi_{-q}^\dagger) |0\rangle. \quad (2.74)$$

In the case  $h < 1$  the state defined in (2.71) has the form

$$|GS^*, h < 1\rangle = \psi_{q=0}^\dagger \prod_{q=1}^{\lfloor \frac{N-1}{2} \rfloor} (\cos \theta_q + \sin \theta_q \psi_q^\dagger \psi_{-q}^\dagger) |0\rangle. \quad (2.75)$$

This state has the right parity so it is also the eigenstate of the full Hamiltonian

$$|GS^-, h < 1\rangle = |GS^*, h < 1\rangle. \quad (2.76)$$

We can conclude that the common odd sector and full Hamiltonian eigenstate with the lowest energy for any magnetic field  $h$  is

$$|GS^-\rangle = \psi_{q=0}^\dagger \prod_{q=1}^{\lfloor \frac{N-1}{2} \rfloor} (\cos \theta_q + \sin \theta_q \psi_q^\dagger \psi_{-q}^\dagger) |0\rangle. \quad (2.77)$$

with the energy

$$E_0^- = \begin{cases} -\frac{1}{2} \sum_{q=0}^{N-1} \Lambda_q & \text{for } h \leq 1 \\ -\frac{1}{2} \sum_{q=0}^{N-1} \Lambda_q + \frac{1}{2}(h-1) & \text{for } h \geq 1 \end{cases} \quad (2.78)$$

We have found the lowest energy eigenstates of the full Hamiltonian with the even and with the odd parity. It can be shown using similar arguments that expressions (2.67) and (2.78) are also valid in the case  $\gamma = 0$ . The excited states are found by applying the raising operators  $\chi_q^\dagger$  in pairs on the states (2.70) and (2.77).

The state (2.70) is the eigenstate of the XY chain Hamiltonian with the lowest energy and with even parity. The state (2.77) is the eigenstate with the lowest energy and odd parity. These states are uniquely determined for a given Hamiltonian parameters  $\gamma$  and  $h$ . However, the energies of two sectors (2.67) and (2.78) might be equal and we might have a degenerate ground state of the full Hamiltonian (2.32). Which one of the ground state energies of the two sectors is bigger and what is the ground state of the full Hamiltonian is a simple question. However, it is non-trivial

to answer and is the topic of Section 3.

## 2.6 Critical properties

Classical phase transition is a change of the physical properties of the system at some critical temperature  $T_c$  [17]. Classical phase transitions are characterized by an order parameter, a quantity that has a vanishing thermal average in one phase, for  $T < T_c$  and a non-zero average in other, for  $T > T_c$ . A measure of order in a system are correlation functions. For example, if the order parameter is magnetization  $\vec{M} = \sum_i \vec{S}_i$  the correlation function  $G$  measures the correlations between spins:

$$G(r) = \langle \vec{S}_i \cdot \vec{S}_j \rangle - \langle \vec{S}_i \rangle \cdot \langle \vec{S}_j \rangle, \quad r = |\vec{r}_i - \vec{r}_j|.$$

Classical phase transitions are further characterized by the correlation length  $\xi$ . It is a characteristic length-scale in the system and describes the asymptotic behavior of the correlation function [17]:

$$G(r) \sim e^{-r/\xi} \quad \text{for } T \neq T_c. \quad (2.79)$$

A class of classical phase transitions, called the phase transitions of *second order* are characterized by a diverging correlation length at the critical point:

$$\xi \rightarrow \infty \quad \text{for } T \rightarrow T_c. \quad (2.80)$$

A characterization of phase transitions using the correlation length can be carried directly to quantum phase transitions. Quantum phase transitions (QPTs) of *second order* are also characterized by a diverging correlation length. The difference from classical phase transitions is that QPTs happen at zero temperature, i. e. when the system is in its ground state, and we change some Hamiltonian parameter instead of temperature, let's denote it by  $\lambda$ . All experiments are necessarily at some non-zero temperatures, though possibly very small, and it is a central task of the theory of QPTs to describe the consequences of a QPT at  $T = 0$  on the physical properties for  $T > 0$  [18]. A theory of QPTs [18] gives also a characterization by a vanishing energy gap. The energy gap can be defined as a difference between the first excited state

and the ground state energy. Explicitly, when the correlation length diverges as

$$\xi \sim \frac{1}{|\lambda - \lambda_c|^\nu} \quad (2.81)$$

the energy gap  $\Delta$  vanishes as

$$\Delta \sim |\lambda - \lambda_c|^{z\nu}. \quad (2.82)$$

Here  $\nu > 0$  and  $z > 0$  are critical indices.

We have reviewed the basic characterizations of QPTs. Now we will find QPTs for the XY chain, based on [36] [14], and justify Figure 1.2. From (2.64) we see that the energy of some excited state

$$\chi_q^\dagger \chi_{q'}^\dagger |GS\rangle$$

is

$$E_0 + \frac{1}{2}(\Lambda_q + \Lambda_{q'}). \quad (2.83)$$

The state has to be excited in pairs because of parity requirements. In the limit of a large system we don't have to worry about the pair excitations and instead of the energy gap we can examine the continuous spectrum [18]

$$\Lambda(x) = \sqrt{(h - \cos x)^2 + \gamma^2 \sin^2 x}. \quad (2.84)$$

The spectrum vanishes in two cases:

$$x = 0, h = 1 \quad \text{and} \quad x = \arccos h, \gamma = 0.$$

For  $x = 0$  the spectrum is equal to

$$\Lambda(0) = \sqrt{|h - 1|} \quad (2.85)$$

If we compare it with (2.82) we can recognize a QPT with the relation between the the critical indices  $z\nu = 1/2$ . For  $x = \arccos h$  the spectrum is equal to

$$\Lambda(\arccos h) = \sin(\arccos h)\gamma \sim |\gamma - 0|. \quad (2.86)$$

and we recognize a QPT with the relation between the critical indices  $z\nu = 1$ . So we have shown that the XY chain has two critical lines,  $\gamma = 0$ ,  $h < 1$  and  $h = 1$ , and justified Figure 1.2.

Two critical lines meet at a bi-critical point  $(\gamma, h) = (0, 1)$ . To show that the bi-critical point is non-conformal we expand the spectrum for small  $x$  at this point

$$\Lambda(x) = \sqrt{\left(1 - 1 + \frac{x^2}{2} \dots\right)^2 + 0} . \quad (2.87)$$

We see that a leading term is quadratic in  $x$

$$\Lambda(x) = \frac{1}{\sqrt{2}}x^2 + \dots , \quad (2.88)$$

while it can be a constant or a linear term in general. Statistical field theory [17] tells us that a point with such quadratic dependence is non-conformal.

There are also points in the phase diagram where the energy difference between two (nearly) degenerate ground states exactly vanish. These are the points where the lowest energies of two sectors,  $E_0^-$  and  $E_0^+$ , are equal. Although this is not the gap appearing in the theory of phase transitions, the properties of the system here are interesting. Moreover, while for finite systems the gap at phase transitions closes polynomially with the system size, the energy difference between the nearly degenerate states closes exponentially [33].

## 2.7 Correlation functions

One of the main topics of the Lieb, Shultz and Mattis article [3] is the long-range order in the XY model. As a measure of the long-range order they introduced the spin-spin correlation functions

$$\rho_{lm}^\mu = \langle \sigma_l^\mu \sigma_m^\mu \rangle = \langle GS^+ | \sigma_l^\mu \sigma_m^\mu | GS^+ \rangle \quad \mu = x, y, z . \quad (2.89)$$

We will examine these correlators in the state  $|GS^+\rangle$  given by (2.70) in the limit of a large chain, based on [2] and [3]. In this limit, as will be discussed in Section 3, for  $h > 1$  the ground state is  $|GS^+\rangle$  while for  $h \leq 1$  can also be some linear combination

with  $|GS^-\rangle$  in general. We don't examine the correlation functions

$$\langle \sigma_l^\mu \sigma_m^\mu \rangle - \langle \sigma_m^\mu \rangle \langle \sigma_l^\mu \rangle , \quad (2.90)$$

because nobody has devised a method to perform a calculation of expectational values  $\langle \sigma_m^\mu \rangle$  directly [2]. Actually, the correlation functions (2.89) are used to conclude something about the expectational values  $\langle \sigma_m^\mu \rangle$ .

The first step in calculating the correlators (2.89) is calculating the correlators  $\langle \psi_j \psi_l \rangle$  and  $\langle \psi_l^\dagger \psi_l \rangle$ . From (2.54) we have:

$$\psi_q = \cos \theta_q \chi_q - \sin \theta_q \chi_{-q}^\dagger . \quad (2.91)$$

Using (2.91) and (2.66) we obtain:

$$\langle \psi_q^\dagger \psi_{q'} \rangle = \frac{1 - \cos 2\theta_q}{2} \delta_{qq'} , \quad (2.92a)$$

$$\langle \psi_q^\dagger \psi_{q'} \rangle = -\frac{1}{2} \sin 2\theta_q \delta_{q, -q'+N} . \quad (2.92b)$$

from which using (2.42) follow the desired correlators

$$\langle \psi_j^\dagger \psi_l \rangle = \frac{1}{N} \sum_q \frac{1 - \cos 2\theta_q}{2} e^{-i\frac{2\pi}{N}q(j-l)} , \quad (2.93a)$$

$$\langle \psi_j \psi_l \rangle = \frac{i}{N} \sum_q \frac{\sin 2\theta_q}{2} e^{i\frac{2\pi}{N}q(j-l)} . \quad (2.93b)$$

These correlators are real and using fermionic relations we obtain simply

$$\langle \psi_j \psi_l^\dagger \rangle = \delta_{jl} - \langle \psi_j^\dagger \psi_l \rangle , \quad \langle \psi_j^\dagger \psi_l^\dagger \rangle = -\langle \psi_j \psi_l \rangle . \quad (2.94)$$

In the limit of a large chain, i.e. large  $N$ , correlators become

$$\langle \psi_j^\dagger \psi_l \rangle = \frac{1}{2} \delta_{jl} - \frac{1}{2\pi} \int_0^{2\pi} \frac{\cos 2\theta \frac{N}{2\pi} x}{2} e^{-ix(j-l)} dx \quad (2.95a)$$

$$= \frac{1}{2} \delta_{jl} - \frac{1}{2\pi} \frac{1}{2} \int_0^{2\pi} \frac{h - \cos x}{|h - \cos x + i\gamma \sin x|} e^{-ix(j-l)} dx, \quad (2.95b)$$

$$\langle \psi_j \psi_l \rangle = \frac{i}{2\pi} \int_0^{2\pi} \frac{\sin 2\theta \frac{N}{2\pi} x}{2} e^{ix(j-l)} dx \quad (2.95c)$$

$$= \frac{i}{2\pi} \frac{1}{2} \int_0^{2\pi} \frac{\gamma \sin x}{|h - \cos x + i\gamma \sin x|} e^{ix(j-l)} dx, \quad (2.95d)$$

where we have used (2.59) to obtain the second equalities. If the integrand has a singularity

$$h - \cos x_0 + i\gamma \sin x_0 = 0$$

we have to think of these as improper integrals

$$\int_0^{x_0} + \int_{x_0}^{2\pi}. \quad (2.96)$$

Now we can proceed in calculating (2.89). Pauli spin operators can be expressed through operators (2.21) as in (2.26) from which we have:

$$\begin{aligned} \rho_{lm}^x &= \langle (\sigma_l^+ + \sigma_l^-) (\sigma_m^+ + \sigma_m^-) \rangle \\ &= \langle (\psi_l + \psi_l^\dagger) \prod_{j=l}^{m-1} (1 - 2\psi_j^\dagger \psi_j) (\psi_m + \psi_m^\dagger) \rangle \end{aligned} \quad (2.97)$$

After noticing

$$\sigma_j^z = 1 - 2\psi_j^\dagger \psi_j = (\psi_j^\dagger + \psi_j) (\psi_j^\dagger - \psi_j) \quad (2.98)$$

we can obtain

$$\rho_{lm}^x = \langle B_l A_{l+1} B_{l+1} \dots A_{m-1} B_{m-1} A_m \rangle, \quad (2.99)$$

where we have defined

$$A_j \equiv \psi_j^\dagger + \psi_j, \quad B_j \equiv \psi_j^\dagger - \psi_j. \quad (2.100)$$



Similarly we obtain

$$\begin{aligned}\rho_{lm}^y &= (-1)^{m-l} \langle A_l B_{l+1} A_{l+1} \dots B_{m-1} A_{m-1} B_m \rangle \\ &= \langle B_{l+1} A_l B_{l+2} A_{l+1} \dots B_m A_{m-1} \rangle ,\end{aligned}\tag{2.101}$$

and

$$\rho_{lm}^z = \langle A_l B_l A_m B_m \rangle .\tag{2.102}$$

These expectation values can be expanded in terms of two-point correlation functions using Wick's theorem [15] from quantum field theory. Wick's theorem, or more precisely its consequence, says:

**Theorem** (Wick's theorem for fermions). *Let  $W_i$  be some linear combination of fermionic operators  $c_i$  and  $c_i^\dagger$ :*

$$W_i = \sum_{j=1}^n (u_{ij} c_j + v_{ij} c_j^\dagger)$$

and let  $|0\rangle$  be the vacuum state:

$$c_i |0\rangle = 0 \quad i = 1, \dots, n .$$

The expectation value of the product  $W_1 W_2 \dots W_n$  in the vacuum state  $|0\rangle$  is given as a sum over all distinct contractions of pairs multiplied with the permutation sign:

$$\langle 0 | W_1 W_2 \dots W_n | 0 \rangle = \sum_{\substack{i_1 < j_1, i_2 < j_2, \dots, i_n < j_n \\ i_1 < i_2 < \dots < i_n}} (-1)^p \langle 0 | W_{i_1} W_{j_1} | 0 \rangle \langle 0 | W_{i_2} W_{j_2} | 0 \rangle \dots \langle 0 | W_{i_n} W_{j_n} | 0 \rangle ,$$

where  $(-1)^p$  is the sign of the permutation in going over from the sequence

$$1, 2, \dots, n$$

into

$$i_1, j_1, i_2, j_2, \dots, i_n, j_n .$$

Here we have assumed that  $n$  is even. Otherwise the expectation value is zero.

Operators  $A_i$  and  $B_i$  can be expressed as a linear combination of the fermionic operators  $\chi_q$  for which the ground state  $|GS+\rangle$  is a vacuum state. That's why we can

use Wick's theorem. The most straightforward pairing contribution to  $\rho_{lm}^x$  is

$$\langle B_l A_{l+1} \rangle \langle B_{l+1} A_{l+2} \rangle \dots \langle B_{m-1} A_m \rangle .$$

All other pairings can be obtained by permuting  $A$ 's among themselves while leaving  $B$ 's fixed. The sign  $(-1)^p$  associated with a given permutation is the sign of the permutation of  $A$ 's. We can write

$$\rho_{lm}^x = \sum_P (-1)^p \langle B_l A_{P(l+1)} \rangle \langle B_{l+1} A_{P(l+2)} \rangle \dots \langle B_{m-1} A_{P(m)} \rangle . \quad (2.103)$$

Using (2.95) and (2.94) we obtain:

$$\langle B_j A_l \rangle = g(j-l) , \quad \langle A_j A_l \rangle = \delta_{ij} , \quad \langle B_j B_l \rangle = -\delta_{ij} , \quad (2.104)$$

where we have defined a function  $g : \mathbb{Z} \rightarrow \mathbb{R}$  with

$$g(l) = -\frac{1}{2\pi} \int_0^{2\pi} \frac{h - \cos x + i\gamma \sin x}{|h - \cos x + i\gamma \sin x|} e^{-ilx} dx . \quad (2.105)$$

Now (2.103) can be expressed as determinant

$$\rho_{lm}^x = \begin{vmatrix} g(-1) & g(-2) & g(-3) & \dots & g(-n) \\ g(0) & g(-1) & g(-2) & \dots & g(-n+1) \\ g(1) & g(0) & g(-1) & \dots & g(-n+2) \\ \vdots & \vdots & \vdots & \ddots & \vdots \\ g(n-2) & g(n-3) & g(n-4) & \dots & g(-1) \end{vmatrix} , \quad (2.106)$$

where  $n = m - l$ . Similar expression can be obtained for  $\rho_{lm}^y$ . For  $\rho_{lm}^z$  it is simpler

$$\rho_{lm}^z = \langle A_l B_l \rangle \langle A_m B_m \rangle - \langle A_m B_l \rangle \langle A_l B_m \rangle = \begin{vmatrix} g(0) & g(n) \\ g(-n) & g(0) \end{vmatrix} . \quad (2.107)$$

Matrices obtained have a special structure. Each of their descending diagonals from left to right is constant. Such matrices are called *Toeplitz matrices* and using their properties the correlation functions are calculated in [16]. We'll simply quote from [2] some results important to our thesis. The results are obtained in the limit

of a large chain. A convenient order parameter is the magnetization along the  $x$ -direction  $\langle \sigma_j^x \rangle$ . As we already said, nobody has found the method to calculate it directly but it can be found from the correlation functions (2.89). It has been found that for  $h > 1$  there is no net magnetization along the  $x$ -direction, while for  $h < 1$  there is a net magnetization. Therefore we may call the phase  $h > 1$  disordered and the phase  $h < 1$  ferromagnetic. The correlation length, which diverges at the critical line  $h = 1$ , is given by

$$\xi = \frac{a}{\left| \ln \left( \frac{h + \sqrt{\gamma^2 + h^2 - 1}}{1 + \gamma} \right) \right|}, \quad (2.108)$$

where  $a$  is the lattice spacing.

### 3 Ground state degeneracy in the XY chain

#### 3.1 Introduction

We have shown that the lowest energy of the  $XY$  chain states with the even parity is

$$E_0^+ = -\frac{1}{2} \sum_{q=0}^{N-1} \Lambda_{q+1/2}. \quad (3.1a)$$

and the lowest energy of states with the odd parity is

$$E_0^- = \begin{cases} -\frac{1}{2} \sum_{q=0}^{N-1} \Lambda_q & \text{for } h \leq 1 \\ -\frac{1}{2} \sum_{q=0}^{N-1} \Lambda_q + \frac{1}{2}(h-1) & \text{for } h \geq 1 \end{cases} \quad (3.1b)$$

In this section we examine which of these energies is the ground state energy and where in the  $(\gamma, h)$  diagram are they equal. The question can be answered numerically with ease for a particular choice of parameters  $(\gamma, h)$ . However, we want to find the general answer. The answer to this question tells us where is the ground state degenerate. We use the term degeneracy in the quantum mechanics textbooks sense. A ground state is degenerate if two or more different states correspond to the lowest energy. Consequently, the answer also tells us where do we have the breaking of the  $Z_2$  symmetry. Namely, the Hamiltonian commutes with the parity operator (2.28) so we have the symmetry

$$PHP = H \quad (3.2)$$

and there exists a basis of common eigenstates of  $H$  and  $P$ . If the ground state is degenerate then we can form linear combinations of two ground states. A linear combination will be the Hamiltonian eigenstate but, in general, not the eigenstate of the parity operator  $P$ , we say that the  $Z_2$  symmetry is broken.

Since the energies  $E_0^-$  and  $E_0^+$ , given by (3.1), are continuous functions of parameters  $(\gamma, h)$  we expect that the points where they are equal form lines in the  $(\gamma, h)$  diagram. In general, these points might also form planes or be isolated. We'll combine the numerical methods with the analytical to try to find an answer. As will be discussed, the question has been answered for the quantum Ising model using com-

plex analysis and Fourier series. Some results already exist for the more general  $XY$  model. We'll review the known results and try to use the method which has given an answer for the quantum Ising model. However, this method will give us results only in some special cases for the  $XY$  chain.

### 3.2 Known results

Immediately from (3.1) we can find the limit of a big system  $N \gg 2$ . It reads:

$$E_0^+ = -\frac{N}{2} \int_0^{2\pi} \Lambda(x) \frac{dx}{2\pi}, \quad (3.3a)$$

$$E_0^- = \begin{cases} E_0^+ & \text{for } h \leq 1 \\ E_0^+ + \frac{1}{2}(h-1) & \text{for } h \geq 1 \end{cases} \quad (3.3b)$$

In the limit of a big system the ground state of the  $XY$  Hamiltonian is always degenerate for  $h \leq 1$ . For  $h > 1$  we have always  $E_0^- > E_0^+$  so in this case the ground state is always the one with the even parity. Since the ground state is everywhere degenerate for  $h \leq 1$  and nowhere for  $h > 1$  in the limit of a big system, the phase transition at  $h = 1$  breaks the  $Z_2$  symmetry of the model.

It has been shown in [28] that the ground state is degenerate for any system size  $N$  on the circle

$$\gamma^2 + h^2 = 1 \quad (3.4)$$

and for odd  $N$  on the line

$$h = 0. \quad (3.5)$$

They have also plotted the difference  $E_0^- - E_0^+$  for different  $N$  and  $h$  where oscillations around zero can be observed.

The equality of the energies  $E_0^-$  and  $E_0^+$  on the line (3.4) can be seen by writing (2.52) in the form

$$\Lambda_x^2 = (1 - \gamma^2) \cos^2 x - 2h \cos x + \gamma^2 + h^2. \quad (3.6)$$

On the line (3.4) it is a square and we have

$$\Lambda_x = 1 - h \cos x , \quad (3.7)$$

from which follows

$$E_0^+ = E_0^- = -\frac{N}{2} \quad (3.8)$$

since the cosines sum up to zero.

On the line  $h = 0$  using (3.6) we find

$$\Lambda_x = \sqrt{(1 - \gamma^2) \cos^2 x + \gamma^2} \quad (3.9)$$

which means that  $\Lambda(x)$  depends only on the square of the cosine. One can check that for odd  $N$  for any  $q \in \{0, 1, \dots, N - 1\}$  there exists  $q' \in \{1/2, 1/2 + 1, \dots, 1/2 + N - 1\}$  such that

$$\frac{2\pi}{N}q = \frac{2\pi}{N}q' + k\pi , \quad (3.10)$$

where  $k = 1$  or  $k = -1$ . This gives

$$\cos\left(\frac{2\pi}{N}q\right) = -\cos\left(\frac{2\pi}{N}q'\right) , \quad (3.11)$$

and from (3.9)

$$E_0^+ = E_0^- . \quad (3.12)$$

For even  $N$  this is not the case.

It has been shown in [29] that in the Ising model, which is a special case of the  $XY$  model for  $\gamma = 1$ , we have

$$E_0^+ > E_0^- \quad \text{for } h > 0$$

and  $E_0^+ = E_0^-$  for  $h = 0$ . The latter is in agreement with what we already know because it is on the line (3.4). We're going to review their method later because we will use it for the more general  $XY$  chain.

It is also good to note that the equation  $E_0^- = E_0^+$  can be easily solved for the system sizes  $N = 2$  and  $N = 3$ . For  $N = 2$  the solution is the circle (3.4), while for  $N = 3$  there is an additional line  $h = 0$ . From this we can conclude that the only line

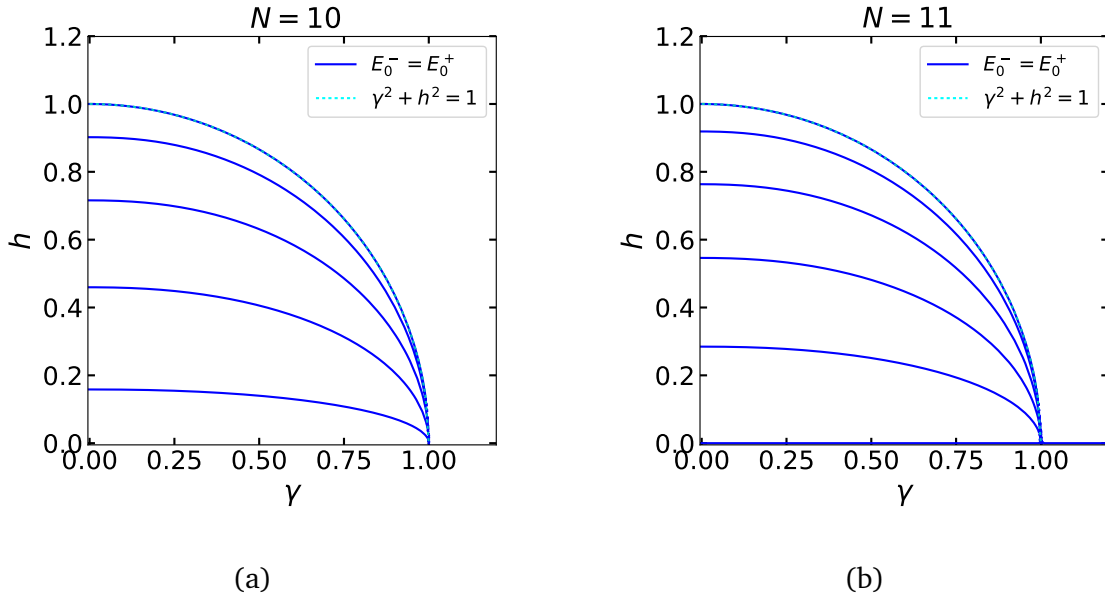


Figure 3.1: Lines where the energies  $E_0^-$  and  $E_0^+$  are equal for the system size (a)  $N = 10$  and (b)  $N = 11$ . The cyan dotted line represents the circle  $\gamma^2 + h^2 = 1$ .

of equality  $E_0^- = E_0^+$  common to all system sizes  $N$  is the circle (3.4) and the only additional line common to all odd system sizes  $N$  is the line  $h = 0$ .

### 3.3 Numerical results

First we'll show our numerical results, obtained in *Python* using the libraries *NumPy* [20] for arithmetic and *matplotlib* [22] for plotting. Numerical results were sometimes an inspiration for our analytical calculations and sometimes a check.

We have found the points in the  $(\gamma, h)$  diagram where the energies  $E_0^-$  and  $E_0^+$  are equal by plotting the difference  $E_0^- - E_0^+$  and indicating in the plot only those lines where the difference is zero. The results are shown for the system size  $N = 10$  and  $N = 11$  in Figure 3.1. The plots of this type are in agreement with the equality  $E_0^- = E_0^+$  on the lines  $\gamma^2 + h^2 = 1$  and  $h = 0$  for odd  $N$ . But they also suggest that there is no such equality outside the circle  $\gamma^2 + h^2 = 1$ , except for  $h = 0$ . In addition, they suggest that inside this circle there are precisely  $\lceil N/2 \rceil$  equality lines and that these lines are ellipses in the limit of big  $N$ . We see the latter when we try to fit the ellipse to the plot. Plots of the type as in Figure 3.1 inspired us to do analytical calculations.

To further examine the relationship between the lowest energies of two sectors we have made plots which show the dependence of the difference  $E_0^- - E_0^+$  on a particular parameter of the Hamiltonian,  $\gamma$ ,  $h$  or  $N$ . In Figure 3.2 the dependence of

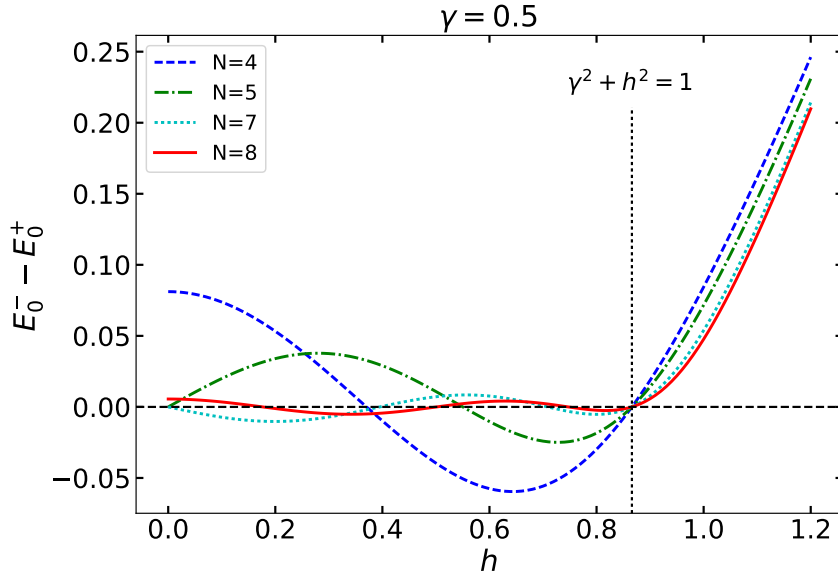


Figure 3.2: The dependence of the difference  $E_0^- - E_0^+$  on the magnetic field  $h$ , for system sizes  $N = 4, 5, 7, 8$ . The anisotropy parameter is  $\gamma = 0.5$ . The value of  $h$  for which  $\gamma^2 + h^2 = 1$  is indicated by black dashed line.

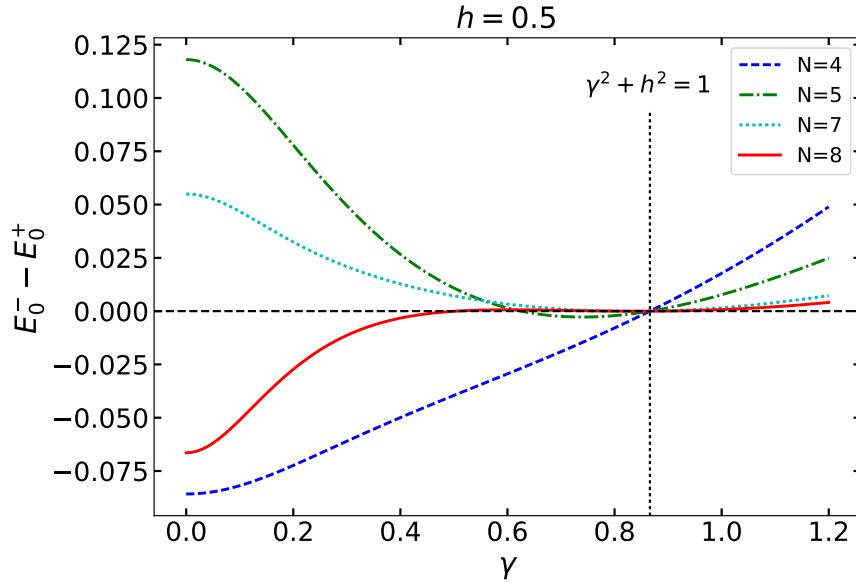


Figure 3.3: The dependence of the difference  $E_0^- - E_0^+$  on the anisotropy  $\gamma$ , for system sizes  $N = 4, 5, 7, 8$ . The magnetic field is  $h = 0.5$ . The value of  $\gamma$  for which  $\gamma^2 + h^2 = 1$  is indicated by black dashed line.

the difference  $E_0^- - E_0^+$  on the magnetic field  $h$  is shown, for different system sizes  $N$ . The anisotropy is  $\gamma = 0.5$ . The oscillations of the difference around zero are visible. The oscillations stop when we reach the circle  $\gamma^2 + h^2 = 1$ . The difference decreases and the number of nodes increases as we increase the system size.

The dependence of the difference  $E_0^- - E_0^+$  on the anisotropy  $\gamma$  is shown in Figure



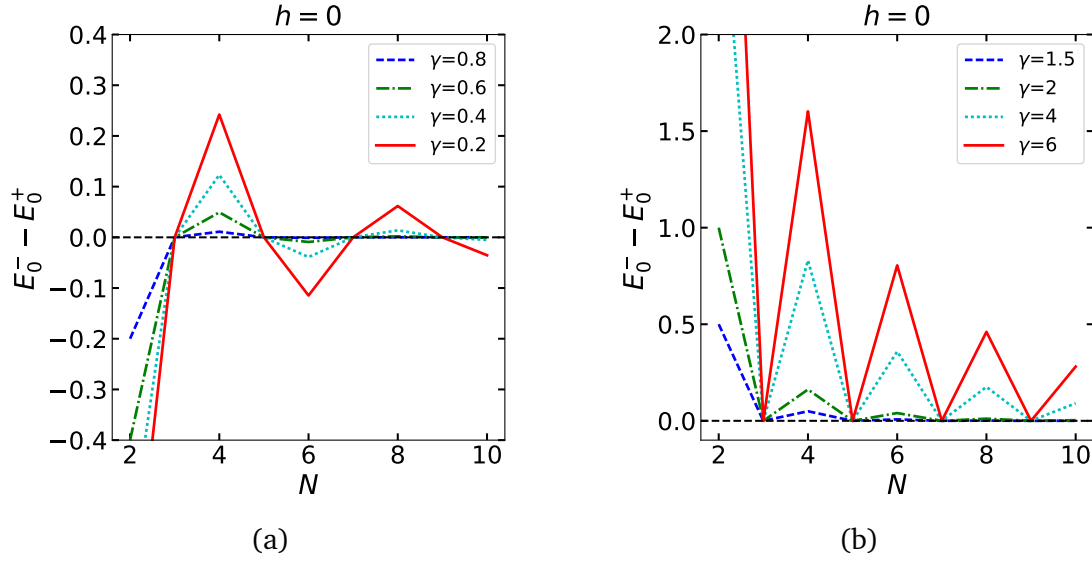


Figure 3.4: The dependence of the difference  $E_0^- - E_0^+$  on the system size  $N$ , for anisotropy (a)  $\gamma = 0.8, 0.6, 0.4, 0.2$  and (b)  $\gamma = 1.5, 2, 4, 6$ . The magnetic field is  $h = 0$ .

3.3, for system sizes  $N = 4, 5, 7, 8$  and the magnetic field  $h = 0.5$ . Again we see the oscillations which stop at the circle  $\gamma^2 + h^2 = 1$ . The difference decreases and the number of nodes increases as we increase the system size  $N$ .

We also show, in Figure 3.4, the dependence of the difference  $E_0^- - E_0^+$  on the system size  $N$ , for the magnetic field  $h = 0$ , to confirm our analytical results later. It is visible in Figure 3.4 that for  $\gamma < 1$  we have oscillations around zero, while for  $\gamma > 1$  the difference is always greater or equal to zero.

### 3.4 Analytical results

We apply the method of [29] used for the Ising chain to the more general XY chain. The first step in the method is to notice that the function (2.52) is periodic with period  $2\pi$  and an even function:

$$\Lambda(x) = \Lambda(x + 2\pi), \quad \Lambda(x) = \Lambda(-x). \quad (3.13)$$

Therefore we could write it as a Fourier series

$$\Lambda(x) = \frac{a_0}{2} + \sum_{n=1}^{\infty} a_n \cos(nx), \quad (3.14)$$

where

$$\begin{aligned}
a_n &= \frac{1}{\pi} \int_0^{2\pi} \Lambda(x) \cos(nx) \, dx \\
&= \frac{1}{\pi} \int_0^{2\pi} \cos(nx) \sqrt{(h - \cos x)^2 + \gamma^2 \sin^2 x} \, dx
\end{aligned} \tag{3.15}$$

Now, we can write the sum in (3.1) as

$$\sum_q \Lambda\left(\frac{2\pi}{N}q\right) = \frac{N}{2}a_0 + \sum_{n=1}^{\infty} a_n \sum_q \cos\left(n\frac{2\pi}{N}q\right). \tag{3.16a}$$

The sum of cosines is equal to

$$\sum_q \cos\left(n\frac{2\pi}{N}q\right) = \frac{1}{2} \sum_q e^{in\frac{2\pi}{N}q} + \frac{1}{2} \sum_q e^{-in\frac{2\pi}{N}q}, \tag{3.17}$$

which can be evaluated using the Lemma from subsection 2.4 . We obtain

$$\begin{aligned}
E_0^- - E_0^+ &= \theta(h - 1)(h - 1) - N \sum_{k=0}^{\infty} a_{(2k+1)N} \\
&= \theta(h - 1)(h - 1) - N(a_N + a_{3N} + a_{5N} + \dots),
\end{aligned} \tag{3.18}$$

where  $\theta$  is the step function to include also the case  $h > 1$  and  $N$  is, as before, the system size. The question of whether  $E_0^- > E_0^+$  now becomes a question of whether the coefficients  $a_N, a_{3N} \dots$  are negative. The coefficients  $a_n$  in (3.18) are all of the same parity. Since  $N \geq 2$  we will always assume in our analysis that we talk about the coefficients for  $n \geq 2$ .

We will further examine the coefficients (3.15) using complex analysis, as in [29]. We use the substitution

$$z = e^{ix}, \tag{3.19}$$

and the definition of a complex square root:

$$\sqrt{re^{i\phi}} = \begin{cases} \sqrt{r}e^{i\frac{\phi}{2}} & , 0 \leq \phi < \pi \\ -\sqrt{r}e^{i\frac{\phi}{2}} & , \pi \leq \phi < 2\pi \end{cases} \tag{3.20}$$

The complex square root defined in such way reduces to a real square root on the positive real axis. It has a branch cut on the negative real axis. If we approach

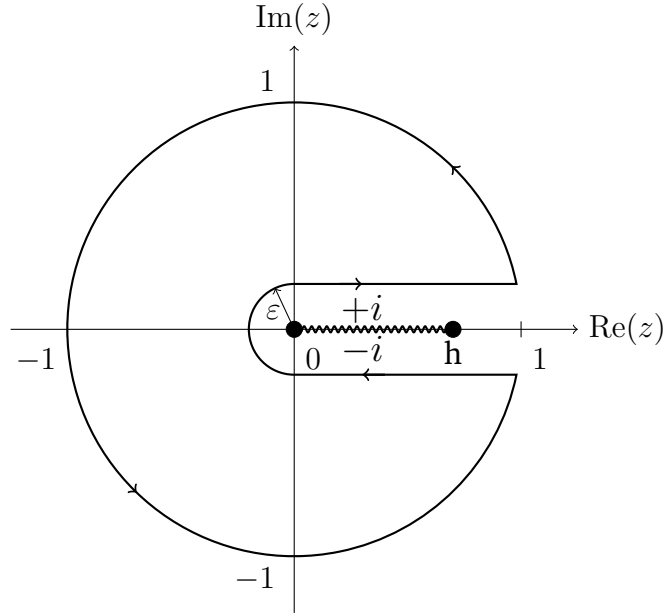


Figure 3.5: The integration countour in the case  $\gamma = 1$ ,  $h < 1$ . The symbols  $\pm i$  indicate that the square root of some function  $\sqrt{f(z = x + iy)}$  reduces to  $\pm i\sqrt{|f(x)|}$  on the real axis where  $f(x) < 0$  as we let  $\epsilon \rightarrow 0$ .

the negative real axis, described by  $y = 0$ ,  $x < 0$ , from above the square root of  $z = x + iy$  becomes  $i\sqrt{|x|}$ , while if we approach it from below it becomes  $-i\sqrt{|x|}$ . More generally, the contour integrals we'll use will contain some square root  $\sqrt{f(z)}$ . This square root will have a branch cut on the real axis where  $f(x) < 0$ . There, depending whether we approach the real axis from above or from below it reduces to  $i\sqrt{f(x)}$  or  $-i\sqrt{f(x)}$ , not necessarily respectively and actually the main difficulty will be to find which one where. We'll indicate whether it reduces to  $i\sqrt{f(x)}$  or  $-i\sqrt{f(x)}$  on the plots of the integration contours with  $+i$  and  $-i$  respectively. First we will discuss the results from the article [29] for the Ising case  $\gamma = 1$  and then our results for the more general XY model.

$\gamma = 1$

In the Ising mode,  $\gamma = 1$ , in the special case of zero magnetic field  $h = 0$  we have  $a_n = 0$  directly from (3.15). Then from (3.18) we have  $E_0^- = E_0^+$ , a result we already know. For non-zero magnetic field  $h$  the coefficients (3.15) can be expressed as complex integrals:

$$a_n = \frac{-i\sqrt{h}}{\pi} \oint_{|z|=1} z^{n-1} \sqrt{-\frac{1}{z}(z-h)(z-\frac{1}{h})} dz . \quad (3.21)$$

The integrand is not a holomorphic function in the whole integration domain. It has branch cuts along the intervals  $(0, h) \cap (1/h, \infty)$ . The integration contour in the case  $h < 1$  used to calculate the integral is shown in Figure 3.5. We obtain

$$a_n = -\frac{2\sqrt{h}}{\pi} \int_0^{1/h} x^{n-1} \sqrt{\left| \frac{1}{x}(x-h) \left(x - \frac{1}{h}\right) \right|} dx . \quad (3.22)$$

The case  $h \geq 1$  is completely analogous. The only difference in that case is that we integrate up to  $h$ . The expression (3.22) is clearly negative which means that in the Ising model we have  $E_0^- > E_0^+$  for  $h > 0$ . The coefficients in (3.18) can be easily summed up using the formula for the sum of the geometric sequence, but we won't go in the details.

$\gamma \neq 1$

In the case  $\gamma \neq 1$  after some algebra we can express the coefficients (3.15) as complex integrals

$$a_n = -\frac{i}{2\pi} \oint_{|z|=1} z^{n-1} \sqrt{-\frac{1}{z^2} P_1(z) P_2(z)} dz , \quad (3.23)$$

where we have defined the quadratic polynomials

$$P_1(z) = (\gamma + 1)z^2 - 2hz - (\gamma - 1) , \quad (3.24a)$$

$$P_2(z) = (\gamma - 1)z^2 + 2hz - (\gamma + 1) . \quad (3.24b)$$

The integrand is not a holomorphic function in the the whole integration domain in general. To calculate the integral we have to find the branch cuts and to find the branch cuts we have to find the roots of the polynomials. If we denote the roots of the polynomials, in the case when they are real, as

$$P_1(\alpha_l) = P_1(\alpha_r) = 0 \quad \alpha_l \leq \alpha_r , \quad (3.25)$$

$$P_2(\beta_l) = P_2(\beta_r) = 0 \quad \beta_l \leq \beta_r .$$

we can express (3.23) as

$$a_n = -\frac{i}{2\pi} \oint_{|z|=1} z^{n-1} \sqrt{\frac{1-\gamma^2}{z^2} (z - \alpha_l)(z - \alpha_r)(z - \beta_l)(z - \beta_r)} dz , \quad (3.26)$$

The roots of  $P_1(z)$  and  $P_2(z)$  are real for  $\gamma^2 + h^2 \geq 1$  and they are equal to

$$\begin{aligned} \alpha_l &= \frac{h - \sqrt{\gamma^2 + h^2 - 1}}{\gamma + 1}, & \alpha_r &= \frac{h + \sqrt{\gamma^2 + h^2 - 1}}{\gamma + 1} \\ \beta_l &= \begin{cases} \frac{-h + \sqrt{\gamma^2 + h^2 - 1}}{\gamma - 1}, & \gamma < 1 \\ \frac{-h - \sqrt{\gamma^2 + h^2 - 1}}{\gamma - 1}, & \gamma > 1 \end{cases}, & \beta_r &= \begin{cases} \frac{-h - \sqrt{\gamma^2 + h^2 - 1}}{\gamma - 1}, & \gamma < 1 \\ \frac{-h + \sqrt{\gamma^2 + h^2 - 1}}{\gamma - 1}, & \gamma > 1 \end{cases}. \end{aligned} \quad (3.27)$$

We managed to bring the integral to a more revealing form in the following special cases:

- $\gamma^2 + h^2 = 1$
- $h = 0$
- $\gamma > 1$ ,  $N = \text{even}$ .

We'll discuss the cases, one by one.

- $\gamma^2 + h^2 = 1$ ,  $\gamma \neq 1$

In the case  $\gamma^2 + h^2 = 1$  we already know the result. The lowest energies of two sectors are equal for any subsystem size  $N$ . However, it's good to note that complex analysis gives us the same result. We have

$$0 < \alpha_l = \alpha_r < \beta_l = \beta_r, \quad (3.28)$$

and it can be shown that we don't have branch cuts. That's why  $a_n = 0$  and  $E_0^- = E_0^+$  as we already know.

- $h = 0$ ,  $\gamma \neq 1$

In the case  $h = 0$  we already know that for odd  $N$  we have  $E_0^- = E_0^+$ . However, the method of complex integrals and Fourier series will give us the answer for any  $N$ . Let's first examine the case  $\gamma > 1$ . In this case it can be shown that the roots (3.27) satisfy the following relation

$$0 < -\alpha_l = \alpha_r = \sqrt{\frac{\gamma - 1}{\gamma + 1}} < 1 < \sqrt{\frac{\gamma + 1}{\gamma - 1}} = \beta_r = -\beta_l. \quad (3.29)$$

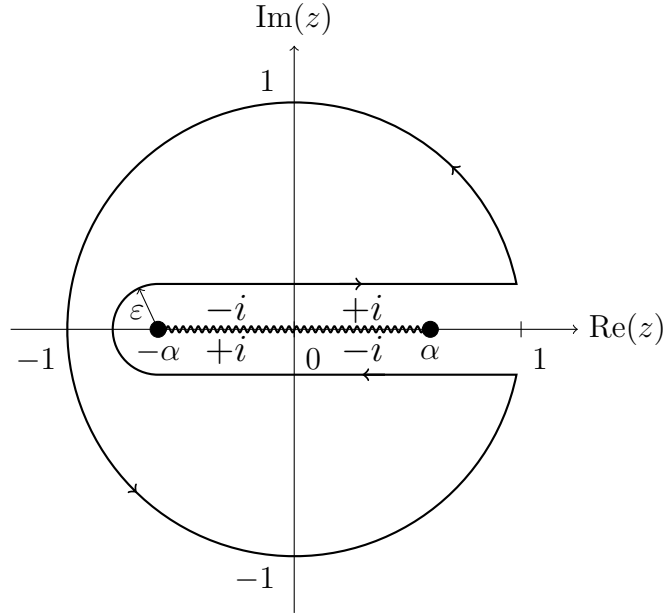


Figure 3.6: The integration contour in the case  $h = 0, \gamma > 1$ .

With the definition

$$\alpha \equiv \alpha_r, \quad \beta \equiv \beta_r \quad (3.30)$$

the coefficients (3.26) become

$$a_n = -\frac{i\sqrt{|\gamma^2 - 1|}}{2\pi} \oint_{|z|=1} z^{n-1} \sqrt{-\frac{1}{z^2}(z^2 - \alpha^2)(z^2 - \beta^2)} dz. \quad (3.31)$$

The square root in the integral has branch cuts along  $(-\infty, -\beta)$ ,  $(-\alpha, \alpha)$  and  $(\beta, \infty)$ . It is indicated in Figure 3.6, where the integration contour is given, to what the square root reduces on the real axis in the interval of interest. The square root acquires opposite signs on the real axis for  $x < 0$  and  $x > 0$ . The branch cuts are of the same length for  $x > 0$  and  $x < 0$ . In addition to square root the integral contains the factor  $x^{n-1}$  which is for  $x < 0$  positive if  $n$  is odd and negative if  $n$  is even. All this gives us

$$a_n = 0, \quad \text{odd } n$$

$$a_n = -\frac{\sqrt{\gamma^2 - 1}}{\pi} \int_0^\alpha x^{n-1} \sqrt{\left| \frac{1}{x^2}(x^2 - \alpha^2)(x^2 - \beta^2) \right|} dx, \quad \text{even } n \quad (3.32)$$

The coefficients  $a_n$  (3.32) are zero for odd  $n$  which using (3.18) implies that  $E_0^- = E_0^+$  for odd  $N$ , a result we already know. For even  $n$  the coefficients are clearly negative

. From this fact we get a new result

$$E_0^- > E_0^+ \quad \text{in the case } h = 0, \gamma > 1, N = \text{even} . \quad (3.33)$$

In the case  $\gamma < 1$  the roots of the polynomials (3.24) are imaginary, given by

$$\pm i\alpha \equiv i\sqrt{\frac{1-\gamma}{1+\gamma}} \quad \text{and} \quad \pm i\beta \equiv i\sqrt{\frac{1+\gamma}{1-\gamma}} . \quad (3.34)$$

and the coefficients (3.23) are given by

$$a_n = -\frac{i}{2\pi} \oint_{|z|=1} z^{n-1} \sqrt{\frac{|\gamma^2-1|}{z^2}} (z^2 + \alpha^2)(z^2 + \beta^2) dz . \quad (3.35)$$

With the substitution  $w = iz$  (3.35) becomes

$$a_n = -i^n \frac{i\sqrt{|\gamma^2-1|}}{2\pi} \oint_{|w|=1} w^{n-1} \sqrt{-\frac{1}{w^2}(w^2 - \alpha^2)(w^2 - \beta^2)} dw . \quad (3.36)$$

But this is basically up to a factor  $i^n$  the same expression as (3.31). For odd  $n$  as before we have  $a_n = 0$  from which we conclude that  $E_0^- = E_0^+$ , a result we already know. For even  $n$  the expression will be positive or negative, depending on the factor  $i^n$ , and we get a new result:

$$\begin{aligned} E_0^- < E_0^+ & \quad \text{in the case } h = 0, \gamma > 1, N = 2, 6, 10, \dots, 4k + 2, \dots , \\ E_0^- > E_0^+ & \quad \text{in the case } h = 0, \gamma > 1, N = 4, 8, 12, \dots, 4k, \dots . \end{aligned} \quad (3.37)$$

This result is clearly in agreement with the numerical one shown in Figure 3.4.

- $\gamma > 1, h \neq 0$

The only other case in which we managed to get results using the method of complex analysis and Fourier series is  $\gamma > 1$  for even  $N$ .

Let's first examine the case  $h > 1$ . It can be shown that in this case

$$0 < -\alpha_l < \beta_r < 1 < \alpha_r < -\beta_l . \quad (3.38)$$

The branch cuts are now along the intervals  $(-\infty, \beta_l)$ ,  $(\alpha_r, \beta_r)$  and  $(\alpha_r, \infty)$ . The integration contour is shown in Figure 3.7, where it is also shown to what the square

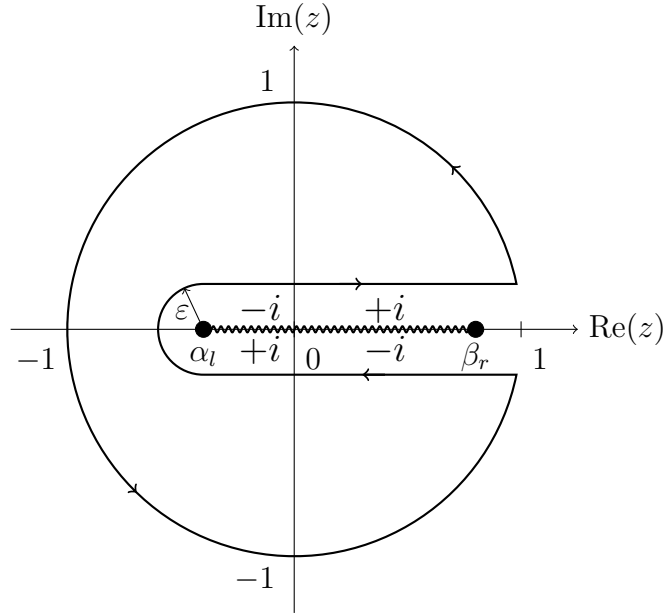


Figure 3.7: The integration contour in the case  $\gamma > 1$ ,  $h > 1$ .

root reduces on the real axis. We obtain

$$a_n = \frac{\sqrt{\gamma^2 - 1}}{2\pi} \left( \int_{\alpha_l}^0 - \int_0^{\beta_r} \right) x^{n-1} \sqrt{\left| \frac{1}{x^2} (x - \alpha_l)(x - \alpha_r)(x - \beta_l)(x - \beta_r) \right|} dx \quad (3.39)$$

For even  $n$  we have  $x^{n-1} < 0$  for  $x < 0$  and therefore in this case the coefficient (3.39) is negative. In the case when  $n$  is odd the two integrals in (3.39) compete and we can't see in this way the sign of the coefficient. So, using (3.18) we find a new result:

$$E_0^- > E_0^+ \quad \text{in the case } \gamma > 1, h > 1, N = \text{even} . \quad (3.40)$$

The case  $h \leq 1$  is completely analogous. In this case it can be shown that

$$0 < -\alpha_l < \alpha_r < 1 < \beta_r < -\beta_l , \quad (3.41)$$

and we have to make a replacement  $\alpha_r \leftrightarrow \beta_r$  in (3.39). The conclusion is:

$$E_0^- > E_0^+ \quad \text{in the case } \gamma > 1, N = \text{even} . \quad (3.42)$$

Our analytical results are summed up in Figure 3.8.



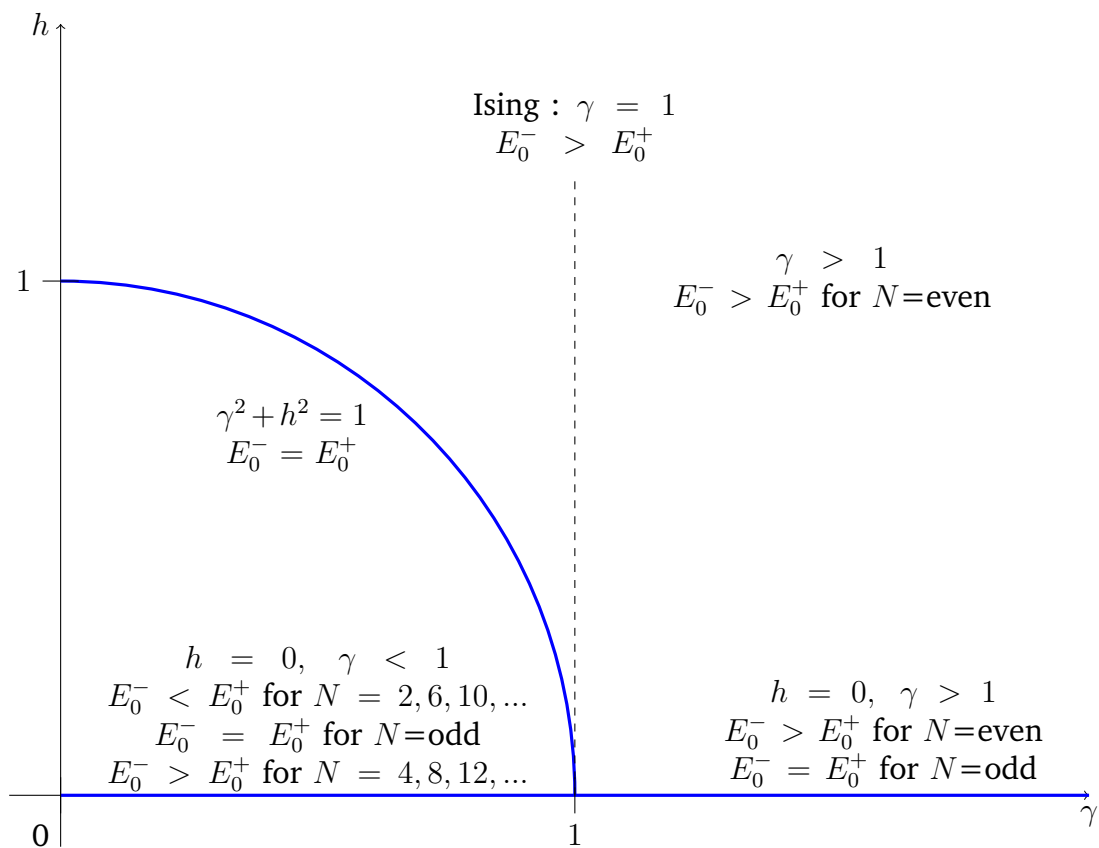


Figure 3.8: Comparison of the lowest energies of two different sectors,  $E_0^-$  and  $E_0^+$ , in the cases where we could obtain it using complex analysis and Fourier series. This method was used in [29] for the Ising model,  $\gamma = 1$ .

## 4 Entanglement in the XY chain

### 4.1 Introduction

In Section 1 we described that the aim of the thesis is to discriminate the non-conformal nature of the bi-critical point in a numerical experiment using quantities accessible also in non-exactly solvable models. Using this approach we want to find in the future a numerical procedure for establishing whether a multi-critical point in an arbitrary model is non-conformal. The quantities accessible also in non-exactly solvable models are the entanglement entropy and the reduced density matrix eigenvalues. In subsection 4.2 we introduce the entanglement entropy and the reduced density matrix in general and in subsection 4.3 we calculate them exactly for the XY chain. In subsection 4.4 we quote some results on the behavior of these quantities in the double-scaling limit. We'll use these results to test our numerical algorithm by comparing them to our results for a finite subsystem. CFT predictions, which will be tested near the bi-critical point and far from it, are also introduced. In subsection 4.5 details of our numerical algorithms are explained. Finally, in subsection 4.6 our numerical results are given. First, comparison of the double-scaling limit predictions and calculated finite-size behavior is given. Then finally, comparison with the CFT prediction is given near and far from the bi-critical point.

### 4.2 Reduced density matrix and the entanglement entropy

In this chapter we introduce the reduced density matrix (RDM) and the entanglement entropy, quantities useful to describe entanglement in a bipartite system. Given a total system in a certain quantum state  $|\Psi\rangle$  we divide it (in space, or in Hilbert space) in two parts. We ask how are the two parts coupled in  $|\Psi\rangle$ . The entanglement entropy and the RDM are quantities useful to give an answer to this question [34]. The system is in a definite state at zero temperature so they are used to describe entanglement in a bipartite system at zero temperature.

First we introduce the RDM and its properties based on [10], [11]. At zero temperature the system is in the ground state, which can be described by pure state density matrix

$$|\Psi\rangle\langle\Psi| .$$

At higher temperatures it is some statistical mixture . Now let's say we have a composite system  $AB$  made out of subsystems  $A$  and  $B$ . The composite system is described by a Hilbert space  $\mathcal{H}^{AB}$  which is a tensor product of the subsystem Hilbert spaces

$$\mathcal{H}^{AB} = \mathcal{H}^A \otimes \mathcal{H}^B .$$

The composite system at zero temperature is described by the density matrix

$$\rho^{AB} = |\Psi\rangle \langle \Psi| . \quad (4.1)$$

The quantum expectation value of any observable, described by a Hermitian operator  $O^{AB}$ , in the state  $|\Psi\rangle$  is given by trace in  $\mathcal{H}^{AB}$

$$\langle O^{AB} \rangle = \text{tr}(\rho^{AB} O^{AB}). \quad (4.2)$$

The RDM for system  $A$  is defined as

$$\rho^A \equiv \text{tr}_B(\rho^{AB}) , \quad (4.3)$$

where  $\text{tr}_B$  is a partial trace over system  $B$ . It is a linear mapping

$$\text{tr}_B : L(\mathcal{H}^{AB}) \rightarrow L(\mathcal{H}^A) , \quad (4.4)$$

defined with

$$\text{tr}_B(|a_1\rangle \langle a_2| \otimes |b_1\rangle \langle b_2|) = |a_1\rangle \langle a_2| \text{tr}(|b_1\rangle \langle b_2|), \quad (4.5)$$

where  $|a_1\rangle, |a_2\rangle$  are any state vectors in  $\mathcal{H}^A$  and  $|b_1\rangle, |b_2\rangle$  in  $\mathcal{H}^B$ . The trace is taken here in  $\mathcal{H}^B$ . The RDM (4.3) is an operator in  $\mathcal{H}^A$ .

Let us now take a look at the observable describing only system  $A$ , which means it acts as identity  $I_B$  in  $\mathcal{H}^B$  and we can write it as  $O \otimes I_B$ . From (4.2) follows that it's expectation value is given by

$$\langle O \rangle = \text{tr}(\rho^A O), \quad (4.6)$$

where trace is now taken in  $\mathcal{H}^A$ . It can be shown [10] that the operator  $\rho^A$  which satisfies (4.6) for an arbitrary observable  $O$  is unique. That's why (4.6) can be taken as a definition of the RDM equivalent to (4.3).

The entanglement entropy [12] is defined through the RDM  $\rho^A$ :

$$S^A = -\text{tr}(\rho^A \ln \rho^A) = -\sum_n \lambda_n \ln \lambda_n , \quad (4.7)$$

where  $\lambda_n$  are eigenvalues of  $\rho^A$ . It can be shown using Schmidt decomposition that for a pure state (4.1) the spectrum of  $\rho^A$  is equal to the spectrum of  $\rho^B$ . That's why  $S^A = S^B$  so one can simply write  $S$  and speak of *the* entanglement entropy. The entanglement entropy (4.7) has the same form as the entropy of a system in a canonical ensemble [13]:

$$S = -k_B \sum_n p_n \ln p_n ,$$

where

$$p_n = \frac{e^{-\beta E_n}}{Z} = \rho_{nn} .$$

We have introduced the desired quantities, the operator RDM and the entanglement entropy which is specified by the eigenvalues of the RDM. Now we'll justify that the entanglement entropy is a measure of entanglement in a bipartite system. When the subsystems are not entangled, i.e. when the state of the composite system can be written in a factorized form

$$|\Psi\rangle = |\Psi^A\rangle \otimes |\Psi^B\rangle \quad (4.8)$$

the RDM  $\rho^A$  is equal to

$$\rho^A = \text{tr}_B(|\Psi\rangle \langle\Psi|) = |\Psi^A\rangle \langle\Psi^A| \quad (4.9)$$

and the entanglement entropy is zero,  $S = 0$ . On the other hand maximally entangled subsystems are described by the state of the composite system

$$|\Psi\rangle = \frac{1}{\sqrt{M}} \sum_{n=1}^M |\Psi_n^A\rangle \otimes |\Psi_n^B\rangle , \quad (4.10)$$

where  $M$  is the dimension of a smaller Hilbert space, let's say  $\mathcal{H}^A$ . The RDM of such state is equal to

$$\rho^A = \text{tr}_B(|\Psi\rangle \langle\Psi|) = \frac{1}{M} \sum_{n=1}^M |\Psi_n^A\rangle \langle\Psi_n^A| \quad (4.11)$$

and the entanglement entropy is maximal,  $S = \ln M$ . Because of such properties the

entanglement entropy is a measure of entanglement in a bipartite system.

In the following subsection we'll find the introduced quantities for the XY chain.

### 4.3 Reduced density matrix of the XY chain

We examine a block of  $L$  subsequent lattice sites in a large XY chain. Because of periodic boundary conditions we may assume without the loss of generality that we examine spins  $1, \dots, L$ .

The block is described by the  $2^L$  dimensional Hilbert space  $\mathcal{H}^A$ . The rest of the composite system is described by the  $2^{N-L}$  dimensional Hilbert space  $\mathcal{H}^B$ . Now we will find the reduced density matrix  $\rho \in L(\mathcal{H}^A)$  of the block for a system in the ground state (2.70), based on [36] [14]. As we have shown in Section 3 for  $h \leq 1$  the ground state can also be some linear combination with (2.77), but the results would qualitatively be the same. The reduced density matrix by definition (4.3) is

$$\rho = \text{tr}_B(|GS^+\rangle \langle GS^+|) . \quad (4.12)$$

However, we will find it by using equivalent definition. We search for an operator that satisfies (4.6) for any observable of the block. Since any  $2 \times 2$  matrix can be expressed as a linear combination of Pauli matrices and a unit matrix, any operator in  $L(\mathcal{H}^A)$  is a linear combination of operators

$$\sigma_1^{\mu_1} \sigma_2^{\mu_2} \dots \sigma_L^{\mu_L} \quad \text{for } \mu_i = 0, x, y, z .$$

Hence it is sufficient to find an operator  $\rho$  that reproduces all the expectation values

$$\langle \sigma_1^{\mu_1} \sigma_2^{\mu_2} \dots \sigma_L^{\mu_L} \rangle \quad \text{for } \mu_i = 0, x, y, z .$$

in the state  $|GS^+\rangle$ . From (2.19) we obtain the property:

$$\text{tr}(\sigma^\mu \sigma^\nu) = 2\delta_{\mu\nu} \quad \text{for } \mu, \nu = 0, x, y, z. \quad (4.13)$$

Using (4.13) and the identity

$$\text{tr}(A \otimes B) = \text{tr}A \text{tr}B$$

one can check that the right operator is

$$\rho = \frac{1}{2^L} \sum_{\mu_1, \dots, \mu_L=0,x,y,z} \langle \sigma_1^{\mu_1} \sigma_2^{\mu_2} \dots \sigma_L^{\mu_L} \rangle \sigma_1^{\mu_1} \sigma_2^{\mu_2} \dots \sigma_L^{\mu_L} . \quad (4.14)$$

One can in principle calculate the expectation values with the procedure similar to the one in section 2.7 and find the spectral decomposition  $\rho$ . However, this might not be an easy task and there is another method.

First, let's notice that the operators (2.21) for  $j = 1, \dots, L$  act only on the block, in the sense that:

$$\psi_j |a\rangle_A \otimes |b\rangle_B = (\psi_j |a\rangle_A) \otimes |b\rangle_B . \quad (4.15)$$

To help us find the RDM we will introduce the Majorana fermions defined with

$$\check{a}_{2j-1} = \psi_j^\dagger + \psi_j , \quad \check{a}_{2j} = i(\psi_j^\dagger - \psi_j) , \quad (4.16)$$

which satisfy the properties

$$\{\check{a}_l, \check{a}_m\} = 2\delta_{lm} , \quad \check{a}_l^\dagger = \check{a}_l . \quad (4.17)$$

They are connected to operators defined in (2.100) with

$$\check{a}_{2j-1} = A_j , \quad \check{a}_{2j} = iB_j . \quad (4.18)$$

From now on operators which satisfy fermionic relations (2.3) we will call Dirac fermions. Dirac fermions (2.21) in terms of Majoranas are given by

$$\psi_j = \frac{\check{a}_{2j-1} + i\check{a}_{2j}}{2} , \quad \psi_j^\dagger = \frac{\check{a}_{2j-1} - i\check{a}_{2j}}{2} . \quad (4.19)$$

From (2.104) we obtain the correlations of Majoranas:

$$\langle \check{a}_{2l-1} \check{a}_{2j} \rangle = -i g(j-l) , \quad \langle \check{a}_{2l-1} \check{a}_{2j-1} \rangle = \langle \check{a}_{2l} \check{a}_{2j} \rangle = \delta_{lj} . \quad (4.20)$$

We'll be interested in the correlations of Majoranas on the block. To express them

we define an antisymmetric  $2L \times 2L$  matrix  $\Gamma^a$  with

$$\langle \check{a}_l \check{a}_j \rangle = \delta_{lj} - i \Gamma_{lj}^a . \quad (4.21)$$

From (4.20) we obtain the explicit form:

$$\Gamma^a = \begin{pmatrix} \Pi_0 & \Pi_1 & \cdots & \Pi_{L-1} \\ \Pi_{-1} & \Pi_0 & \cdots & \Pi_{L-2} \\ \vdots & \vdots & \ddots & \vdots \\ \Pi_{-(L-1)} & \Pi_{-(L-2)} & \cdots & \Pi_0 \end{pmatrix} , \quad (4.22)$$

where we have defined the  $2 \times 2$  matrices

$$\Pi_j \equiv \begin{pmatrix} 0 & g(j) \\ -g(-j) & 0 \end{pmatrix} . \quad (4.23)$$

The function  $g$  is defined in (2.105).

Matrix (4.22) is real and skew-hermitian. Any such matrix can be carried to a block-diagonal form

$$\Gamma^b = \bigoplus_{j=1}^L \begin{pmatrix} 0 & \nu_j \\ -\nu_j & 0 \end{pmatrix} , \quad (4.24)$$

by real orthogonal transformation [1]

$$\Gamma^b = V \Gamma^a V^T . \quad (4.25)$$

Orthogonal matrix  $V$  defines a set of another Majorana operators

$$\check{b}_l \equiv \sum_{j=1}^{2L} V_{lj} \check{a}_j , \quad \check{a}_l \equiv \sum_{j=1}^{2L} V_{jl} \check{b}_j . \quad (4.26)$$

Indeed, using (4.17), the orthogonality and reality of  $V$  we obtain

$$\{\check{b}_l, \check{b}_m\} = 2\delta_{lm} , \quad \check{b}_l^\dagger = \check{b}_l . \quad (4.27)$$

Using (4.21) we can obtain the correlations of new Majorans:

$$\langle \check{b}_l \check{b}_j \rangle = \delta_{lj} - i (V \Gamma^a V^T)_{lj} . \quad (4.28)$$

from which, using (4.24), follows

$$\langle \check{b}_{2l-1} \check{b}_{2j} \rangle = -i\delta_{lj}\nu_j, \quad \langle \check{b}_{2l-1} \check{b}_{2j-1} \rangle = \langle \check{b}_{2l} \check{b}_{2j} \rangle = \delta_{lj}. \quad (4.29)$$

The correlators of new Majoranas have simpler form and this was the reason for introducing Majorana operators. We'll return to the more familiar language of Dirac Fermions and define

$$c_j = \frac{\check{b}_{2j-1} + i\check{b}_{2j}}{2}, \quad c_j^\dagger = \frac{\check{b}_{2j-1} - i\check{b}_{2j}}{2}. \quad (4.30)$$

They satisfy

$$\{c_l, c_j\} = 0, \quad \{c_l, c_j^\dagger\} = \delta_{lj}. \quad (4.31)$$

and are uncorrelated

$$\langle c_l^\dagger c_j \rangle = \delta_{lj} \frac{1 + \nu_j}{2}, \quad \langle c_l c_j \rangle = 0. \quad (4.32)$$

Operators (4.30) are some linear combination of operators  $\psi_j$  and they act only on the block. One basis of  $\mathcal{H}^B$ , as in (2.14), are states of the form

$$|n_1 n_2 \dots n_L\rangle = (c_1^\dagger)^{n_1} (c_2^\dagger)^{n_2} \dots (c_L^\dagger)^{n_L} |0\rangle, \quad (4.33)$$

where  $|0\rangle$  is state annihilated by every  $c_i$ . Since any basis state  $|n'_1 n'_2 \dots n'_L\rangle$  can be obtained from another (4.33) by applying  $c_i$  for  $n'_i < n_i$  and  $c_i^\dagger$  for  $n'_i > n_i$  any operator on the block can be expressed as a linear combination of the operators

$$(c_1^\dagger)^{\alpha_1} c_1^{\beta_1} (c_2^\dagger)^{\alpha_2} c_2^{\beta_2} \dots (c_L^\dagger)^{\alpha_L} c_L^{\beta_L}, \quad \alpha_i, \beta_i, \dots, \alpha_L, \beta_L = 0, 1. \quad (4.34)$$

Because operators  $c_i$  are a linear combination of operators  $\psi_j$  they will also be some linear combination of the operators  $\chi_q$ , defined in (2.54), and their conjugates. Since the state  $|GS^+\rangle$  is a vacuum state for operators  $\chi_q$  we can use Wick's theorem, stated in Section 2, to find the expectation values of operators (4.34) in the ground state  $|GS^+\rangle$ . Using Wick's theorem and (4.32) the expectation values of operators (4.34) take a simple form

$$\langle (c_1^\dagger)^{\alpha_1} c_1^{\beta_1} (c_2^\dagger)^{\alpha_2} c_2^{\beta_2} \dots (c_L^\dagger)^{\alpha_L} c_L^{\beta_L} \rangle = \langle c_1^\dagger c_1 \rangle^{\alpha_1} \langle c_2^\dagger c_2 \rangle^{\alpha_2} \dots \langle c_L^\dagger c_L \rangle^{\alpha_L} \delta_{\alpha_1 \beta_1} \delta_{\alpha_2 \beta_2} \dots \delta_{\alpha_L \beta_L}. \quad (4.35)$$



We will search for a reduced density matrix as for an operator which reproduces the expectation values of operators (4.34), as in (4.6). By performing the trace with respect to the basis (4.33) and using (4.35) one can easily check that the right operator is

$$\rho = ( \langle c_1^\dagger c_1 \rangle c_1^\dagger c_1 + \langle c_1 c_1^\dagger \rangle c_1 c_1^\dagger ) ( \langle c_2^\dagger c_2 \rangle c_2^\dagger c_2 + \langle c_2 c_2^\dagger \rangle c_2 c_2^\dagger ) \dots ( \langle c_L^\dagger c_L \rangle c_L^\dagger c_L + \langle c_L c_L^\dagger \rangle c_L c_L^\dagger ) . \quad (4.36)$$

To sum up, we have found the RDM for the ground state  $|GS^+\rangle$ . It is given by (4.36) and now we can easily read its eigenvalues. Using (4.32) we see that they are given by

$$\lambda_{\alpha_1 \alpha_2 \dots \alpha_L} = \prod_{j=1}^L \frac{1 + (-1)^{\alpha_j} \nu_j}{2} , \quad \alpha_1, \dots, \alpha_L = 0, 1 . \quad (4.37)$$

There are  $2^L$  eigenvalues of the reduced density matrix and it is remarkable that they can be obtained from a  $2L \times 2L$  correlation matrix (4.24).

The entanglement entropy is given by its definition (4.7):

$$S = - \sum_{\alpha_1, \alpha_2, \dots, \alpha_L = 0, 1} \lambda_{\alpha_1, \alpha_2, \dots, \alpha_L} \ln \lambda_{\alpha_1, \alpha_2, \dots, \alpha_L} . \quad (4.38)$$

After some algebra and noticing

$$\sum_{\alpha_i, \alpha_{i+1}, \dots, \alpha_L = 0, 1} \frac{1 + (-1)^{\alpha_i}}{2} \frac{1 + (-1)^{\alpha_{i+1}}}{2} \dots \frac{1 + (-1)^{\alpha_L}}{2} = 1 , \quad (4.39)$$

we obtain a simple expression for the entanglement entropy

$$S_L = - \sum_{j=1}^L \left( \frac{1 - \nu_j}{2} \ln \frac{1 - \nu_j}{2} + \frac{1 + \nu_j}{2} \ln \frac{1 + \nu_j}{2} \right) . \quad (4.40)$$

We have added the index  $L$  to the entropy to note that it depends on the subsystem size  $L$ . It is a remarkable fact that the entanglement entropy which is a trace in a  $2^L$  dimensional Hilbert space can be obtained from a  $2L \times 2L$  correlation matrix.

We can simply calculate the entropy at the bi-critical point  $(\gamma, h) = (0, 1)$ . There from the definition (2.105) we have  $g(0) = -1$  and  $g(l) = 0$  for  $l \neq 0$ . That's why (4.22) is already in the block diagonal form (4.24) with  $\nu_j = -1$  for any  $j$ . The entropy (4.40) is then equal to zero for any size of the subsystem  $L$ .

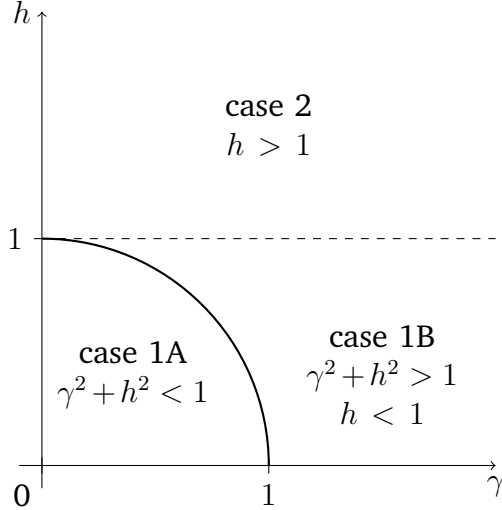


Figure 4.1: Definition of the cases in the expression (4.43) for the elliptic parameter.

#### 4.4 Double scaling limit

A double scaling limit (DSL) is a limit of a large subsystem in a very large system. It is a limit  $L \rightarrow \infty$  in a limit  $N \rightarrow \infty$ . In the whole phase diagram of the XY chain, exact computational methods were used to extract the DSL. Close to criticality, the DSL can also be described by CFT. We review results important for the thesis.

Let's start with the behavior of the entropy far from the critical line  $h = 1$ . This regime is called the *gapped* regime and is characterized by  $L \gg \xi$ . First we introduce some quantities. The complete elliptic integral of first kind is defined by

$$I(k) = \int_0^{\frac{\pi}{2}} \frac{d\theta}{\sqrt{1 - k^2 \sin^2 \theta}} \quad (4.41)$$

We define the quantity

$$\tau_0 = \frac{I(k')}{I(k)}, \quad k' = \sqrt{1 - k^2}. \quad (4.42)$$

The elliptic parameter  $k$  is given by

$$k = \begin{cases} \gamma / \sqrt{\gamma^2 + h^2 - 1}, & \text{case 1A} \\ \sqrt{1 - \gamma^2 - h^2} / \sqrt{1 - h^2}, & \text{case 1B} \\ \gamma / \sqrt{\gamma^2 + h^2 - 1}, & \text{case 2} \end{cases} \quad (4.43)$$

where the cases are defined in Figure 4.1. It has been shown in [24] that in the DSL

limit the values  $\nu_j$  in the block diagonal form (4.24) are given by

$$\nu_n = \begin{cases} \tanh(n\pi\tau_0), & h < 1 \\ \tanh[(n+1)\pi\tau_0], & h > 1 \end{cases} \quad (4.44)$$

for  $n = 0, 1, 2, \dots$  and their multiplicity is 2. The entanglement entropy in the DSL is completely specified by (4.44). The RDM spectrum in the DSL has also been found, in [25]. Before stating the result we have to introduce some other quantities. Let  $p_{\mathbb{N}}^{(1)}(n)$  denote the number of partitions of a number  $n$  into distinct natural numbers and let  $p_O^{(1)}(n)$  denote the number of partitions of  $n$  into distinct odd natural numbers. By definition  $p_O^{(1)}(0) = p_{\mathbb{N}}^{(1)}(0) = 1$ . The RDM eigenvalues are given by

$$\lambda_n = \begin{cases} e^{\frac{1}{6} \ln \frac{k'}{4k^2} - 2\pi\tau_0 \left[ n + \frac{1}{12} \right]}, & h < 1 \\ e^{\frac{1}{6} \ln \frac{k'}{4} - \pi\tau_0 \left[ n - \frac{1}{12} \right]}, & h > 1 \end{cases} \quad (4.45)$$

for  $n = 0, 1, 2, \dots$  and their multiplicity  $g_n$  is given by

$$g_n = \begin{cases} 2 \sum_{l=0}^n p_{\mathbb{N}}^{(1)}(l) p_{\mathbb{N}}^{(1)}(n-l), & h < 1 \\ \sum_{l=0}^n p_O^{(1)}(l) p_O^{(1)}(n-l), & h > 1 \end{cases} \quad (4.46)$$

The entanglement entropy in the DSL is completely specified by these expressions. As noted in the article, the number of partitions is given by generating functions [26]

$$\sum_{n=0}^{\infty} p_{\mathbb{N}}^{(1)}(n) q^n = \prod_{k=1}^{\infty} (1 + q^k), \quad (4.47a)$$

$$\sum_{n=0}^{\infty} p_O^{(1)}(n) q^n = \prod_{k=1}^{\infty} (1 + q^{2k-1}). \quad (4.47b)$$

It has also been shown that the DSL predictions (4.44) and (4.45) are good approximations to the finite-size behavior as long as  $L \gg \exp(1/\tau_0)$ , with  $\tau_0$  defined in (4.42). That's why we can consider  $\exp(1/\tau_0)$  as another characteristic length-scale in the system.

The behavior of the entropy on the critical line and close to the criticality is given

by CFT. The entropy scales logarithmically with the size of the block [35]:

$$S_L = \frac{c}{3} \ln \frac{L}{a} + c'_1, \quad (4.48)$$

where  $c$  is the central charge of the QFT in question and  $c'_1$  some correction constant which is negligible for large  $L$ . In the XY chain the central charge of the QFT at  $h = 1$  is  $c = 1/2$  [2] so using (4.48) we have

$$S_L = \frac{1}{6} \ln L + C(\gamma), \quad (4.49)$$

where  $C(\gamma)$  is a correction independent of  $L$ . It has been shown numerically in [36] [14] that this correction is such that

$$\lim_{L \rightarrow \infty} [S_L(\gamma) - S_L(\gamma = 1)] = \frac{1}{6} \ln \gamma. \quad (4.50)$$

The CFT also gives us a simple relation between the entropy and the largest RDM eigenvalue  $\lambda_{\max}$  [9]:

$$S_L = -2 \ln \lambda_{\max} \quad (4.51)$$

We have shown exactly in subsection 4.3 that the entanglement entropy at the bi-critical point in the XY chain vanishes for any size of the subsystem  $L$ . This is clearly in disagreement with (4.49) from which we can conclude, in another way, that the bi-critical point is non-conformal. It has been shown in [6] that the bi-critical point is an essential singularity of the entanglement entropy in the double-scaling limit. They have shown that the curves of constant entropy are ellipses and hyperbolas, and they all meet at the bi-critical point. Depending on the approach to the bi-critical point, the entropy can take any real positive value. On the other hand, exactly on the bi-critical point the entropy is zero and therefore a singularity. This observation is the primary motivation for the aim of the thesis, to see if one can discriminate conformal and non-conformal point through the quantities describing entanglement.

Our goal will be to calculate the entanglement entropy in the XY chain using (4.40) and the RDM eigenvalues using (4.37), and then test the breaking of the CFT predictions (4.49) and (4.51) close to the bi-critical point. Before testing the breaking of the CFT predictions we'll compare our finite-size results to the DSL predictions, one reason for this being to test our algorithm. Specifically, we'll test predictions (4.44),

(4.50) and (4.45).

## 4.5 Methodology

All numerics in this thesis is performed in *Python* programming language. We are using the *mpmath* Python library which allows real and complex floating-point arithmetic with arbitrary precision [19] and the *NumPy* library for creating arrays [20]. The precision is set at the beginning of the code. The plots are made using Python plotting library *matplotlib* [22].

We'll describe our method of finding the reduced density matrix eigenvalues. The first step in calculating the RDM eigenvalues is finding the values of  $\nu_j$  in the block diagonal form (4.24) of the correlation matrix (4.21). In order to find those values we notice that the antisymmetric correlation matrix multiplied with an imaginary unit is Hermitian

$$(i\Gamma^a)^\dagger = i\Gamma^a, \quad (4.52)$$

and  $\pm\nu_j$  are it's eigenvalues. With a unitary transformation  $U$  it can be brought to form

$$\bigoplus_{j=1}^L \begin{pmatrix} \nu_j & 0 \\ 0 & -\nu_j \end{pmatrix} = U^\dagger i\Gamma^a U. \quad (4.53)$$

That's why to find the values of  $\nu_j$  we are going to diagonalize the Hermitian matrix (4.52). This also allows us to use the algorithm for diagonalization of a Hermitian matrix, which is faster than the one for diagonalization of an arbitrary matrix and more precise. To construct the matrix (4.52) we calculate the function  $g(l)$  defined in (2.105) for  $l = -(L-1), \dots, 0, 1, \dots, L-1$ , multiply it with an imaginary unit and save it into an array(s). We have three parameters, magnetic field  $h$ , anisotropy gamma  $\gamma$  and the subsystem size  $L$  for which we set a value at the beginning of the code. To calculate the integral in (2.105) we use the function *quad* from the *mpmath* library. Here we have to be careful in the special case  $\gamma = 0$ . Then we have the singularity  $x_0 = \arccos h$  and we have to perform the integration as in (2.96). Once the function  $g(l)$  is calculated we construct the correlation matrix (4.52) row by row. We diagonalize it with the function *eighe* for the diagonalization of the Hermitian matrices from the *mpmath* library.

Once the matrix is diagonalized the entanglement entropy can be immediately

calculated using (4.40). If this is the only quantity we are interested in we stop here. If we are interested in the eigenvalues of the RDM we proceed further. The eigenvalues of the matrix (4.52), made out of  $\pm\nu_j$  are saved into array. For convenience in further calculations we sort this array of  $2L$  elements and keep only the  $L$  non-negative elements. We'll assume that  $+\nu_j$  are positive, so we keep only them. Let's denote this array with  $\nu$ :

$$\nu[0] = \nu_1, \nu[1] = \nu_2, \dots, \nu[L-1] = \nu_L. \quad (4.54)$$

Of course we can calculate the entanglement entropy using only the array  $\nu$  of non-negative values  $\nu_j$ . We define a function

$$f(x) = -\frac{1+x}{2} \ln \frac{1+x}{2} - \frac{1-x}{2} \ln \frac{1-x}{2}, \quad (4.55)$$

and sum it for  $i = 0, 1, \dots, L-1$  with  $x = \nu[i]$ . To avoid potential problems with logarithms of very small numbers which may happen because  $\nu_j$  is very close to 1 we use

$$f(x) = 0 \quad \text{for } x > 1 - \frac{1}{\text{precision}/2}. \quad (4.56)$$

in the definition of function  $f$ . Here *precision* is the number of decimal places we work with, which we set at the beginning of the code. To sum up, we calculate the entanglement entropy by summing (4.55) with  $x = \nu[i]$  under the restriction (4.56).

To calculate the RDM eigenvalues first we define an empty array for storing the eigenvalues and a two dimensional  $2 \times L$  array  $A$ :

$$A[i][0] = 1 + \nu[i], \quad A[i][1] = 1 - \nu[i], \quad i = 0, 1, \dots, L-1. \quad (4.57)$$

Then we create a loop which goes over all  $L$ -tuples  $a$  defined with

$$a = [\alpha_1, \alpha_2, \dots, \alpha_L], \quad a[i] = \alpha_{i-1}, \quad \alpha_i = 0, 1 \text{ for } i = 0, \dots, L-1. \quad (4.58)$$

Such loop can be created using the Python library *itertools* [21]. In each iteration

one RDM eigenvalue is calculated with

$$\lambda_{\alpha_1\alpha_2\dots\alpha_L} = \frac{1}{2^L} \prod_{i=0}^{L-1} A[i] [ a[i] ] \quad (4.59)$$

and appended to the array of the calculated RDM eigenvalues. In this way all the eigenvalues are obtained. Calculation of the eigenvalues  $\nu_j$  requires only the diagonalization of an  $2L \times 2L$  matrix. While it is possible to obtain all the  $\nu_j$  up to very large  $L$ , making all of the  $2^L$  products to obtain the full spectrum of the RDM requires far too much memory on a personal computer [27]. Also, the smallest eigenvalues are very small numbers for any reasonable precision. We can handle these problems to some extent by truncation of the RDM spectrum. Let's say we want to know only the largest eigenvalue. Then it is sufficient to calculate (4.37) with  $\alpha_j = 0$  for all  $j$ , which means to calculate (4.59) with  $a[i] = 0$ . But let's say we want to calculate 50 largest eigenvalues. The array  $\nu$  is ordered. The values of  $\nu[j]$  will be mostly close to 1 and  $(1 + \nu[j])/2 \approx 1$ . It is a non-trivial question how to truncate the spectrum because in principle we don't know whether

$$(1 - \nu[3])(1 - \nu[4]) > (1 - \nu[5]) \quad \text{or} \quad (1 - \nu[3])(1 - \nu[4]) < (1 - \nu[5]) . \quad (4.60)$$

However we can try for example to calculate all the eigenvalues

$$w_{\alpha_1\alpha_2\dots\alpha_K 0\dots 0} = \prod_{j=1}^K \frac{1 + (-1)^{\alpha_j} \nu_j}{2} \prod_{j=K+1}^L \frac{1 + \nu_j}{2} , \quad \alpha_1, \dots, \alpha_K = 0, 1 . \quad (4.61)$$

for some  $K < L$  such that  $2^K > 50$ . To do this we define a two-dimensional  $2 \times K$  array  $A$  as in (4.57) for  $L = K$  and create a loop over all  $K$ -tuples as in (4.58) for  $L = K$ . In each iteration we calculate the product

$$\lambda_{\alpha_1\alpha_2\dots\alpha_K 0\dots 0} = \frac{1}{2^L} \prod_{i=0}^{K-1} A[i] [ a[i] ] \prod_{i=K}^L (1 + \nu[i]) . \quad (4.62)$$

In this way we calculate  $2^K$  eigenvalues. In principle we don't calculate exactly the  $2^K$  largest eigenvalues here, but we can use this approach if we examine the agreement with some relation. For sufficiently big  $K$  we should find the agreement. However, we can be sure that we calculate the two largest eigenvalues when we set  $K = 1$ .

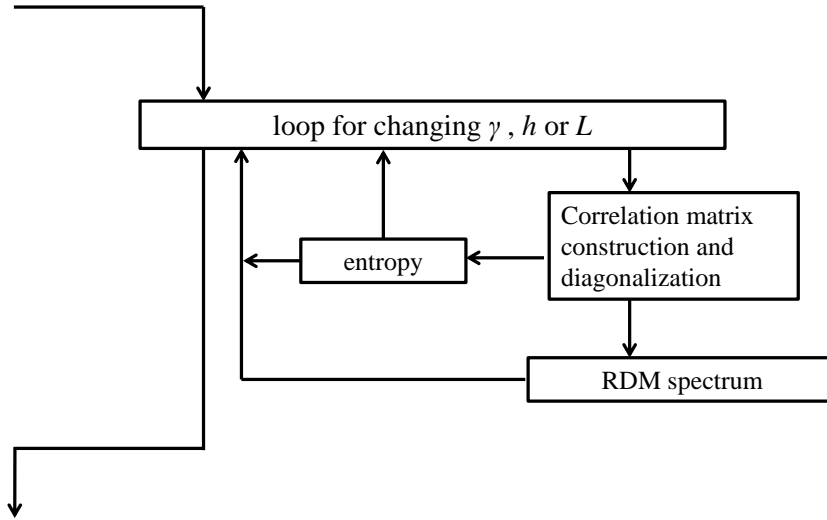


Figure 4.2: Schematic representation of our numerical algorithm.

The calculation of the DSL of  $\nu_j$ , given by (4.44), is straightforward. We compute the elliptic parameter (4.43) and use the function *ellipk* from the *mpmath* library to calculate the elliptic integrals in (4.42). Then we use (4.44) to calculate the DSL limit of  $\nu_j$ . Each value in (4.44) we have to plot, or print, two times starting from  $n = 0$  because of its multiplicity. The exception is the value for  $n = 0$  in the case  $h < 1$  because this value is zero and it has corresponding  $-\nu_j$  approaching to it.

To calculate the DSL of the RDM eigenvalues, given by (4.45), we use the quantities (4.43) and (4.42), calculated in the same way as to find the DSL of the  $\nu_j$ . The RDM eigenvalues in the DSL have the multiplicities given by (4.46). To find these multiplicities we use the generating functions. We notice that a partition of a number  $N$  into natural numbers cannot be formed with numbers greater than  $N$ . Actually, a partition of a number  $N$  into distinct odd natural numbers cannot be formed by numbers greater than  $2\lceil \frac{N}{2} \rceil - 1$ . Using (4.47) we conclude that to find partitions into distinct natural numbers  $p_{\mathbb{N}}^{(1)}(n)$  of numbers  $n \leq N$  it is sufficient to use the generating functions

$$\prod_{k=1}^N (1 + q^k), \quad (4.63a)$$

and to find partitions  $p_O^{(1)}(n)$  of numbers  $n \leq N$  it is sufficient to use

$$\prod_{k=1}^{\lceil \frac{N}{2} \rceil} (1 + q^{2k-1}). \quad (4.63b)$$



We use the Python library *SymPy* [23] for symbolic mathematics to construct the generating functions (4.63). These functions are polynomials and the numbers of partitions are simply found as polynomial coefficients. The multiplicities of the RDM eigenvalues are then calculated using (4.46). To reduce the computational time the multiplicities are calculated once and saved into a text file which can be called upon when needed. For our purposes it is sufficient to calculate the multiplicities of the first 50 eigenvalues in the case  $h < 1$  and first 75 in the case  $h > 1$ .

To make our code more elegant we have made separate codes for construction and diagonalization of the correlation matrix (4.52), and for calculating the RDM eigenvalues and their DSL. These codes are called upon and executed when needed. For example, for calculation of the entanglement entropy only the first one is needed while for plotting the RDM eigenvalues compared to the DSL we need both. Our algorithm is shown schematically in Figure 4.2.

## 4.6 Results

First, we have examined the behavior of the entanglement entropy exactly on the critical line  $h = 1$ . We have tried to reproduce the numerical result (4.50). That's why we have calculated the dependence of the entropy (4.40) on the anisotropy parameter  $\gamma$  for the subsystem sizes  $L = 5, 10, 20$  and compared it to (4.50). Results are given in Figure 4.3. The agreement with (4.50) clearly grows with the subsystem size  $L$  and that's why result (4.50) is reproduced.

Next, we have calculated values of  $\nu_j$ , defined in (4.24), for a finite subsystem and compared them to their double-scaling limit prediction (4.44) which should be a good approximation as long as  $L \gg \exp(1/\tau_0)$ , with  $\tau_0$  defined in (4.42). The results are given in Figure 4.4. The calculation is made for  $\gamma = 5$ ,  $h = 2$  and  $\gamma = 5$ ,  $h = 0.5$  for subsystem sizes  $L = 5, 10, 20$ . These are points far from the criticality and will also be used in Figure (4.5), where the explicit value of  $\exp(1/\tau_0)$  is given and this value satisfies  $L > \exp(1/\tau_0)$ . We see in the results in Figure 4.4 that the agreement with (4.44) becomes better, overall, as we increase the subsystem size  $L$ , which is a desired result.

So far our algorithm has given us the results for the entropy on the critical line and for the values of  $\nu_j$  in agreement with predictions. We proceed to calculate the RDM

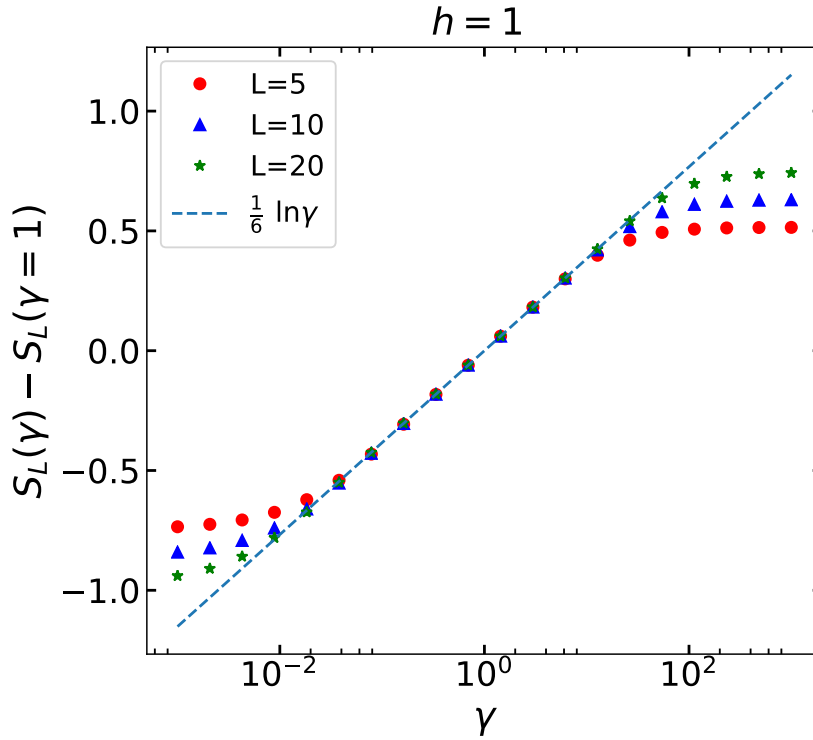


Figure 4.3: Dependence of the difference  $S_L(\gamma) - S_L(\gamma = 1)$ , where  $S_L$  given by (4.40), on the anisotropy parameter  $\gamma$  for subsystem sizes  $L = 5, 10, 20$ , on the critical line  $h = 1$ . Result (4.50) is given by blue dashed line. Agreement with (4.50) is better as we increase the subsystem size  $L$ .

eigenvalues, given by (4.37). We have calculated them both in the case  $h < 1$  and in the case  $h > 1$ , and compared them to the DSL prediction (4.45). Results are given in Figure 4.45 for subsystem sizes  $L = 10, 25$  and show 60 largest RDM eigenvalues. To calculate the eigenvalues for  $L = 25$  we had to use the procedure of truncation of the spectrum, which is explained in subsection 4.5. Again, the DSL prediction should be a good approximation as long as  $L \gg \exp(1/\tau_0)$ , with  $\tau_0$  defined in (4.42). The value of  $\exp(1/\tau_0)$  is indicated in Figure 4.5. We can see clearly how our finite-size results approach the DSL prediction as we increase the subsystem size, and this is the desired result.

Our algorithm has so far been successful and we can finally proceed to examine the CFT predictions near and far from the bi-critical point. We calculate the entanglement entropy (4.40) and the largest RDM eigenvalue, let's denote it by  $\lambda_{\max}$ . The largest eigenvalue  $\lambda_{\max}$  is calculated by truncation of the spectrum with  $K = 1$ , a procedure described in subsection 4.5. First we have examined the behavior of  $S_L$  and  $\lambda_{\max}$  exactly on the critical line  $h = 1$ . Exactly on the critical line for a given subsystem sizes  $L$  we find the breaking of CFT prediction as we approach the bi-critical point. However, this is not surprising because the entropy is zero,  $S_L = 0$ , exactly at the bi-critical point for any subsystem size  $L$ , as we have shown in subsection 4.3,

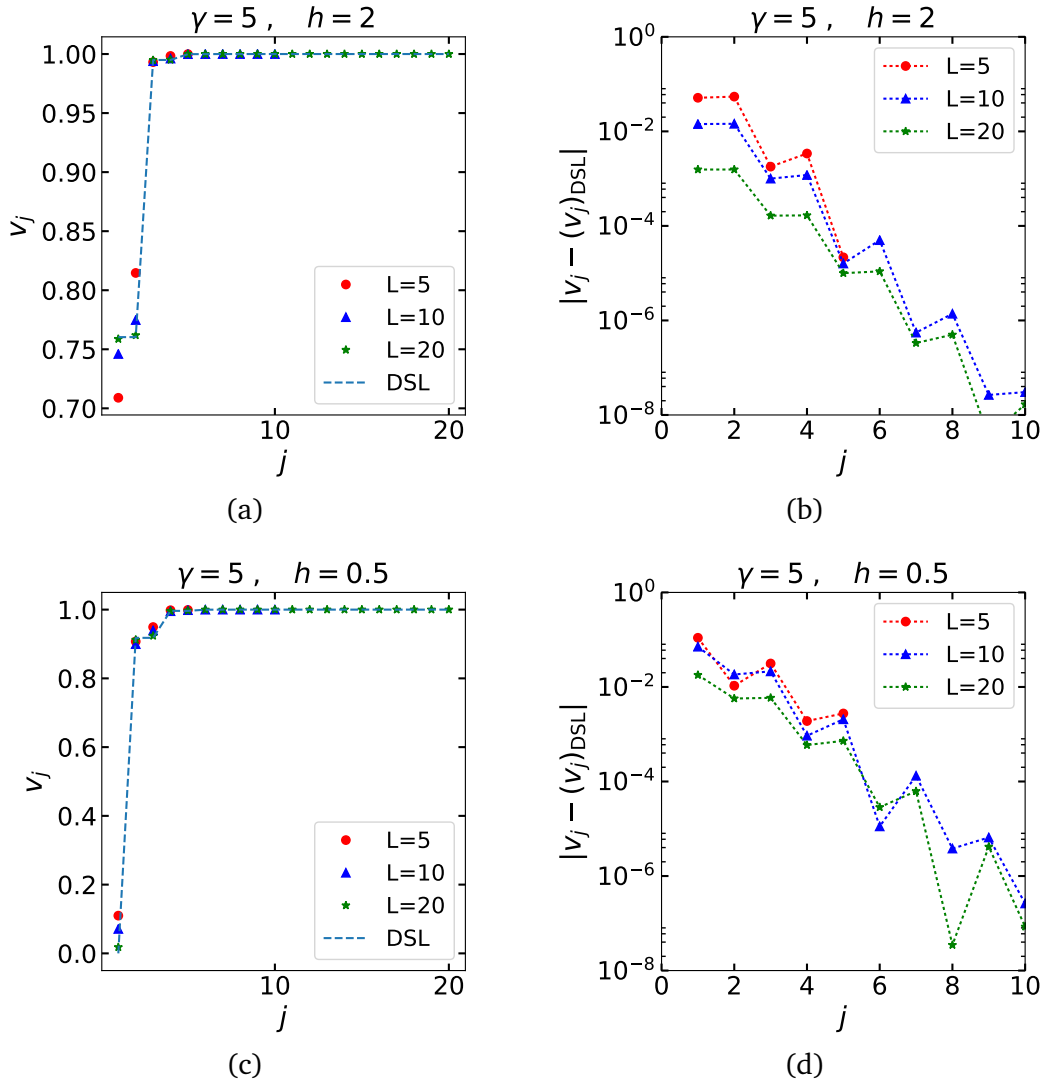
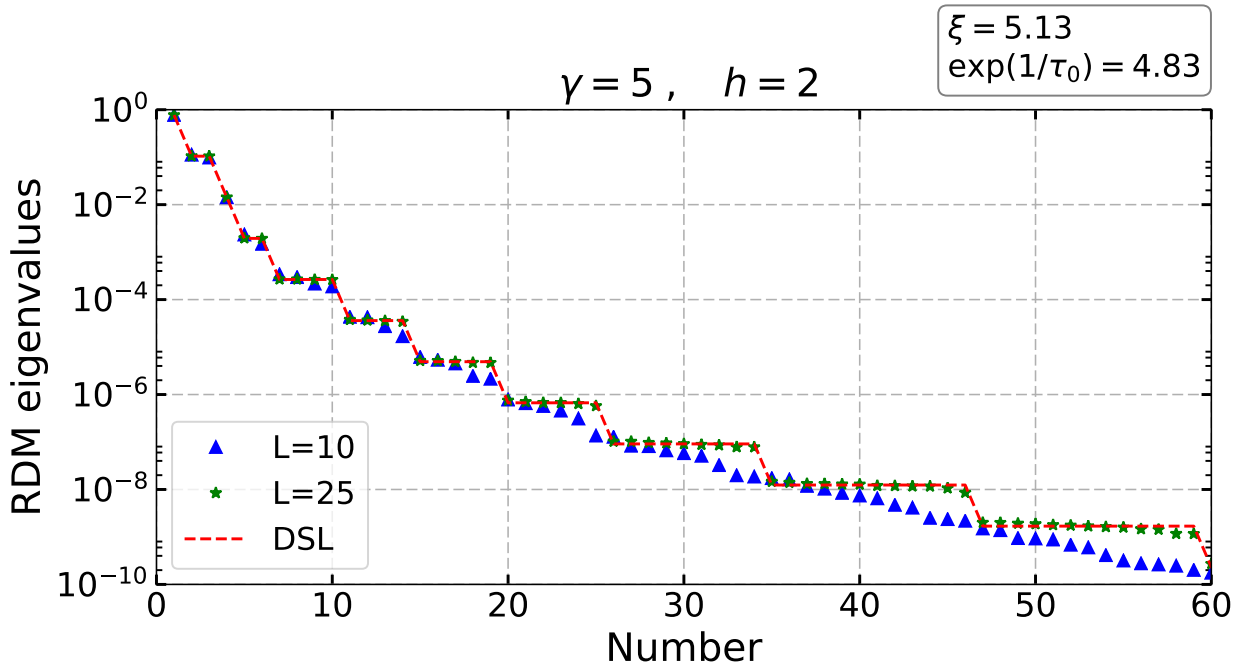
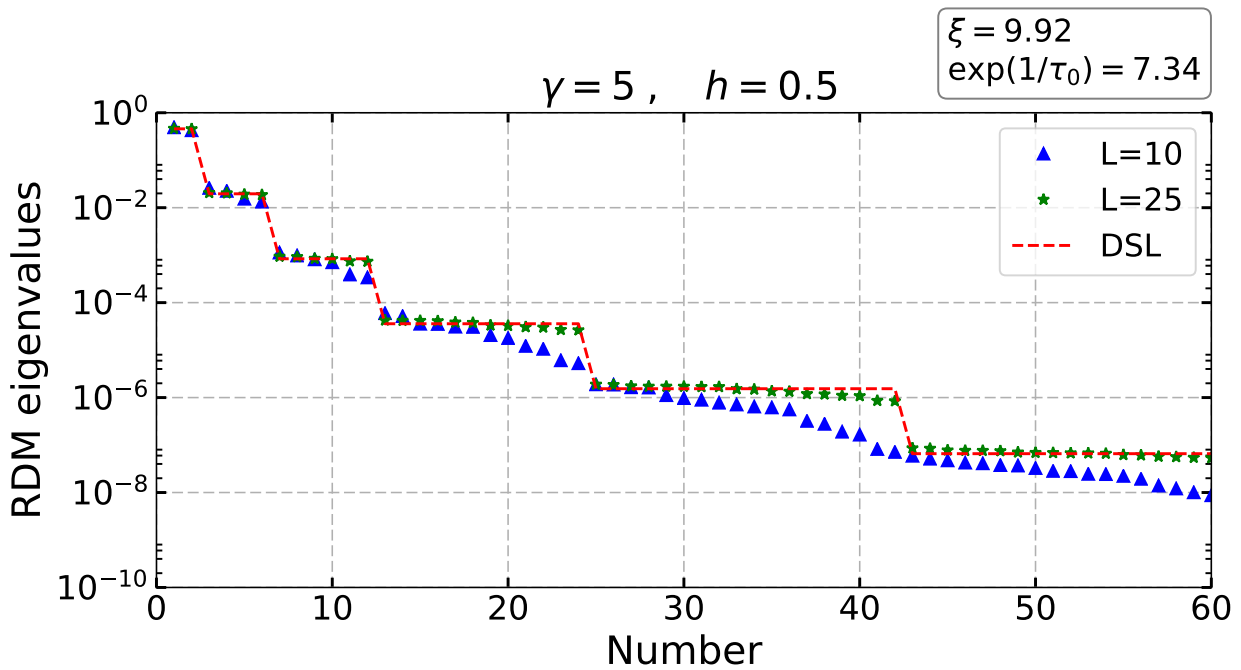


Figure 4.4: Calculated values  $\nu_j$ , defined in (4.24), compared to the DSL prediction (4.44), denoted with  $(\nu_j)_{DSL}$  for three different subsystem sizes  $L = 5, 10, 20$ . In (a) and (b) the magnetic field is smaller than 1,  $h = 0.5$ . In (c) and (d) it is bigger,  $h = 1.5$ . The anisotropy parameter is  $\gamma = 5$  in both cases. (b) and (d) show the difference between the calculated finite-size values and the DSL prediction (4.44) in the log scale.



(a)



(b)

Figure 4.5: Calculated RDM eigenvalues compared to the DSL prediction (4.45) for two different magnetic fields, (a)  $h = 0.5$  and (b)  $h = 2$ . The anisotropy parameter is  $\gamma = 5$  in each case. The eigenvalues are calculated for two different subsystem sizes in each case,  $L = 10, 25$ . The eigenvalues for  $L = 25$  are calculated by truncation of the spectrum. The agreement with (4.45) is better for bigger subsystem size  $L$ . The characteristic length-scales  $\xi$  and  $\exp(1/\tau_0)$  are also indicated.

and we have to approach this behavior sooner or later. Moreover, exactly on the critical line the correlation length  $\xi$  diverges and there is no characteristic length-scale in the system. This makes it harder to define the vicinity of the bi-critical point through universal parameters. That's why to explore points with similar microscopic conditions we have decided to go outside the critical line where the correlation length (2.108) is  $\xi \approx 1000$  in the units of lattice spacings  $a$ .

Results for the entanglement entropy  $S_L$  and  $-2 \ln \lambda_{\max}$  for four different phase diagram points where  $\xi \approx 1000$  are given in Figure 4.6. In all four cases the range of subsystem sizes is the same,  $L = 20, 21, \dots, 60$ . Results are compared to CFT predictions (4.49) and (4.51). The comparison is made by plotting the functions  $1/6 \ln L + C_1$  and  $1/6 \ln L + C_2$  where  $C_1$  and  $C_2$  are constants chosen so that the functions coincide with  $S_L$  and  $-2 \ln \lambda_{\max}$  for largest subsystem size  $L$ , i.e. for  $L = 60$ .

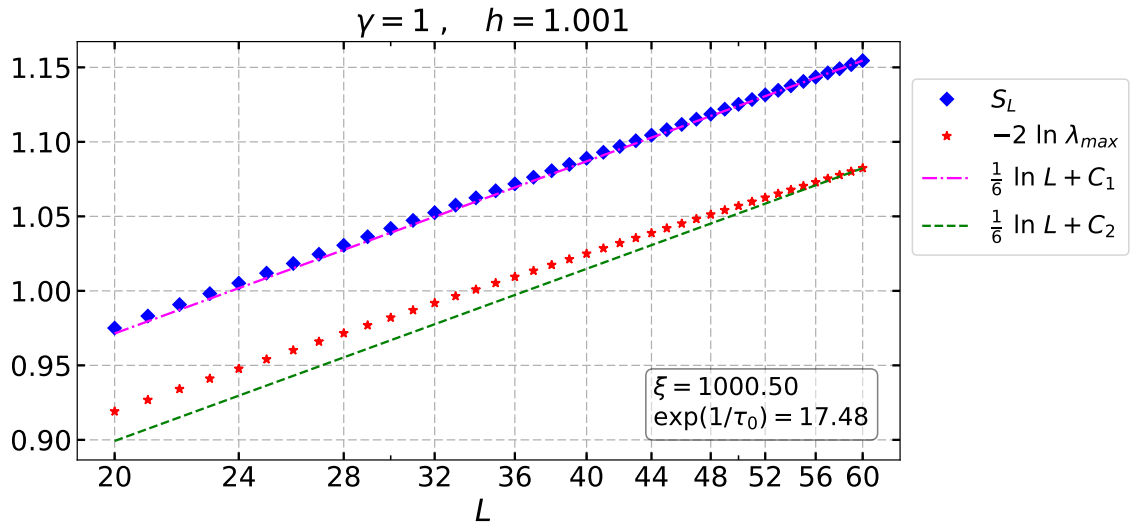
In Figure 4.6a the anisotropy parameter is  $\gamma = 1$  and the appropriate magnetic field to be in the regime  $\xi \approx 1000$  is  $h = 1.001$ . We see that the entanglement entropy  $S_L$  is in agreement with the CFT relation (4.49). The values of  $-2 \ln \lambda_{\max}$  differ from the entropy. But the slope only slightly differ from  $1/6$  so the CFT relation (4.51) is violated mostly up to an additive constant. The difference up to an additive constant can be explained as a finite-size effect. Another reason for deviations from the CFT predictions is the fact that we are not exactly on the critical-line. Similar situation is in Figure 4.6b where the anisotropy parameter is  $\gamma = 10$  and we are farther from the bi-critical point than in Figure 4.6a. The appropriate magnetic field to have  $\xi \approx 1000$  is  $h = 1.01$ . The microscopic conditions are similar to Figure 4.6a and the violation of the CFT relations is similar. Now we'll move closer to the bi-critical point. Figure 4.6c is obtained for the anisotropy  $\gamma = 0.01$ . The appropriate magnetic field to have similar microscopic conditions,  $\xi \approx 1000$ , is in this case  $h = 1.00001$ . Figure 4.6c shows greater violation of the CFT relations than Figures 4.6a and 4.6b. This is a desired result because a greater violation might be an effect of the vicinity of non-conformal point. In all cases in Figure 4.6 a characteristic length scale  $\exp(1/\tau_0)$  is also indicated. This characteristic length-scale differs most significantly from another, the correlation length  $\xi \approx 1000$ , in Figure 4.6c, which is another aspect of being close to a non-conformal point.

We have also calculated  $S_L$  and  $-2 \ln \lambda_{\max}$  very far from the critical point, for  $\gamma = 100$  and  $h = 1.1$ , with similar microscopic conditions,  $\xi \approx 1000$ , and for the same

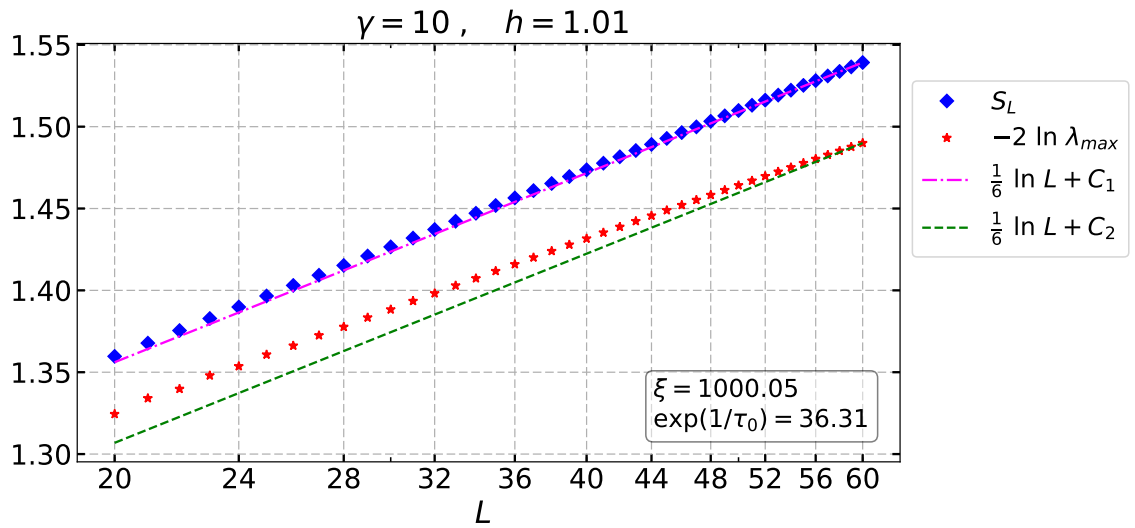
subsystem sizes  $L$ . Results are given in Figure 4.6d. Results show different behavior of  $-2 \ln \lambda_{\max}$  for even and odd  $L$ . CFT relation (4.49) is violated to the same extent as in Figure 4.6c which is obtained close to the non-conformal point. CFT relation (4.51) is violated for even  $L$  to the same extent as in 4.6c and for odd  $L$  to an even larger extent. Different behavior for even and odd  $L$  might be a finite-size effect. It has been explained in [9] why the approach to the CFT predictions might be slower for odd  $L$ . It seems that the finite-size effects are more visible here than in Figure 4.6. However, greater disagreement with CFT relations (4.49) and (4.51) than in Figures 4.6a and 4.6b might be also a sign that a point  $\gamma = \infty$  is non-conformal. We leave this as an open question.

The entanglement entropy  $S_L$  and  $-\ln \lambda_{\max}$  show a greater violation of the CFT relations (4.49) and (4.51) in the vicinity of the bi-critical point than far from it for a similar microscopic conditions. The method of establishing whether a multi-critical point in an arbitrary model is non-conformal by examining the behavior of the entanglement entropy and the RDM eigenvalues chain near and far from it might be useful. To further examine it we suggest testing other CFT predictions close to the bi-critical point in the XY chain and testing CFT predictions close to the non-conformal points in other exactly solvable models. Other exactly solvable models which contain a non-conformal multi-critical point that can be investigated are for example the XYZ chain, studied in [37], and  $t_1 - t_2$  models, studied in [38].

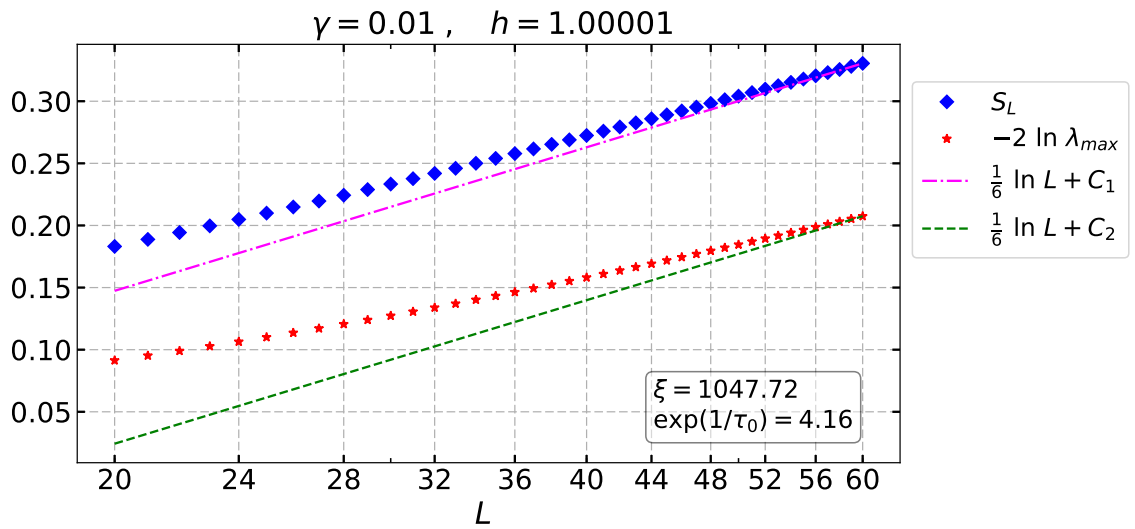
To recap, we have constructed the numerical algorithm for finding the reduced density matrix eigenvalues and the entanglement entropy for a finite subsystem in a large XY chain. After testing our algorithm on some results for the DSL and finding agreement we have moved to test CFT predictions on these quantities close to the criticality. We have accomplished to discriminate the non-conformal nature of the bi-critical point by comparing the entanglement entropy and the largest reduced density matrix eigenvalue to their CFT predictions near and far from the bi-critical point. But to construct a test whether a given multi-critical point is non-conformal which can be used in an arbitrary models we suggest taking other CFT predictions and other exactly solvable models with non-conformal points in the consideration.



(a)



(b)



(c)

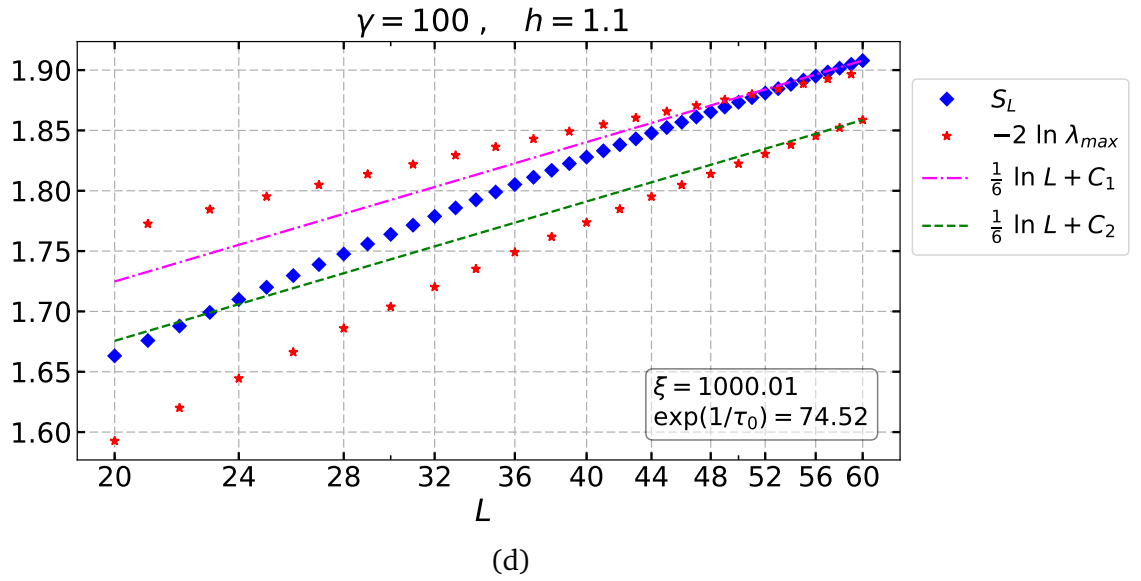


Figure 4.6: The dependence of the entanglement entropy  $S_L$ , given by (4.40), and  $-2 \ln \lambda_{\max}$ , where  $\lambda_{\max}$  is the largest RDM eigenvalue, on the subsystem size  $L$ . The subsystem sizes range from  $L = 20$  to  $L = 60$  and are shown in log scale. The Hamiltonian parameters are as indicated: (a)  $\gamma = 1, h = 1.001$ , (b)  $\gamma = 10, h = 1.01$ , (c)  $\gamma = 0.01, h = 1.00001$ , (d)  $\gamma = 100, h = 1.1$ . The dashed lines are functions  $1/6 \ln L + C_1$  and  $1/6 \ln L + C_2$  where  $C_1$  and  $C_2$  are constants chosen so that the functions coincide with  $S_L$  and  $-2 \ln \lambda_{\max}$  for the largest  $L$ , i.e.  $L = 60$ . These functions are useful to compare results to CFT predictions (4.49) and (4.51). The characteristic length-scales  $\xi$  and  $\exp(1/\tau_0)$  are also indicated.



## 5 Conclusion

The aim of this thesis was to observe the non-conformal nature of the bi-critical point in the XY chain in a numerical experiment through quantities accessible also in non exactly solvable models. Using this approach we want to construct in the future a numerical test whether a multi-critical point in an arbitrary model is non-conformal.

First we have introduced the XY chain and brought its Hamiltonian to a form of free fermions by separating the theory in two parity sectors. Using the free form we have found the Hamiltonian spectrum. Critical properties were discussed using two different approaches, studying the Hamiltonian spectrum and studying the correlation functions. All this computational work has given us a microscopic description of the XY chain.

Exact degeneracy of the XY chain ground state happens when the lowest energies of states belonging to two different parity sectors,  $E_0^-$  and  $E_0^+$ , are equal. We have introduced known results on the exact degeneracy in the XY chain and because of their incompleteness we have explored it further using numerical and analytical methods. Specifically, the method using complex analysis and Fourier series which has given a definite answer for the Ising model was introduced. Using this method we have found the dependence of the existence of the exact degeneracy in some special cases of the more general XY chain. Namely, we have shown the explicit dependence of the exact degeneracy on the number of spins  $N$  in the case of zero magnetic field  $h$  and we have shown the absence of the exact degeneracy in the case  $\gamma > 1$ , for any magnetic field  $h$ , when the number of spins  $N$  is even. Numerically, we have plotted the dependence of the difference  $E_0^- - E_0^+$  on Hamiltonian parameters  $\gamma$ ,  $h$  or  $N$ , where the oscillations around zero are visible. We have also examined numerically the lines in the  $(\gamma, h)$  parameter space where the XY chain has degenerate ground state. Results suggest that there is no exact degeneracy outside the circle  $\gamma^2 + h^2 = 1$  for  $h > 0$  and that inside the circle there is precisely  $\lceil N/2 \rceil$  such lines.

Coming back to the aim of the thesis, we have derived the reduced density matrix and the entanglement entropy of a finite subsystem in the XY chain. Then we have constructed the numerical algorithm for calculating the entanglement entropy and the reduced density matrix eigenvalues, which are quantities accessible also in non exactly solvable models, in the XY chain. After testing our algorithm on some results

for the double-scaling limit and finding agreement we have moved to test conformal field theory (CFT) predictions on these quantities close to the criticality. We have accomplished to discriminate the non-conformal nature of the bi-critical point by comparing the entanglement entropy and the largest reduced density matrix eigenvalue to their CFT predictions near and far from the bi-critical point. To construct a test in the future whether a given multi-critical point in an arbitrary model is non-conformal we have suggested taking other CFT predictions and other exactly solvable models with non-conformal points in the consideration.

## 6 Prošireni sažetak

### 6.1 Uvod

Jednodimenzionalni XY lanac je egzaktno rješiv model koji se koristi za proučavanje magnetskih uređenja u sistemima spinova. Model je generalizacija jednodimenzionalnog Isingovog modela i također opisuje lanac spinova koji interagiraju s najbližim susjedima. Općenitiji je od Isingovog modela jer  $x$  i  $y$  komponente spinova mogu različito interagirati, a razlika je opisana parametrom anizotropije  $\gamma$ . XY lanac opisan je Hamiltonijanom:

$$H = J \sum_{j=1}^N [(1 + \gamma)S_j^x S_{j+1}^x + (1 - \gamma)S_j^y S_{j+1}^y + hS_j^z].$$

Uvedeni Hamiltonijan opisuje  $N$  trodimenzionalnih spinova  $1/2$  na jednodimenzionalnoj rešetki i pretpostavljamo da se interakcija spinova može zanemariti u smjeru magnetskog polja, smjeru pozitivne  $z$  osi. Iznos magnetskog polja opisan je parametrom  $h$ . Jednodimenzionalni Isingov model dobiva se za  $\gamma = 1$ . Drugi specijalni slučaj,  $\gamma = 0$ , poznat je u literaturi kao XX model. Pretpostavljamo periodične rubne uvjete  $S_{N+1}^\alpha = S_1^\alpha$ . Zbog simetrija modela može se također bez smanjenja općenitosti pretpostaviti  $\gamma \geq 0$ ,  $h \geq 0$ . Parametar  $J$  opisuje energetska skalu. U ovom radu proučavamo feromagnetski slučaj  $J < 0$ .

XY lanac je egzaktno rješiv i slobodan model. Energija osnovnog stanja, pobuđenja, entropija zapetljanosti i gotovo svaka druga veličina može se pronaći egzaktno, što čini XY model dobrim za testirati nove teorijske hipoteze. Jednodimenzionalni sistemi su važni općenito zbog postojanja egzaktnih i aproksimativnih metoda za njihovo rješavanje. S druge strane moguće ih je eksperimentalno realizirati, npr. hladnim atomima u optičkoj rešetki. Jednodimenzionalni sistemi i XY model posebno također dobivaju na važnosti u području kvantnih računala i kvantnih informacija.

XY lanac ima bogat  $(\gamma, h)$  fazni dijagram. Naime, pokazuje dva fazna prijelaza na temperaturi apsolutne nule. Kritične linije su  $h = 1$  i  $\gamma = 0$ ,  $h \leq 1$ , i sijeku se u bikritičnoj točki  $(\gamma, h) = (1, 0)$ .

Jedno od osnovnih svojstava kvantne mehanike je zapetljanost. Veličina koja se pokazala uspješnom za kvantitativno izražavanje tog svojstva je entropija zapetljanosti. Prvenstveni razlog za uspjeh entropije zapetljanosti su njezini jednostavni

zakoni skaliranja na  $i$  u blizini kritičnih točaka, koje daje konformalna teorija polja (CFT). CFT je snažna analitička metoda za opisivanje sistema na  $i$  u blizini kritičnosti. Problem sa konformalnom teorijom polja je što ona sama po sebi ne daje informaciju o režimima svoje valjanosti. Postoje određeni postupci za odrediti te režime, koji mogu ovisiti i o veličinama koje opisujemo, no za njih je često potrebno imati i mikroskopsko rješenje modela.

Multikritične točke, tj. točke gdje se susreće više kvantnih prijelaza, imaju posebno mjesto u konformalnoj teoriji polja. Postoje multikritične točke, koje nazivamo nekonformalnim, u blizini kojih metoda prestaje vrijediti. Općenito, nekad je teško odrediti je li multikritična točka nekonformalna. U XY lancu može se pokazati da je bikritična točka nekonformalna.

U ovom radu želimo uočiti nekonformalnu prirodu bikritične točke u XY lancu u numeričkom eksperimentu kroz veličine dostupne također u modelima koji nisu egzaktno rješivi. Na taj način želimo u budućnosti predložiti numeričke provjere je li multikritična točka u proizvoljnom modelu konformalna ili nije. Da bi postupak bio primjenjiv na razne modele on mora uključivati veličine koje se mogu dobiti za svaki model. Takve veličine su entropija zapetljanosti i reducirana matrica gustoće zbog postupka koji se naziva renormalizacijska grupa reducirane matrice gustoće (DMRG). Ideja je proučiti ponašanje tih veličina u egzaktno rješivom XY lancu i vidjeti kako CFT predviđanja prestaju vrijediti u blizini nekonformalne bikritične točke. Možda bi slično ponašanje bilo vidljivo u blizini nekonformalnih točaka i u drugim modelima. XY lanac je rješiv i stoga znamo njegove mikroskopske detalje te možemo izračunati karakterističnu skalu duljine za procijeniti gdje bi CFT predviđanja trebala biti valjana. Ideja je najprije uspostaviti slaganje s CFT predviđanjima za neku karakterističnu skalu duljine u sistemu daleko od bikritične točke. Zatim se približiti bikritičnoj točki i istražiti jesu li, i na koji način, CFT predviđanja prekršena.

U poglavlju 2 rješavamo XY lanac. Pronalazimo energiju osnovnog stanja i pobuđenja te razmatramo njegova kritična svojstva i korelacijske funkcije. Općenito, osnovno stanje XY lanca može biti degenerirano, što je također povezano s lomljenjem diskretne  $Z_2$  simetrije, a ta degeneracija ovisi i o veličini sistema  $N$ . Zbog manjka rezultata o degeneraciji u XY lancu posvećujemo joj cijelo poglavlje 3. U poglavlju 4 nalazimo reduciranu matricu gustoće i entropiju zapetljanosti za konačni blok spinova velikog XY lanca. Zatim uvodimo CFT predviđanja i neka dobivena drugim metodama o pon-

ašanju tih veličina u limesu dvostrukog skaliranja, što znači limes velikog podsistema u jako velikom sistemu. Uspoređujemo numerički dobivene vrijednosti za konačni sistem sa limesom dvostrukog skaliranja. Zatim, konačno, proučavamo kršenje CFT predviđanja u blizini bikritične točke.

## 6.2 Rješavanje XY lanca

XY lanac rješava se najprije preslikavanjem spinova u sustav fermiona, a zatim dijeljenjem teorije u dva sektora. U svakom sektoru Hamiltonijan se dovodi u formu slobodnih fermiona. Hamiltonijan XY lanca zapisan pomoću Paulijevih operatora dizanja i spuštanja,

$$\sigma^\pm = \frac{1}{2}(\sigma^x \pm i\sigma^y)$$

glasi

$$H = \frac{J}{2} \sum_{j=1}^N \left[ (\sigma_j^+ \sigma_{j+1}^- + \gamma \sigma_j^+ \sigma_{j+1}^+ + \text{h.c.}) + h\sigma_j^z \right],$$

Pritom su  $\sigma^\alpha$  za  $\alpha = x, y, z$  Paulijeve matrice. Hamiltonijan preslikavamo u sustav fermiona pomoću Jordan-Wigner transformacije

$$\psi_j \equiv \left( \prod_{l=1}^{j-1} \sigma_l^z \right) \sigma_j^+, \quad \psi_j^\dagger \equiv \left( \prod_{l=1}^{j-1} \sigma_l^z \right) \sigma_j^-,$$

kojom definiramo fermionske operatore

$$\begin{aligned} \{\psi_i, \psi_j\} &= 0, \\ \{\psi_i, \psi_j^\dagger\} &= \delta_{ij}. \end{aligned}$$

Hamiltonijan zapisan pomoću fermiona glasi

$$H = \frac{1+P}{2} H^+ + \frac{1-P}{2} H^-,$$

gdje je  $P$  operator pariteta

$$P = \prod_{l=1}^N \sigma_l^z = \prod_{l=1}^N (1 - 2\psi_l^\dagger \psi_l).$$

koji ima svojstvene vrijednosti  $\pm 1$  te  $H^+$  i  $H^-$  su redom Hamiltonijani parnog i neparnog sektora, definirani s

$$H^\pm = -\frac{J}{2} \sum_{j=1}^N (\psi_j \psi_{j+1}^\dagger + \gamma \psi_j \psi_{j+1} + \text{h.c.}) - Jh \sum_{j=1}^N \psi_j^\dagger \psi_j + \frac{1}{2} JNh.$$

Hamiltonijan komutira s operatorom pariteta

$$[H, P] = 0.$$

Hamiltonijani pojedinih sektora mogu se dovesti do forme slobodnih fermiona

$$H^\pm = -J \sum_q \Lambda_q (\chi_q^\dagger \chi_q - \frac{1}{2}).$$

gdje su  $\chi_q$  fermionski operatori. U parnom sektoru sumira se  $q \in \{1/2, 3/2, \dots, N - 1/2\}$ , a u neparnom  $q \in \{0, 1, 2, \dots, N - 1\}$ . Spektar je dan s

$$\Lambda_q \equiv \Lambda\left(\frac{2\pi}{N}q\right) \equiv \sqrt{\left[h - \cos\left(\frac{2\pi}{N}q\right)\right]^2 + \gamma^2 \sin^2\left(\frac{2\pi}{N}q\right)}.$$

Iz forme slobodnih fermiona nalaze se svojstvena stanja u pojedinim sektorima. Pola stanja iz parnog sektora,  $P = 1$ , i pola iz neparnog,  $P = -1$ , su svojstvena stanja ukupnog Hamiltonijana  $H$ . Najniže energije u pojedinim sektorima, a da su pripadana stanja svojstvena stanja  $H$ , dane su s

$$E_0^+ = -\frac{1}{2} \sum_{q=0}^{N-1} \Lambda_{q+1/2},$$

$$E_0^- = \begin{cases} -\frac{1}{2} \sum_{q=0}^{N-1} \Lambda_q & \text{for } h \leq 1 \\ -\frac{1}{2} \sum_{q=0}^{N-1} \Lambda_q + \frac{1}{2}(h-1) & \text{for } h \geq 1 \end{cases}$$

Kritična svojstva XY lanca mogu se proučavati pomoću spektra  $\Lambda_q$  i pomoću korelacijskih funkcija

$$\rho_{lm}^\mu = \langle \sigma_l^\mu \sigma_m^\mu \rangle = \langle GS^+ | \sigma_l^\mu \sigma_m^\mu | GS^+ \rangle, \quad \mu = x, y, z.$$

Spektar može isčezavati u dva slučaja. Prvi je

$$\Lambda(0) = \sqrt{|h - 1|}$$

za  $h = 1$ , a drugi

$$\Lambda(\arccos h) = \sin(\arccos h)\gamma \sim |\gamma - 0|.$$

za  $\gamma, h \leq 1$ . Teorija kvantnih faznih prijelaza kaže da su zbog takvog ponašanja linije  $h = 1$  i  $\gamma, h \leq 1$ , kritične linije. Bikritična točka  $(\gamma, h)$  na kojoj se te kritične linije susreću je nekonformalna zato jer ukoliko razvijemo spektar po malom argumentu na bikritičnoj točki imamo

$$\Lambda(x) = \frac{1}{\sqrt{2}}x^2 + \dots$$

Spektar je kvadratičan i statistička teorija polja kaže da su takve točke nekonformalne.

U limesu dugog lanca, tj. velikog  $N$ , korelacijske funkcije mogu se korištenjem svojstava fermionskih operatora iz Jordan-Wigner transformacije i Wickovog teorema iz kvantne teorije polja zapisati kao determinante Toeplitzovih matrica. Npr. korelacijska funkcija  $\rho_{lm}^x$  dana je s

$$\rho_{lm}^x = \begin{vmatrix} g(-1) & g(-2) & g(-3) & \cdots & g(-n) \\ g(0) & g(-1) & g(-2) & \cdots & g(-n+1) \\ g(1) & g(0) & g(-1) & \cdots & g(-n+2) \\ \vdots & \vdots & \vdots & \ddots & \vdots \\ g(n-2) & g(n-3) & g(n-4) & \cdots & g(-1) \end{vmatrix},$$

a slične su i korelacijske funkcije za ostale komponente spinova. Pritom smo definirali realnu funkciju

$$g(l) = -\frac{1}{2\pi} \int_0^{2\pi} \frac{h - \cos x + i\gamma \sin x}{|h - \cos x + i\gamma \sin x|} e^{-ilx} dx.$$

Korištenjem svojstava Toeplitzovih matrica mogu se dobiti informacije o fazama u XY lancu i izraz za korelacijsku duljinu. Za  $h < 1$  postoji neto magnetizacija u lancu, dok za  $h > 1$  ne postoji. Korelacijska duljina je karakteristična duljina u sustavu i ona divergira na faznom prijelazu. Korelacijska duljina, koja divergira na prijelazu  $h = 1$ ,

dana je izrazom

$$\xi = \frac{a}{\left| \ln \left( \frac{h + \sqrt{\gamma^2 + h^2 - 1}}{1 + \gamma} \right) \right|},$$

gdje je  $a$  razmak spinova u rešetki.

### 6.3 Degeneracija osnovnog stanja u XY lancu

U ovom poglavlju istražujemo degeneraciju osnovnog stanja u XY lancu. Osnovno stanje je degenerirano ukoliko su najniže energije iz dvaju različitih sektora jednake, tj. ukoliko  $E_0^- = E_0^+$ . Spomenimo simetriju  $PHP = H$  i da ukoliko nema degeneracije svojstvena stanja Hamiltonijana su i svojstvena stanja operatora pariteta  $P$ . No u slučaju degeneracije moći ćemo formirati linearne kombinacije stanja koje će biti osnovna stanja, ali neće biti svojstvena stanja operatora pariteta. Tada kažemo da je došlo do lomljenja  $Z_2$  simetrije.

Navodimo do sada poznate rezultate. Osnovno stanje degenerirano je u limesu velikog sistema, tj. velikog  $N$ , svugdje za  $h \leq 1$ , a za  $h > 1$  osnovno stanje je ono iz parnog sektora jer imamo  $E_0^+ < E_0^-$ . Zatim, poznato je da je linija  $\gamma^2 + h^2 = 1$  degenerirana za sve veličine sistema  $N$  te da je linija  $h = 0$  degenerirana za sisteme s neparnim brojem spinova, tj. s neparnim  $N$ . Također pokazano je da je u Isingovom modelu, koji je specijalan slučaj  $\gamma = 1$  XY lanca, za  $h > 0$  uvijek  $E_0^+ < E_0^-$ . Pokazano je korištenjem kompleksne analize i Fourierovog reda. Mi ćemo probati upotrijebiti metodu u općenitijem XY lancu. Metoda će nam dati rezultate samo u nekim posebnim slučajevima. Neki članci navode i numeričke rezultate gdje se vide oscilacije razlike  $E_0^- - E_0^+$  oko nule dok mijenjamo neki od parametara  $\gamma, h, N$ .

Sada navodimo naše numeričke rezultate koji su nekad bili inspiracija za naše analitičke račune, a nekad potvrda. Dobiveni su korištenjem programskog jezika *Python*. Pronašli smo točke u  $(\gamma, h)$  dijagramu gdje su energije  $E_0^-$  i  $E_0^+$  jednake tako da smo grafički prikazali razliku  $E_0^- - E_0^+$  samo tamo gdje ona iščezava. Rezultati su dani na slici 3.1 za  $N = 10$  i  $N = 11$ . Rezultati ovog tipa sugeriraju da se degeneracija ne može javiti izvan kruga  $\gamma^2 + h^2 = 1$ , a točno na kružnici ona je uvijek prisutna, što je u skladu s dosad rečenim. Također sugeriraju da je unutar kruga točno  $\lceil N/2 \rceil$  linija gdje postoji degeneracija te da su te linije elipse u limesu velikog sistema, tj. velikog  $N$ . Nadalje, grafički smo prikazali ovisnost razlike  $E_0^- - E_0^+$  o pojedinim parametrima



modela,  $h$ ,  $\gamma$ ,  $N$ . Rezultati su redom za svaki od njih dani na slikama 3.2, 3.3 i 3.4. Jasno se mogu vidjeti oscilacije oko nule.

Analitičke rezultate dobili smo metodom koja je dala odgovor o (ne)postojanju degeneracije u Isingovom modelu. Metoda započinje primjećivanjem periodičnosti i parnosti spektra:

$$\Lambda(x) = \Lambda(x + 2\pi) , \quad \Lambda(x) = \Lambda(-x) ,$$

što omogućuje razvoj u Fourierov red

$$\begin{aligned} a_n &= \frac{1}{\pi} \int_0^{2\pi} \Lambda(x) \cos(nx) \, dx \\ &= \frac{1}{\pi} \int_0^{2\pi} \cos(nx) \sqrt{(h - \cos x)^2 + \gamma^2 \sin^2 x} \, dx . \end{aligned}$$

Korištenjem Fourierovog reda dobiva se

$$\begin{aligned} E_0^- - E_0^+ &= \theta(h - 1)(h - 1) - N \sum_{k=0}^{\infty} a_{(2k+1)N} \\ &= \theta(h - 1)(h - 1) - N(a_N + a_{3N} + a_{5N} + \dots) , \end{aligned}$$

gdje je  $\theta$  step funkcija zbog uključivanja i slučaja  $h > 1$ , a  $N$  je kao i dosad veličina sistema.

Razliku  $E_0^- - E_0^+$  dalje istražujemo korištenjem kompleksne analize. Pretpostavit ćemo da uvijek govorimo o koeficijentima  $a_n$  za  $n \geq 2$ . Koristimo supstituciju  $z = e^{ix}$  i definiciju korijena u skupu kompleksnih brojeva

$$\sqrt{re^{i\phi}} = \begin{cases} \sqrt{r}e^{i\frac{\phi}{2}} & , 0 \leq \phi < \pi \\ -\sqrt{r}e^{i\frac{\phi}{2}} & , \pi \leq \phi < 2\pi \end{cases}$$

Tako definirani korijen ima rez na pozitivnoj realnoj osi. Približavamo li se realnoj osi  $x > 0$  odozgo korijen  $\sqrt{x + iy}$  svodi se na  $i\sqrt{|x|}$ , a ukoliko se približavamo odozdo svodi se na  $-i\sqrt{|x|}$ . Slično, korijen funkcije  $\sqrt{f(x + iy)}$  može postati  $i\sqrt{|f(x)|}$  ili  $-i\sqrt{|f(x)|}$  tamo gdje je  $f(x) < 0$  i pitanje na koji oblik se točno svodi jedno je od pitanja koje najviše otežava uporabu metode. Na prikazima integracijskih krivulja naznačeno je sa  $i$  ili  $-i$  redom na koji od dva navedena izraza se podintegralna

funkcija koju ćemo susresti svodi.

Najprije razmatramo već poznati rezultat za Isingov model,  $\gamma = 1$ . U slučaju  $h = 0$  već znamo da je degeneracija prisutna. U ostalim slučajevima koeficijent iz Fourierovog reda jednak je

$$a_n = \frac{-i\sqrt{h}}{\pi} \oint_{|z|=1} z^{n-1} \sqrt{-\frac{1}{z}(z-h)(z-\frac{1}{h})} dz ,$$

što se upotrebom integracijske krivulje na slici 3.5 svodi na

$$a_n = -\frac{2\sqrt{h}}{\pi} \int_0^{1/h} x^{n-1} \sqrt{\left| \frac{1}{x}(x-h)\left(x-\frac{1}{h}\right) \right|} dx$$

za  $h > 1$ , a izraz je potpuno analogan za  $h \leq 1$ , iz čega se zaključuje da je  $E_0^- > E_0^+$ .

Osnovno stanje Isingovog modela je nedegenerirano za  $h > 0$ .

U općenitijem XY lancu za koeficijent Fourierovog reda dobivamo

$$a_n = -\frac{i}{2\pi} \oint_{|z|=1} z^{n-1} \sqrt{-\frac{1}{z^2} P_1(z) P_2(z)} dz ,$$

gdje smo definirali polinome drugog reda

$$P_1(z) = (\gamma + 1)z^2 - 2hz - (\gamma - 1) ,$$

$$P_2(z) = (\gamma - 1)z^2 + 2hz - (\gamma + 1) .$$

Slučajevi u kojima smo uspjeli pojednostaviti koeficijente i u kojima se metoda uspostavila korisnom su sljedeći:

- $\gamma^2 + h^2 = 1$
- $h = 0$
- $\gamma > 1$  ,  $N = \text{paran}$

U prvom slučaju rezultat je već poznat. U drugom slučaju,  $h = 0$ , za  $\gamma > 1$  korištenjem integracijske krivulje na slici 3.6 dobivamo

$$a_n = 0 \quad , \text{ neparan } n$$

$$a_n = -\frac{\sqrt{\gamma^2 - 1}}{\pi} \int_0^\alpha x^{n-1} \sqrt{\left| \frac{1}{x^2}(x^2 - \alpha^2)(x^2 - \beta^2) \right|} dx \quad , \text{ paran } n$$

gdje su  $\pm\alpha$  i  $\pm\beta$  nultočke uvedenih polinoma drugog reda, eksplicitno dane s

$$\alpha = \sqrt{\frac{\gamma-1}{\gamma+1}}, \quad \beta = \sqrt{\frac{\gamma+1}{\gamma-1}}.$$

Za  $\gamma < 1$  izrazi su slični, ali javlja se i faktor  $i^n$ . Iz ovih relacija može se zaključiti odnos energija  $E_0^-$  i  $E_0^+$ . Rezultati su dani na slici 3.8.

U trećem slučaju,  $\gamma > 1$ , označimo nultočke polinoma  $P_1$  s  $\alpha_l < \alpha_r$  i nultočke polinoma  $P_2$  s  $\beta_l < \beta_r$ . One zadovoljavaju

$$0 < -\alpha_l < \beta_r < 1 < \alpha_r < -\beta_l$$

i korištenjem integracijske krivulje na slici 3.7 dobivamo

$$a_n = \frac{\sqrt{\gamma^2-1}}{2\pi} \left( \int_{\alpha_l}^0 - \int_0^{\beta_r} \right) x^{n-1} \sqrt{\left| \frac{1}{x^2} (x-\alpha_l)(x-\alpha_r)(x-\beta_l)(x-\beta_r) \right|} dx$$

iz čega se može zaključiti jedino da je  $E_0^- > E_0^+$  kada je  $N$  paran. Svi naši analitički rezultati sažeti su na slici 3.8.

## 6.4 Zapetljanost u XY lancu

Entropija zapetljanosti definira se pomoću svojstvenih vrijednosti  $\lambda_n$  reducirane matrice gustoće  $\rho$  kao

$$S = -\text{tr}(\rho \ln \rho) = -\sum_n \lambda_n \ln \lambda_n.$$

Entropija zapetljanosti je mjera koliko su dva podsistema u nekom sistemu zapetljana.

Definiramo  $2L \times 2L$  matricu korelacija

$$\Gamma^a = \begin{pmatrix} \Pi_0 & \Pi_1 & \cdots & \Pi_{L-1} \\ \Pi_{-1} & \Pi_0 & \cdots & \Pi_{L-2} \\ \vdots & \vdots & \ddots & \vdots \\ \Pi_{-(L-1)} & \Pi_{-(L-2)} & \cdots & \Pi_0 \end{pmatrix},$$

gdje je

$$\Pi_j \equiv \begin{pmatrix} 0 & g(j) \\ -g(-j) & 0 \end{pmatrix} .$$

Matrica korelacija je antisimetrična i može se dovesti u blok-dijagonalnu formu

$$\Gamma^b = \bigoplus_{j=1}^L \begin{pmatrix} 0 & \nu_j \\ -\nu_j & 0 \end{pmatrix} ,$$

Svojtvene vrijednosti reducirane matrice gustoće podsistema veličine  $L$  u XY lancu jednake su

$$\lambda_{\alpha_1 \alpha_2 \dots \alpha_L} = \prod_{j=1}^L \frac{1 + (-1)^{\alpha_j} \nu_j}{2} , \quad \alpha_1, \dots, \alpha_L = 0, 1 ,$$

a entropija zapetljanosti dana je s

$$S_L = - \sum_{j=1}^L \left( \frac{1 - \nu_j}{2} \ln \frac{1 - \nu_j}{2} + \frac{1 + \nu_j}{2} \ln \frac{1 + \nu_j}{2} \right) .$$

Pritom su  $\pm \nu_j$  koeficijenti koji se javljaju u blok-dijagonalnoj formi matrice korelacija, a mi ćemo ih dobivati numerički dijagonalizacijom hermitske matrice  $i\Gamma^a$ .

Limes dvostrukog skaliranja (DSL) je limes velikog podsistema u velikom sistemu. To je limes  $L \rightarrow \infty$  u limesu  $N \rightarrow \infty$ . U blizini kritičnosti DSL se može opisati konformalnom teorijom polja (CFT). U cijelom faznom dijagramu XY lanca DSL je pronađen egzaktnim metodama.

CFT relacija o skaliranju entropije zapetljanosti na  $i$  u blizini kritičnih linija primijenjena na kritičnu liniju  $h = 1$  u XY lancu glasi

$$S_L = \frac{1}{6} \ln L + C(\gamma) ,$$

gdje je  $C(\gamma)$  konstanta koja ne ovisi o veličini podsistema  $L$ . CFT daje vezu entropije zapetljanosti i najveće svojstvene vrijednosti, označimo je s  $\lambda_{\max}$ , reducirane matrice gustoće:

$$S_L = -2 \ln \lambda_{\max} .$$

Naš cilj je izračunati entropiju zapetljanosti i svojstvene vrijednosti reducirane

matrice gustoće i testirati jesu li uvedena CFT predviđanja o ponašanju tih veličina prekršena u blizini nekonformalne bikritične točke. Numeričke izračune i izradu grafova obavili smo u programskom jeziku *Python*. Naš numerički algoritam sastoji se od konstrukcije i diagonalizacije matrice korelacija  $i\Gamma^a$  te izračunavanja entropije zapetljanosti i svojstvenih vrijednosti reducirane matrice gustoće.

Prije testiranja kršenja CFT predviđanja testirali smo naš algoritam uspoređujući naše rezultate za konačni podsistem s limesom dvostrukog skaliranja. Rezultati su dani na slikama 4.3, 4.4 i 4.5. Nakon utvrđenog slaganja krenuli smo testirati CFT predviđanja u blizini i daleko od bikritične točke. Računamo entropiju zapetljanosti i  $\lambda_{\max}$  za jednake veličine podsistema blizu i daleko od bikritične točke. Želimo uvijek isti odnos veličina  $La$  i  $\xi$ , gdje je  $a$  udaljenost spinova u rešetki. Budući da na samoj kritičnoj liniji  $h = 1$  nema karakteristične skale duljine potrebno se malo odmaknuti od kritične linije. Zato smo odlučili tražiti točke blizu i daleko od bikritične točke, za  $h > 1$ , koje će sve imati  $\xi \approx 1000$ . Koristili smo veličine podsistema  $L = 20, 21, \dots, 60$ . Rezultati su prikazani na slici 4.6. Slike 4.6b i 4.6c pokazuju manje odstupanje od CFT predviđanja nego slika 4.6a u blizini nekonformalne točke, što je željeni rezultat. Odstupanja postoje u svim razmatranim točkama. Uzrok su efekti konačne veličine i to što nismo točno na kritičnoj liniji. Zanimljivo, slika 4.6d dobivena je najdalje od bikritične točke i pokazuje odstupanja, a također pokazuje različita ponašanja za parne i neparne  $L$ , što je znak efekata konačne veličine. No moguće je i da je točka  $\gamma = 100$  nekonformalna. To pitanje ostavljamo otvorenim. Bitno je da za  $\xi \approx 1000$  i iste veličine podsistema  $L$  dobivamo veće odstupanje za  $\gamma = 0.01$ , u blizini bikritične točke, nego za  $\gamma = 1$  i  $\gamma = 10$ , daleko od bikritične točke. Za konstruirati test u budućnosti je li multikritična točka u proizvoljnom modelu nekonformalna predložimo napraviti analizu uzimanjem u obzir drugih CFT predviđanja i drugih modela sa nekonformalnim multikritičnim točkama.

## 6.5 Zaključak

Cilj diplomskog rada bio je primijetiti nekonformalnu prirodu bikritične točke XY lanca u numeričkom eksperimentu koji uključuje veličine dostupne i u modelima koji nisu egzaktno rješivi. Koristeći takav pristup u budućnosti želimo napraviti numerički test je li multikritična točka u proizvoljnom modelu nekonformalna.

Uveli smo XY lanac i doveli njegov Hamiltonijan do forme slobodnih fermiona podijelivši teoriju u dva sektora različitog pariteta. Koristeći formu slobodnih fermiona pronašli smo spektar Hamiltonijana. Diskutirali smo kritična svojstva XY lanca koristeći dva različita pristupa, proučavanje spektra i proučavanje korelacijskih funkcija. Sve zajedno, došli smo do mikroskopskog opisa XY lanca.

Degeneracija osnovnog stanja XY lanca postoji ukoliko su najniže energije stanja iz dva različita sektora pariteta,  $E_0^-$  i  $E_0^+$ , jednake. Uveli smo dosad poznate rezultate o degeneraciji osnovnog stanja XY lanca i zbog njihovog manjka dalje je istražili koristeći numeričke i analitičke metode. Posebno, uveli smo metodu koja je dala odgovor za Isingov model. Metoda koristi kompleksnu analizu i Fourierov red i koristeći je pronašli smo odgovor postoji li degeneracija u nekim slučajevima općenitijeg XY lanca. Pokazali smo eksplicitnu ovisnost postojanja degeneracije o broju spinova  $N$  u slučaju isčezavajućeg magnetskog polja  $h$ . Također, pokazali smo odsutnost degeneracije u slučaju  $\gamma > 1$ , za proizvoljno magnetsko polje, kada je broj spinova  $N$  paran. Grafički smo prikazali numerički dobivenu ovisnost razlike  $E_0^- - E_0^+$  o parametrima Hamiltonijana  $\gamma$ ,  $h$ ,  $N$ , gdje su jasno vidljive oscilacije oko nule. Također, numerički smo istražili linije u  $(\gamma, h)$  prostoru parametara gdje postoji degeneracija osnovnog stanja XY lanca. Rezultati sugeriraju da degeneracija ne postoji izvan kruga  $\gamma^2 + h^2 = 1$  za  $h > 0$  i da unutar kruga postoji točno  $\lceil N/2 \rceil$  takvih linija.

Vraćajući se na cilj diplomskog rada, izveli smo reduciranu matricu gustoće i entropiju zapetljanosti za konačni podsistem XY lanca. Konstruirali smo numerički algoritam koji računa entropiju zapetljanosti i svojstvene vrijednosti reducirane matrice gustoće za konačni podsistem XY lanca, a to su veličine dostupne i u modelima koji nisu egzaktno rješivi. Nakon testiranja našeg algoritma uspoređujući dobivene rezultate za konačni podsistem sa limesom dvostrukog skaliranja krenuli smo testirati predviđanja konformalne teorije polja (CFT) o tim veličinama u blizini kritičnosti. Uspjeli smo primijetiti nekonformalnu prirodu bikritične točke usporedivši entropiju zapetljanosti i najveću svojstvenu vrijednost reducirane matrice gustoće s pripadnim CFT predviđanjima. Za konstruirati numerički test je li multikritična točka u proizvoljnom modelu nekonformalna predložili smo uzeti u obzir ostala CFT predviđanja i druge egzaktno rješive modele s nekonformalnim bikritičnim točkama.

## 6.6 HR nazivi slika i tablica

1.1	Grafički prikaz XY lanca . . . . .	2
1.2	Fazni dijagram XY lanca . . . . .	3
3.1	Linije $E_0^- = E_0^+$ . . . . .	36
3.2	Ovisnost razlike $E_0^- - E_0^+$ o magnetskom polju $h$ . . . . .	37
3.3	Ovisnost razlike $E_0^- - E_0^+$ o anizotropiji $\gamma$ . . . . .	37
3.4	Ovisnost razlike $E_0^- - E_0^+$ o veličini sistema $N$ . . . . .	38
3.5	Integracijska krivulja u slučaju $\gamma = 1, h < 1$ . . . . .	40
3.6	Integracijska krivulja u slučaju $h = 0, \gamma > 1$ . . . . .	43
3.7	Integracijska krivulja u slučaju $\gamma > 1, h > 1$ . . . . .	45
3.8	Odnos energija $E_0^-$ i $E_0^+$ u posebnim slučajevima . . . . .	46
4.1	Slučajevi u definiciji eliptičkog parametra $k$ . . . . .	55
4.2	Shematski prikaz numeričkog algoritma . . . . .	61
4.3	Ovisnost razlike $S_L(\gamma) - S_L(\gamma = 1)$ o anizotropiji $\gamma$ . . . . .	63
4.4	Usporedba vrijednosti $\nu_j$ konačnog podsistema i limesa dvostrukog skaliranja . . . . .	64
4.5	Svojstvene vrijednosti reducirane matrice gustoće konačnog podsistema u usporedbi s limesom dvostrukog skaliranja . . . . .	65
4.6	Ovisnost entropije zapetljanosti $S_L$ i $-2 \ln \lambda_{\max}$ o veličini podsistema $L$ , u blizini i daleko od nekonformalne bikritične točke . . . . .	69

## Bibliography

- [1] See, e.g., Gantmacher, F. R. The theory of matrices. Vol. 1. New York : Chelsea Publishing company, 1959.
- [2] Franchini, F. An introduction to integrable techniques for one-dimensional quantum systems. Berlin : Springer, 2017.
- [3] Lieb, E.; Schultz, T.; Mattis, D. Two Soluble Models of an Antiferromagnetic Chain. // Annals of Physics. Vol. 16, 407-466 (1961).
- [4] Katsura, S. Statistical Mechanics of the Anisotropic Linear Heisenberg Model. // Phys. Rev. Vol. 127, 1508-1518 (1962).
- [5] Niemeijer, T. Some exact calculations on a chain of spins 1/2. // Physica. Vol 36, 377-419 (1967).
- [6] Franchini F.; Its, A. R.; Jin B.-Q.; Korepin V. E. Ellipses of constant entropy in the XY spin chain. // J. Phys. A: Math. Theor. Vol. 40, 8467-8478 (2007).
- [7] See, e.g., Sakurai, J. J.; Napolitano J. Modern Quantum Mechanics. 2nd ed. San Francisco : Addison-Wesley, 2011.
- [8] Complete notes on fermions and the Jordan-Wigner transform, (7/29/2005), <http://michaelnielsen.org/blog/complete-notes-on-fermions-and-the-jordan-wigner-transform/>, 6/6/2017
- [9] Calabrese P.; Cardy J. Entanglement entropy and conformal field theory. // arXiv:0905.4013 [cond-mat.stat-mech], 2009.
- [10] Nielsen M.; Chuang I. Quantum Computation and Quantum Information. New York : Cambridge University Press, 2010.
- [11] Cheong S. A.; Henley C. L. Many-body density matrices for free fermions. // Phys. Rev. B Vol 69, 075111 (2004).
- [12] Peschel I.; Eisler V. Reduced density matrices and entanglement entropy in free lattice models. // arXiv:0906.1663 [cond-mat.stat-mech], 2009



- [13] See e.g., Kittel C. Elementary Statistical Physics. New York : Wiley, 1958.
- [14] Latorre J. I.; Rico E.; Vidal G. Ground state entanglement in quantum spin chains. // arXiv:quant-ph/0304098, 2003.
- [15] See, e.g., Bogoliubov N.N.; Shirkov D. V. Introduction To The Theory Of Quantized Fields. 3rd ed. New York : Wiley, 1980.
- [16] Barouch E.; McCoy B. M. Statistical Mechanics of the XY Model. II. Spin-Correlation functions. // Phys. Rev. A Vol. 3, 786-804 (1971).
- [17] Mussardo G. Statistical Field Theory. New York : Oxford University Press, 2010.
- [18] Sachdev S. Quantum Phase Transitions. 2nd ed. New York : Cambridge University Press, 2011.
- [19] <http://mpmath.org/>
- [20] <http://www.numpy.org/>
- [21] <https://docs.python.org/3.6/library/itertools.html>
- [22] <https://matplotlib.org/>
- [23] <http://www.sympy.org>
- [24] Its A. R.; Jin B.-Q.; Korepin V. E. Entanglement in the XY spin chain.// J. Phys. A: Math. Gen. Vol. 38, 2975-2990 (2005).
- [25] Franchini, F.; Its, A.R.; Korepin, V.E. *et al.* Spectrum of the density matrix of a large block of spins of the XY model in one dimension.// Quantum Inf Process Vol. 10, 325–341 (2011).
- [26] Andrews G. E. The Theory of Partitions. Massachusetts : Addison-Wesley, 1976.
- [27] Calabrese P.; Lefevre A. Entanglement spectrum in one-dimensional systems.// Phys. Rev. A Vol 78, 032329 (2008).
- [28] De Pasquale A.; Facchi P. XY model on the circle: Diagonalization, spectrum, and forerunners of the quantum phase transition.// Phys. Rev. A Vol 80, 032102 (2009).

- [29] Damski B.; Rams M. M. Exact results for fidelity susceptibility of the quantum Ising model: the interplay between parity, system size, and magnetic field.// J. Phys. A: Math. Theor. Vol 47, 025303 (2014).
- [30] Lewenstein M.; Sanpera A.; Ahufinger V. Ultracold Atoms in Optical Lattices. Oxford : Oxford University Press, 2012.
- [31] Bose S. Quantum Communication through an Unmodulated Spin Chain.// Phys. Rev. Lett. Vol. 91, 207901 (2003).
- [32] Giamarchi T. Quantum Physics in One Dimension. New York : Oxford University Press, 2003.
- [33] Laumann C. R.; Moessner R.; Scardicchio A.; Sondhi S. L. Quantum Adiabatic Algorithm and Scaling of Gaps at First-Order Quantum Phase Transitions.// Phys. Rev. Lett. Vol. 109, 030502 (2012).
- [34] Peschel I. Entanglement in solvable many-particle models. // arXiv:1109.0159 [cond-mat.stat-mech] (2011).
- [35] Calabrese P.; Cardy C. Entanglement entropy and quantum field theory.// J. Stat. Mech. P06002 (2004).
- [36] Vidal G.; Latorre J. I.; Rico E.; Kitaev A. Entanglement in Quantum Critical Phenomena.// Phys. Rev. Lett. Vol. 90, 227902 (2003).
- [37] Ercolessi E.; Evangelisti S.; Franchini F.; Ravanini F. Essential singularity in the Renyi entanglement entropy of the one-dimensional XYZ spin-1/2 chain.// Phys. Rev. B Vol. 83, 012402 (2011).
- [38] Sudan J.; Luscher A.; Laeuchli A. Emergent multipolar spin correlations in a fluctuating spiral - The frustrated ferromagnetic  $S=1/2$  Heisenberg chain in a magnetic field.// Phys. Rev. B Vol. 80, 140402(R) (2009).